UNIVERSITÀ
DEGLI STUDI
FIRENZE

DOTTORATO DI RICERCA IN
SCIENZE CHIMICHE

CICLO XXVII

COORDINATORE Prof. Adrea Goti

Electrochemical Genosensors for Tumor Biomarker Detection: the case of miRNAs

Settore Scientifico Disciplinare CHIM/01

Dottorando
Dott. Voccia Diego

Tutore
Prof. Palchetti Ilaria

Coordinatore
Prof. Goti Andrea

Anni 2012/2014

Abstract

This thesis describes the implementation of different types of genosensors for microRNA (miRNA) electrochemical detection.

miRNAs are intensely studied as candidates for diagnostic and prognostic biomarkers. They are naturally occurring small RNAs (approximately 22 nucleotides in length) that act as regulators of protein translation. Because many diseases are caused by the misregulated activity of proteins, miRNAs have been implicated in a number of diseases including a broad range of cancers, heart diseases, immunological and neurological diseases. Therefore, a great deal of effort has been devoted to develop analytical methods for miRNA analysis with a PCR-free approach.

In this thesis, miRNA 221 and 222 detection was studied since it is well known that these two sequences are involved into different type of lung, liver and brain cancers. Both electrochemical and photoelectrochemical transduction method was adopted.

The analytical approaches were based on a recognition event through the hybridization of miRNAs to a specific capture probe. Several modifications of the sensor surface were studied in order to obtain the optimal analytical performances.

In a first approach, the genoassay was developed using disposable screen printed gold electrodes (SPGE). The surface of a SPGE was modified with a thiol-tethered DNA capture probe, a spacer thiol, and then exposed to the target miRNA sequence. Electrochemical Impedence Spectroscopy (EIS) was chosen as electroanalytical technique due to its intrinsic property that allows a label-free detection scheme. Moreover, in order to increase the sensitivity of the assay, an enzyme amplification route was investigated. In this case, the hybrid formed on the electrode surface was labeled using the enzyme Alkaline-Phosphatase. The electrochemical transduction of the hybridization process was performed by means of EIS, after a biocatalyzed conversion of a soluble substrate into an insoluble and insulating product. Enzyme-decorated liposomes were then tested as labels in order to amplify the miRNA-electrochemical sensing. The possibility to further increase the sensitivity of the assay by nanostructuration of the working electrode surface was also investigated using

carbon screen printed electrodes modified with gold nanoclusters through electrodeposition, obtaining a detection limit in the picomolar range.

In another approach, an electroconductive polymer film was investigated in order to obtain a label-free assay. In particular, a biotinylated bisthiophene monomer was potentiodynamically polymerized to form films on the SPGEs surface. On top of these films, streptavidin was immobilized by complexing the biotin moieties of the polymer. Finally, biotinylated oligonucleotide capture probe was immobilized by complexing the surface-immobilized streptavidin. This structure served as recognition element of the complementary miRNA sequence via hybridization event. EIS was chosen as electroanalytical technique. The use of conductive polymer resulted in a label-free assay with sensitivity in the picomolar range.

The last part of the thesis was focused on the development of a photoelectrochemical system for miRNAs detection. Recently, with the emergence of novel photo-electrochemically active species and new nanomaterials, photoelectrochemistry has received increasing attention in the field of biosensors. Commercial ITO-nanoTiO_2 electrodes were modified with gold nanorods and characterized in order to develop an enzyme-based genosensor. A white LED was used as a light source.

Index

Chapter 1 – Introduction

1.1 Cancer

Cancer is a major public health problem in Italy and in many other parts of the world. According to ISTAT, 1 of 3 deaths in Italy is due to cancer [1]. The words “cancer”, “neoplasia” and “tumor” are referred to a complex disease in which cells in a specific tissue are no longer fully responsive to the signals within the tissue that regulate cellular differentiation, survival, proliferation and death. As a result, these cells accumulate within the tissue, causing local damage and inflammation. In normal conditions, for an adult, the number of cells is widely constant. The transformation from a normal cell into a tumor cell is a multistage process, typically a progression from a pre-cancerous lesion to malignant tumors. These changes are the result of the interaction between a person's genetic factors and external agents, like physical carcinogens (ultraviolet and ionizing radiation), chemical carcinogens (food and water contaminant, components of tobacco smoke) and biological carcinogens (infections from certain viruses, bacteria or parasites) [2]. Actually, there are over 200 different types of cancer. According the International Agency for Research on Cancer, cancers figure among the leading causes of death worldwide, accounting for 8.20 million deaths in 2012 with 32.55 million people living with cancer (within 5 years of diagnosis). Europe counts 1.28 million deaths in 2012 (15.6% of total) with 7.25 million people (22.3% of total) living with cancer (within 5 years of diagnosis). Italy, instead, counts 0.17 million deaths in 2012 (13.3% of Europe) with 1.01 million people (14.0% of Europe) living with cancer (within 5 years of diagnosis). In Italy, according ISTAT’s evaluation, cancer is the second death cause (30.9% of total) after cardiovascular diseases (42.3% of total), with an highest mortality for men respect to women [3]. The most common causes of cancer death in Italy, according to WHO, are summarized in table 1.1. The highest incidence in Italy, in 2012, is connected to breast cancer for women (33.0% of total women cancer incidence) and prostate cancer for men (24.8% of total men cancer incidence). For the total of the sample analyzed breast cancer results the one with highest incidence (15.2% of the total) followed by colorectum cancer (14.4% of the total).

	mortality	%
Lung	33531	22.4%
Colorectum	19279	12.9%
Breast	12796	8.6%
Pancreas	10637	7.1%
Stomach	9917	6.6%
Prostate	7814	5.2%
Others	55452	37.1%
Total	149426	

Table 1.1 – Cancer mortality in 2012 according the International Agency for Research on Cancer [3].

Temporal trends analysis, in terms of cancer incidence and mortality, represents one of the main tools for efficiency evaluation of preventions, therapies, as well as changes in habits and exposition to environmental factors of the population. As reported in the AIRTUM bulletin of 2013 "I numeri del cancro in Italia", in the temporal range from 1996 to 2007, it is evident a statistically significant reduction in mortality for the totality of tumors in both sexes. In particular emerges a 17% and 10% decrease, for men and women respectively, in the observed period. This reduction in mortality can be attributed to the effect of a reduction in the number of people who is affected by neoplasia, or the introduction of more effective treatments with a consequent improved survival. In example, mortality decreasing trends in lung cancer in men are probably connected to the reduction of incidence; mortality decreasing trends in breast cancer in women is mainly due to the effectiveness of new therapies associated to intervention for early diagnosis. The increased mortality in some cases is related to the increase in number of subjects affected by tumor in absence of therapies available. The increase in incidence is a complex phenomenon and can be attributed to several factors, including increased exposure to risk factors related to tumor, or to anticipation of diagnosis due to screening programs introduced (e.g. is notable an increased number of incidence linked to the spread of the test of detection diffused in the early 90's of the last century).

Knowledge about the causes of cancer, and interventions to prevent and manage the disease is extensive. Cancer can be reduced and controlled by implementing evidence-based strategies for cancer prevention, early detection of cancer and management of patients with cancer. Many cancers have a high chance of cure if detected early and

treated adequately. Cancer mortality can be reduced if cases are detected and treated early. There are two components of early detection efforts: the awareness of early signs and symptoms (for cancer types such as cervical, breast, colorectal and oral) in order to get them diagnosed and treated early before the disease becomes advanced; screening aims to identify individuals with abnormalities suggesting a specific cancer or pre-cancer and refer them promptly for diagnosis and treatment.

Carcinogenesis is a process by which normal cells are transformed into cancer cells. It is characterized by a progression of changes at the cellular, genetic and epigenetic level that ultimately reprogram a cell to undergo uncontrolled cell division, thus forming a malignant mass. Cell division is a physiological process that occurs in almost all tissues and under many circumstances. Under normal circumstances, the balance between proliferation and programmed cell death, usually in the form of apoptosis, is maintained by regulation of both processes to ensure the integrity of tissues and organs. Changes in DNA that lead to cancer interrupt these orderly processes by disrupting the regulation of this process. In the beginning of 80's of the last century, Berenblum gave great attention to carcinogenesis permitting to arrive to the generally accepted multistep theory [4], in which there are three distinct stages: the initiation stage, the promotion stage and the progression stage. If the first two stages underlie the triggering of cell transformation, the third stage determines the transformation of a benign tumor into a malignant form, with the maintenance and evolution of malignancy. The period between the fixation of a carcinogen to chromosomal DNA and the appearance of a population of neoplastic cells can be divided in the following stages: initiation, promotion and progression [5].

Initiation represent the starting stage with the action of the carcinogen on chromosomal DNA, inducing a lesion, which can be repaired or reproduced. The biological mechanisms of repair are complex. In the repair of a cell lesion, the time factor is essential. Thus, if mitosis is delayed, DNA can be repaired; if not, the lesion will be replicated and transmitted to the new cells. The initiation stage of a cell starts with the impossibility of repairing of the DNA lesion.

Promotion is the stage in which genetic alterations of the initiated cell determine the neoplastic transformation and the appearance of cells that are capable of autonomous growth. The promoter is applied several times after the simple administration of an initiating carcinogen. Carcinogens are agents that induce cancer without the need for the subsequent action of a promoter. Tumor promotion is to a great extent associated with epigenetic factors that alter, directly or indirectly, the genomic DNA expression [6].

Promotion would consist of events occurring in the genetic program of terminal proliferation and differentiation. The promoted cell does no longer recognize the differentiation signals, which would normally remove it from the replication population. Unlike initiators, promoters do not bind to DNA, their major target being the cell membrane.

Progression is characterized by marked malignancy and the tendency to induce changes that cause the death of the host. Cells in the progression stage are characterized by genetic changes, gene alterations and rearrangements and the tumor is phenotypically characterized by a rapid proliferation rhythm, invasive and metastasizing properties, with biochemical and morphological changes.

Studies have shown that there are genetic mechanisms involving hereditary transmissible DNA alterations, as well as epigenetic mechanisms that involve the expression of one or several genes. Genetic mechanisms have been demonstrated by the presence of hereditary cancer or by the increased incidence of cancer in congenital chromosomal lesions or in disorders characterized by DNA repair deficiencies. Spandidos and Anderson mention three main classes of genes [7]:

- oncogenes, which derive from altered normal genes, proto-oncogenes, so that they become activated;
- modeling genes, which can predispose to cancer and are submitted to a mutation. In general, there is a group of heterogeneous genes, some of which are involved in the repair of damaged DNA;
- onco-suppressor genes, which is a very diverse group of genes which share the property of inhibiting the cancer phenotype. The mode of functioning and identification of onco-suppressor genes is difficult; it seems that their role is to inhibit cell proliferation, not to directly regulate oncogenes.

The involvement of mutations in various phases of carcinogenesis is certain; it seems that some epigenetic events also contribute to the development of cancerous cells. These events cannot be avoided and include DNA, RNA and protein changes that can influence the cell phenotype, but not the genotype. Differentiation, which can be estimated to derive from a series of epigenetic changes, can modify the tumorigenic phenotype of the cells.

The results of the investigations regarding oncogenes and onco-suppressor genes suggest possible applications in practical oncology. In this sense, the use for diagnosis (tumor classification, malignancy diagnosis, early metastasizing); prognosis (oncogene

amplifications); therapy (monoclonal antibodies and radiochemotherapy); and epidemiology (genetic consultation) is intended. The determination of changes in oncogenes and onco-suppressor genes in tumors can be useful for diagnosis, prognosis and the therapeutic approach. The molecular hybridization technique involving tumor DNA or RNA, as well as immunohistochemical techniques, can be used in determining quantitative and/or qualitative changes of oncogenes and onco-suppressor genes, as well as their expression.

The discovery of cellular microRNA and its functions, in particular, has provided important data on cell biology, especially on the understanding of cancer diseases. In cancer cell cultures, microRNA has been shown to delay cell division, consequently acting as tumor suppressor. Another important function of microRNA is to regulate the amount of messenger RNA produced in a cell. The actions and functions of microRNAs are multiple, on the one hand due to their diversity, and on the other hand due to the diversity of their targets, which makes them essential in cell differentiation. It has been demonstrated that each tumor type possesses a specific "expression profile" of microRNA, which opens the perspective for a certainty diagnosis of the tumor type and, implicitly, for the application of adequate therapy.

A cancer diagnosis results really important in order to assign the best therapy for patients. Possible signs and symptoms include: a new lump, abnormal bleeding, a prolonged cough, unexplained weight loss, and a change in bowel movements, among others. While these symptoms may indicate cancer they may also occur due to other issues. For this reason, specific test are necessary. One of the possible diagnosis is nearly always made by an expert looking at cell or tissue samples under a microscope. The procedure that takes a sample for this testing is called a biopsy, and the tissue sample is called the biopsy specimen. The testing process is sometimes referred to as pathology. Lumps that might be cancer might be found by imaging (radiology) studies or felt as lumps during a physical exam, but they still must be sampled and looked under a microscope to find out what they really are. Not all lumps are cancer. In fact, most tumors are benign (not cancer). A malignant tumor (cancer) can spread into nearby tissues and even to distant parts of the body. A benign tumor cannot do this. In order to confirm a diagnosis, lab tests of specific molecules like cells proteins, DNA, and RNA can help to make the diagnosis. These tests can also help in choosing the best treatment options. These molecules could be altered in patients affected by tumors, and their analysis could help confirming a specific diagnosis. These molecules are known as biomarkers.

1.2 Biomarkers

Biological marker, better known as "biomarker" refers to medical signs that are objective indications of a medical state and that is possible to measure accurately and reproducibly. It is important to note that medical signs are in contrast with symptoms, that are instead indications of health or illness perceived by patients. There are several definitions of biomarkers in the literature, but in 1998, the National Institutes of Health Biomarkers Definitions Working Group defined a biomarker as "*a characteristic that is objectively measured and evaluated as an indicator of normal biological processes, pathogenic processes, or pharmacologic responses to a therapeutic intervention*" [8]. Another definition has been proposed by the International Programme on Chemical Safety, led by the World Health Organization (WHO) and in coordination with the United Nations and the International Labor Organization: "*any substance, structure, or process that can be measured in the body or its products and influence or predict the incidence of outcome or disease*" [9]. A biomarker associated with cancer is commonly defined "*tumor marker*". Tumor markers are substances that are produced by malignant cells and that can be determined in body fluids or tissues. Tumor markers can be either substances that can be found in normal organisms in much lower or higher concentrations. Ideally, a tumor marker would always be detected, but only when a certain type of cancer is present. In reality, tumor markers are rarely like that. In order to evaluate a good candidate as tumor marker is important to know its sensitivity and specificity. The sensitivity of a marker reports the proportion of patients bearing a specific type of tumor in which the marker concentration is elevated: the more patients with the same type of cancer have an elevated level, the more sensitive is the marker, and the lower is the expected number of false negative determinations. The specificity of a marker represents the proportion of individuals who have a certain type of malignancy and in whom the marker level is present at high level. That means that the lower is the number of individuals not bearing a certain type of tumor and having a low marker level, the higher is the specificity, and lower is the expected number of false positive determinations. The ideal case of 100% of specificity and sensitivity is not yet possible. In order to increase sensitivity, it is possible to combine two or more tumor markers associated with a specific cancer, but we have to consider that in this way, the specificity of detection is decreased. The choice of combining tumor marker must be focused bearing in mind that specificity can be slightly

lowered, while the sensitivity is significantly increased. The prerequisite for a proper combination of different markers is their high specificity and complementarity for the type of tumor. In example, the CA125 tumor marker is used to help predict the presence of ovarian cancer [10]. Because elevated CA125 levels occur in many benign gynecologic conditions, combining other biomarkers that would increase the sensitivity and specificity of CA125 is necessary. In literature is reported a logistic regression model for a set of markers and their combinations, with cross-validation analysis performed to obtain the sensitivities keeping specificities at 95%. In this study, CA125 had a low sensitivity of 43%, instead HE4 marker had a sensitivity of 73%. Comparatively, combining CA125 and HE4 sensitivity increase to 76% [11]. This result show how CA125 and HE4 combination gives a more accurate predictor of malignancy than either alone, but also how is difficult to obtain good sensitivities and specificities. Because of these limitations, a tumor marker could only be considered as a probabilistic indication of the presence of a certain type of cancer, not a specific diagnosis: the only way to have a precise diagnosis is biopsy. Anyway, it is important to underline all the potentiality of a tumor marker in clinical oncology: it could be used in order to evaluate the response to treatment detecting its level before and after the beginning of the therapy; it could also be used in order to identify the presence of new metastasis. Even if tumor markers present limits, in clinical oncology their detection for monitoring the course of cancer is an established and often an irreplaceable oncological laboratory method. Tumor markers are reliable predominately in monitoring the treatment response, as well as in early detection of disease recurrence. Tumor markers can be classified according to their chemical structure or types of cancer in which they are elevated: tumor antigens, enzymes, hormones, oncogens and nucleic acids. Tumor antigen is an antigenic substance produced in tumor cells, i.e., it triggers an immune response in the host. In this group we could find: *Carcino Embryonic Antigen* (CEA) that is specific marker for colon carcinoma [12]; and *Alpha FetoProtein* (AFP) that is specific marker for hepatocellular carcinoma [13]. Enzymes represent good markers if they result overproduced by cancer cells: *Alkaline phosphatase* is normally synthesized in the liver, bones or placenta and an elevated serum concentration could be associated to liver cancer or osteosarcoma [14]. Hormones represent good tumor markers when the cancer affect their natural secretions. This group comprises hormones of malignant endocrine tumors as parathyroid hormone, insulin and others. An oncogene is a gene that has the potential to cause cancer and in tumor cells are often mutated or expressed at high levels. Effective diagnosis and

surveillance of complex multi-factorial disorders such as cancer can be improved by screening of easily accessible biomarkers. Highly stable Circulating Nucleic Acids (CNA) have been discovered in the blood, plasma and other fluids of humans. Alterations in CNA levels are strong predictors of the utility of this biomarker class as promising clinical indicators [15]. Towards this goal, microRNAs (a class of naturally occurring small non-coding RNAs of 19–25 nt in length) have emerged as an important set of biomarkers that can associate their specific expression profiles with cancer status.

1.3 microRNA

Starting from the initial discovery by Ambros group in 1993 [16], over the last decade has become more clear that a large class of small noncoding RNAs with approximately 22 nucleotides in length, better known as microRNAs (miRNAs), play important role in many biological process as modulator of gene expression. Ambros group identified two strands of small RNAs studying the developmental pathways of the soil nematode *Caenorhabditis elegans* (figure 1.1): they discovered that lin-4 gene does not encode a protein product, but instead gives rise to a precursor gene that matured to a more abundant small transcript. In parallel, Ruvkun group founded that lin-14 protein synthesis is regulated posttranscriptionally and that lin-14 levels are inversely proportional to those of lin-4 gene [17]: analyzing the sequences the lin-4 RNA is complementary to the 3′ untranslated region of the lin-14 gene. These discoveries revealed the possibility of a base pair regulation of lin-14 by lin-4: in other words, they revealed the first miRNA and mRNA target interaction.

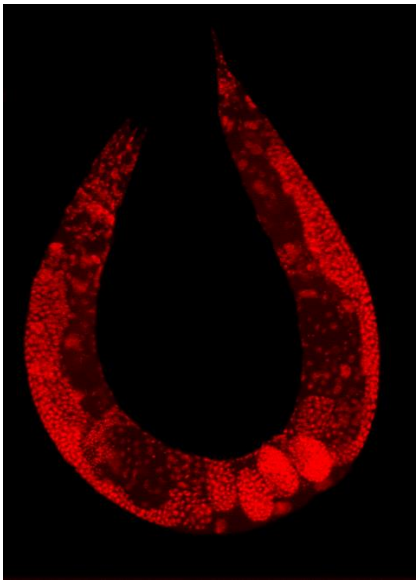

Figure 1.1 - Wild-type Caenorhabditis elegans hermaphrodite stained to highlight the nuclei of all cells [18]

RNA lin-4 was considered an anomaly until 2000, when Ruvkun group discovered another small RNA, called let-7 [19], which is complementary to elements in the 3' untranslated regions of the heterochronic genes lin-14, lin-28, lin-41, lin-42 and daf-12, indicating that expression of these genes may be directly controlled by let-7. Moreover, the same lab identified let-7 homologs in many vertebrate species including humans [20], demonstrating that miRNAs are evolutionarily conserved across many species and are often ubiquitously expressed. Since that time, has become clear that this class of small noncoding RNAs plays important role in many biological processes as modulator of gene expression.

miRNAs have a peculiar mechanism of action and biogenesis. The main biological role of miRNAs is to perform gene regulation either directly through cleavage of mRNA or indirectly through translational repression. In either case, miRNA hybridizes with its target mRNA strand at the mRNA's 3′ untranslated region. Initially, miRNA is part of a much larger piece of RNA with stem-loop structures, which may contain multiple potential miRNAs as reported in figure 1.2. This long strand of RNA, known as primary miRNA (pri-miRNA) is transcribed by RNA polymerase II in the nucleus of the cell [21]. Next, the pri-miRNA is cleaved by an RNase III endonuclease known as Drosha, which cuts the RNA into an approximately 60-base stem-loop structure [22]. This piece of RNA is known as pre-miRNA. The pre-miRNA is then exported to the cytoplasm via the carrier protein Exportin-5 (Exp-5). Once the Exp-5 has mediated pre-miRNA delivery

into the cytoplasm, the pre-miRNA separates from the Exp-5, and is cleaved by an RNase III enzyme known as Dicer, which results in the mature form of miRNA [23].

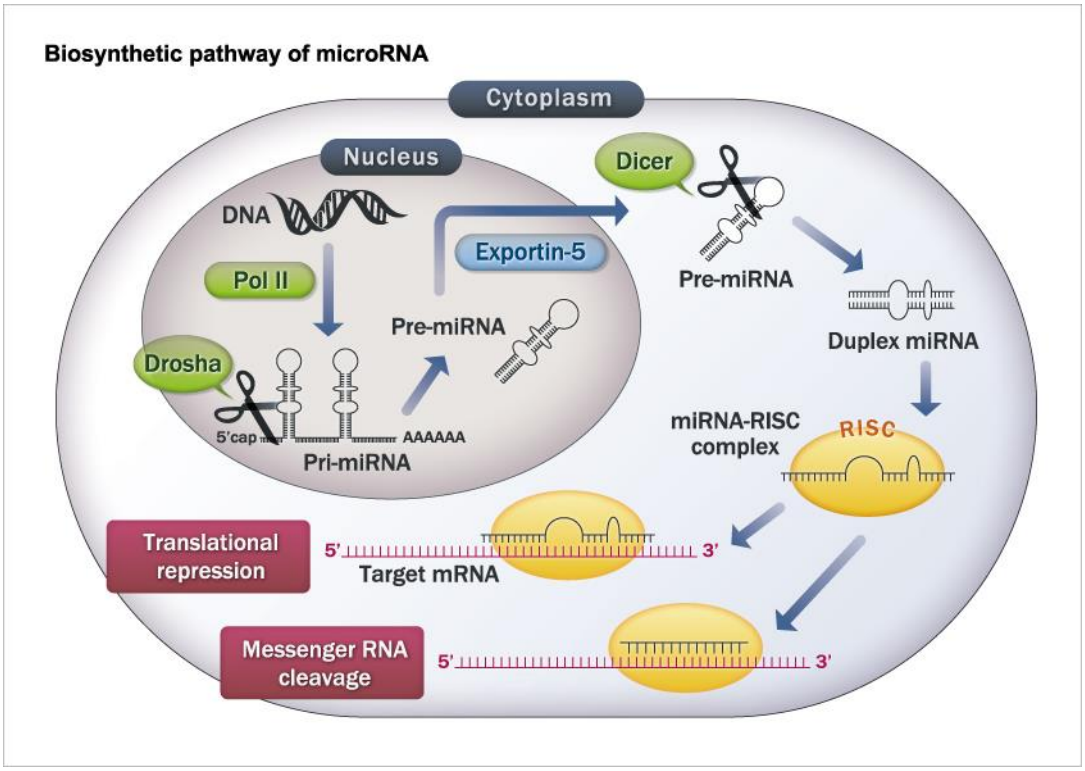

Figure 1.2 - Biosynthetic pathway of miRNA. Reproduced from [24]

An abnormal miRNA expression (overexpression or downexpression) could be linked to many diseases, like cardiovascular pathologies [25], cancer [15], immunological [26] and neurological [27] diseases. For instance in cancer, miRNAs are implicated in each one of the main essential features of cancer progression: from cell proliferation to inhibition of cell apopotosis and in the same cancer type, different miRNAs can be up-or down-regulated respect to a basal level.

The first evidence of involvement of miRNAs in human cancer came from molecular studies which revealed that two miRNAs, mir-15 and mir-16, were involved in chronic lymphocytic leukemias (CLL) [28]. Particularly, these first studies were performed in an attempt to identify tumor suppressors at chromosome 13q14, frequently deleted in CLL. Indeed, as demonstrated later by the same group and other groups, chromosomal regions encompassing microRNAs involved in the negative regulation of a transcript encoding a known tumor suppressor gene can be amplified in cancer development. This amplification would result in the increased expression of the microRNA and consequent silencing of the tumour suppressor gene. Conversely, microRNAs repressing oncogenes

are often located in fragile loci, where deletions or mutations can occur and result in reduced microRNA levels and overexpression of the target oncogene. microRNAs playing an oncogenic role by targeting oncosuppressor molecules are called oncomiRs, instead microRNAs playing an oncosuppressive role by targeting oncogenes are tumor suppressor miRNAs. In Table 1.2, are reported some examples of miRNA expression deregulated in human cancer. These deregulated miRNAs may function as either tumour suppressors or oncogenes by targeting each one of these features.

miRNA profiles can distinguish not only between normal and cancerous tissue and identify tissues of origin, but they can also discriminate different subtypes of a particular cancer, or even specific oncogenic abnormalities. Gene expression profiling has already demonstrated its effectiveness at subtyping various cancers. However, miRNA profiles are equally discriminatory and can even be more informative, as expression changes can provide insights into the multitude of gene permutations observed in various cancer subtypes [29].

miRNA	Tumor associated	Type of Targeting
miR-15/16	Chronic lymphocytic leukemia [30]	Tumor suppressor gene
miR-17/92	Colon [31]	Oncogene
miR-21	Cholangio carcinoma [32]	Oncogene
miR-34	Gastric cancer [33]	Tumor suppressor gene
miR-155	Breast cancer [34]	Oncogene
miR-200 family	Bladder cancer [35]	Tumor suppressor gene
miR-222/221	Glioblastoma [36], prostate [37], and thyroid carcinoma [38]	Oncogene

Table 1.2 - Tumor-suppressor and oncogene microRNAs

Following this initial discover, other researches were focused on the investigation of miRNA expression deregulation in human cancer. For example mir143 and mir145 are down-regulated in colon carcinomas [39] and mir122 is involved in breast cancer [40]. For all these reasons and considering that they are more stable than long mRNA,

miRNAs are intensely studied as candidates for diagnostic, prognostic and predictive tumor markers.

1.3.1 microRNA as tumor marker

microRNAs have revealed a great potential as tumor markers, and especially as early diagnosis markers. Indeed, they are able to discriminate tumor origins, subtypes, oncogenic mutations and cancer predisposition. Moreover, since miRNAs regulate the most important cellular processes, they can be useful to predict also cancer prognosis and/or response to specific therapies. Furthermore, the presence of miRNAs not only in body cells and tissues, but also in body fluids (circulating miRNAs) may be an important feature for minimally invasive analysis [41, 42]. However, these circulating miRNA are present at very low level and in some cases are secreted from cells packaged in microparticles (exosomes, microvesicles, and apoptotic bodies) or by their association with RNA-binding proteins, including Argonaute 2 or lipoprotein complexes such as high-density lipoprotein (HDL) [43]. For these reasons, proper extraction procedures have to be performed. Moreover, the composition of these fluids is quite dissimilar, which implies that isolation methods cannot be directly transposed from one tissue/fluid to another [44]. Obviously, these findings complicate the detection of miRNA in biological fluids.

Thus, to use miRNAs as reliable diagnostic, predictive or prognostic tumor markers, the development or optimization of efficient, sensitive and reproducible detection methods, including robust sample extraction selection or preparation procedure, are of primary importance [29]. Since deregulated miRNA expression is an early event in patients with cancer, measuring circulating miRNA levels may also be useful for early diagnostic, with high advantages to the success of treatment. How miRNAs are selected for secretion is still unknown. Cells secrete miRNAs as lipoprotein complexes, small membranous vesicles known as exosomes [45]. It is important to note that these findings do not yet eliminate the necessity of using invasive cancer screening techniques.

1.3.2 miRNA 221 and miRNA 222

The miR-222/221 cluster is among the most dysregulated miRNAs implicated in cancer. Expression of miR-222/221 is highly upregulated in a variety of solid tumors, including lung cancer [46], hepatocarcinoma [47], breast cancer [48], thyroid cancer [38], and melanoma cells [49].

The miR-221 is one of the most frequently and consistently up-regulated miRNAs in human cancer. It has been demonstrated that miR-221 may act as a tumor promoter with a concomitant down-regulation of miR-221 target proteins (i.e., cyclin-dependent kinase inhibitor [Cdkn]1b/p27, Cdkn1c/p57, and B-cell lymphoma 2–modifying factor) [50].

Stinson et al. [51] reported that miR-221 and miR-222 decrease expression of epithelium-specific genes and increase expression of mesenchymespecific genes. They showed that the transcription factor FOSL1 directly stimulates the transcription of miR-222/221, which in turn, by targeting TRPS1 (trichorhinophalangeal syndrome type 1, a Zeb2 inhibitor), reduces Ecadherin abundance, contributing to the aggressive clinical behavior of basal-like breast cancer. Elevated miR-221 and miR-222 expression is linked not only to proliferation [52] and migration [51] but also to apoptosis [53]. Despite advances in standard treatment, non small cell lung cancer and hepatocellular carcinoma, are often diagnosed at an advanced stage and have poor prognoses. The development of innovative early diagnosis represent an important goal for the treatment of these cancers. For these reasons, in this thesis different genosensors for miRNA 221 and 222 detection are studied in order to obtain a fast and simple method of detection.

1.3.3 microRNA detection

Actually, there are different methods for the detection of miRNAs, each of them with their own unique advantages and disadvantages. Many detection methods rely on hybridization event with a complementary sequence. The hybridization event could occur either with solid-phase approach (a capture probe is adsorbed or bound to a solid surface for hybridization to the target) or with a solution-phase approach (target hybridization occurs in solution). Solution-phase methods often result in much more

rapid analysis times, while solid-phase methods, in general, are more appropriate for high-throughput analysis. Once the hybridization event occurs, it is necessary to translate the event in something that is possible to detect. Northern blotting is the most widely used miRNA detection method because it is generally a readily available technology for laboratories and does not require special equipment and technical knowledge. In general, target RNA run on an electrophoresis gel and then it is transferred, by blotting, onto a membrane to which the RNA is covalently bound. Finally, the membrane is incubated with a labeled probe, which is a single-stranded DNA, forming a duplex with its target. The hybrid can be revealed by a radioactive or by an enzyme label (e.g. alkaline phosphatase or horseradish peroxidase). However, this method is time-consuming, semi quantitative and is characterized by a low sensitivity. In order to increase sensitivity, locked nucleic acid (LNA)-modified oligonucleotide probes were used to enhance the efficiency of hybridization [54].

The use of microarray is another classical detection method and require immobilized oligonucleotides on a support with the same sequence as the target miRNA in order to detect cDNA from a sample [55]. The cDNA is produced via reverse transcription from a sample's RNA using fluorescent or enzyme labeled primers. Recently, Quantum Dots (QDs) as fluorescent labels have been introduced because of the high extinction coefficient and high quantum yield, which should dramatically increase the sensitivity for microarray detection [56]. Even if microarrays can analyze thousands of samples in a day, they are very expensive to fabricate. Thus, the high cost limits the wide applications of miRNAs microarray, especially in clinical diagnosis.

Another standard method of detection is the quantitative reverse transcriptase polymerase chain reaction (RT-PCR), which can detect miRNA in real time and is one of the most used due to the inherent sensitivity and reliability. Because of their small size, (similarly to the primers), miRNA detection based on PCR is complicated (i.e. ligation is needed), is low throughput and time consuming.

A great deal of effort, therefore, has been devoted to developing new analytical methods for miRNA analysis that possess appropriate sensitivity, appropriate dynamic range and multiplexing capability without PCR.

Alternative methods include bioassays and biosensor based on surface-enhanced Raman Scattering (SERS), surface plasmon resonance (SPR), surface plasmon resonance imaging, fluorescence, and bioluminescence-based techniques [57]. However, many of these methods are laborious and require the use of a well- equipped

laboratory with specialized and well-trained personnel, and are neither feasible for routine determination of miRNAs nor applicable for point-of-care (POC) testing.

Electrochemical biosensors are emerging options for miRNA detection. In comparison with other techniques, like optical methods, electrochemistry is considered as one of the most appealing techniques in term of cost, ease of operation and automation.

1.4 Electrochemical biosensor for microRNA detection

Electrochemical biosensors have emerged as particularly attractive options for miRNA detection in terms of simplicity of use, low assay time, small amount of sample required. The role of electrochemical biosensors for miRNAs detection has been reviewed recently [58-60]. In this section the definition of electrochemical biosensors will be introduced and examples of miRNA detection using electrochemical biosensor will be discussed.

1.4.1 Electrochemical biosensor: definition and classification

According to the International Union of Pure and Applied Chemistry (IUPAC) an electrochemical biosensor is "*a self-contained integrated device, which is capable of providing specific quantitative or semi-quantitative analytical information using a biological recognition element (biochemical receptor) which is retained in direct spatial contact with an electrochemical transduction element*" [61]. There are two classes of different biosensors classified according to the biologically active part: catalytic and affinity biosensors. Catalytic biosensors are based on a biological catalysts such as enzymes, cells, microorganisms or biomimetic catalysts, which promote a specific reaction with the target analyte to produce a species to which the electrode responds [62]. Because of their immediate application in clinical tests and ease of preparation, these biosensors have been very popular, with thousands of articles published. Affinity biosensors instead are based on biomolecules able to selectively and reversibly bind specific ligands [63]. In this way, it is possible to monitor and quantify the binding of antibodies to antigens, cell receptors to their ligands, nucleic acid (DNA, RNA) with a complementary sequence and aptamers to

specific proteins. Biosensors based on antibodies and antigens, commonly known as immunosensors, have been the most investigated due their high affinity, versatility and commercial availability of the biological elements. However, the use of antibodies in biosensing has some limitations [64]: antibodies are labile and the identification and selection of rare antibodies is laborious. In order to overcome these limitations, new biorecognition elements are under study, like aptamers [65], which offer new perspectives for the realization of affinity biosensors with higher selectivity, sensitivity and stability.

Both physical and chemical methods have been developed for immobilizing the biological element on the sensor surface. Physical strategies comprise adsorption or entrapment in permeable membranes, while chemical methods rely on the covalent binding or cross-linking of reactive residues present within the biomolecule such as amine, carboxylic, aldheydic or thiolic groups. The immobilization step is a crucial aspect in biosensor development, which must be studied and optimized in order to avoid the denaturation of the receptor, with consequent loss of recognition ability, and to control steric hindrance, thus assuring a good accessibility for the analytes.

Another key aspect is the transduction system. With respect to other transduction systems (optical, piezoelectric, acoustic, gravimetric, magnetic, calorimetric), electrochemical devices are highly sensitive, inexpensive, easy-to-use, portable and compatible with microfabrication technologies [66].

An important class of affinity biosensors are genosensors [67], which employ an oligonucleotide sequence as bio-recognition element. In this case recognition derives from complementary base coupling (hybridization).

In particular, genosensors are analytical devices that result from the integration of a sequence-specific probe, usually a short synthetic DNA oligonucleotide, [67, 68] and a signal transducer. The probe, immobilized onto the transducer surface, acts as the biorecognition molecule and recognizes the target DNA (or RNA), while the transducer is the component that converts the biorecognition event into a measurable signal [66].

1.4.2 Electrochemical genosensors: key aspects

Electrochemical genosensors monitor the reaction among a capture probe with its target nucleic acid [67]. The reaction being monitored electrochemically typically

generates a measurable current (amperometry, voltammetry), a measurable charge accumulation or potential (potentiometry) or alters the conductive properties of the medium between electrodes (conductometry). Use of electrochemical impedance spectroscopy by monitoring both resistance and reactance in the biosensor is also becoming more common.

Amperometry is based on the application of a constant potential promoting a redox reaction, while in voltammetry current is measured upon varying the potential in a proper range. In both techniques the resulting current is proportional to the bulk concentration of electroactive species [69]. Potentiometry measures the accumulation of a charge or a potential at the working electrode (usually known as indicator electrode) compared to the reference electrode when zero or no significant current flows between them. In other words, potentiometry provides information about the ion activity in an electrochemical reaction. Conductometric detection monitors changes in the electrical conductivity of the sample solution, as the composition of the solution changes in the course of the chemical reaction. Electrochemical impedance spectroscopy (EIS), measures the resistive and capacitive properties of electrode materials upon perturbation of a system by a small amplitude sinusoidal ac excitation signal typically of 2–10 mV. The frequency is varied over a wide range to obtain the impedance spectrum. The in-phase and out-of-phase current responses are then determined to obtain the resistive and capacitive components of impedance, respectively. Impedance methods are powerful because they are capable of sampling electron transfer at high frequency and mass transfer at low frequency. Tipically, this technique is used for the direct monitoring of the changes in conductivity or capacitance of an electrode as a result of the immobilization of DNA/RNA duplex, onto the electrode surface. In photoelectrochemical measurements, light is used to excite active species on the electrode and photocurrent is obtained as the detection signal. A photoelectrochemistry-based analytical method, has the advantages of both optical and electrochemical methods. Due to its separate source for excitation and detection, it is potentially very sensitive. As an additional benefit in comparison with all optical detection methods, such as fluorescence that have to use complex and expensive optical imaging devices and sophisticated image recognition software, the low cost inherent to electronic detection makes the photoelectrochemical instrumentation simple and low cost [70, 71]. Despite the advantages mentioned above only rather limited photoelectrochemical biosensors have been reported for nucleic

acid determination in the past decade. The emergence of nanomaterials with enhanced photoelectrochemical properties [72-75] shows great potential in the field of photoelectrochemical biosensors [76-79].

The probe immobilization step plays an important role in determining the overall performance of a genosensor. Both physical and chemical methods have been developed for immobilizing the capture probe on the sensor surface. Physical strategies comprise adsorption or entrapment in permeable membranes, while chemical methods rely on the covalent binding or cross-linking of reactive residues present within the biomolecule such as amine, carboxylic, aldheydic or thiolic groups. The probes have to be immobilized in a way that retains their stability, reactivity, accessibility to target analyte and optimal orientation. Sensor surface coverage by DNA probes is also important in minimizing nonspecific binding.

The nature and the composition of the working electrode surface become important in order to choose the better immobilization procedure for a specific application. The achievement of high sensitivity and selectivity requires maximization of the hybridization efficiency and minimization of non-specific adsorption, respectively. Several kind of electrode surface have been investigated as electrochemical transducers in genosensor development: glassy carbon [80], screen printed carbon [81], screen printed gold [82-84], gold [85], indium tin oxide (ITO) electrodes [86]. Generally, use of disposable electrodes that avoid the regeneration step, appear to be the most promising approach [66]. Depending on the electrode surface, the immobilization of the probe could occur in different ways. One of the most simply method of immobilization on carbon based electrodes is adsorption at controlled potential. The biggest advantage of this method is the possibility to avoid capture probe modifications. A pretreatment of the carbon surface is necessary in order to enhance the immobilization of the probe [87]. However, in this immobilization procedure, washing steps must be performed carefully in order to avoid desorption. Moreover, immobilized DNA probe uses bases to interact with the surface, resulting not totally accessible for hybridization and, consequently, reducing hybridization efficiency. Another probe immobilization method with carbon based electrodes requires the use of N-hydroxysulfosuccinimide with ethyl(dimethylaminopropyl) carbodiimide to activate carboxylate groups on the electrode surface in order to covalently immobilize single-stranded DNA probe [88]. The high stability of covalent

bound allows the regeneration of the probe-modified surface denaturating the hybrid formed for the detection.

The use of gold electrodes for genosensor development is widely used. Self-assembly provide one of the most elegant approaches to obtain well defined and organized surfaces that can be an excellent platform for biosensor applications. One of the widely used approaches in literature involves the direct chemisorption of thiol-modified DNA probes onto gold surfaces. The self-assembly of thiolated molecules was characterised at the beginnings of the 80's [89]. Sulfur based molecules coordinate very strongly onto a variety of metals, but gold is the most favored, because it is reasonably inert. The assumed reaction between a thiolate compound and a gold substrate is:

$$RSH + Au \leftrightarrow RS\text{-}Au + e^- + H^+$$

Chemisorption of thiolated single-stranded DNA probes (HS-ssDNA) onto gold substrates was extensively characterized using X-ray photoelectron spectroscopy (XPS), ellipsometry, ^{32}P-radiolabeling, neutron reflectivity and electrochemical methods [90-92]. The ionic strength of HS-ssDNA solutions was found to have an effect on surface coverage, with chemisorption greatly enhanced at high salt concentrations. The authors hypothesized that intermolecular electrostatic repulsion between neighboring DNA strands was minimized under the high ionic strength conditions, as the charged strands were better electrostatically shielded. More precise control over surface coverage and probe availability was achieved by creating mixed monolayers of the HS-ssDNA and a spacer thiol, like mercaptohexanol (MCH), by a two-step method, where first the gold substrate was exposed to a micromolar solution of HS-ssDNA, followed by exposure to a millimolar solution of MCH. The post-treatment with MCH allow DNA molecules to "stand up" from an initial disordered layer. Thus, the DNA strand is more accessible for specific hybridization.

As the specificity of the hybridization reaction is essentially dependent on the biorecognition properties of the capture oligonucleotide, design of the capture probe is undoubtedly one of the most important pre-analytical step. The probes can be linear oligonucleotides or structured (hairpin) oligonucleotides, which are being used with increasing frequency [93, 94]. Design of linear probes takes great advantage of many commercially available softwares which can design capture oligonucleotides within

the hypervariable or highly conserved regions of different genomes after their assembly and alignment. Candidate sequences, usually 18–22 nucleotides in length, are finally tested for theoretical melting temperature (T_m), hairpins and dimers formation and for homologies using a Basic Local Alignment Search Tool (BLAST) search [93].

The experimental variables affecting the hybridization event at the transducer–solution interface are referred to as stringency and they generally include hybridization and post-hybridization-washing buffers composition and reaction temperature. When dealing with complex sets of probes the basic requirement for a functional system is the ability of all the different probes to hybridize their target sequences with high affinity and specificity under the same stringency conditions.

In addition, a number of probes, variable for chemical composition and conformational arrangement, have been used to assemble genosensors. Peptide Nucleic Acids (PNAs) are DNA mimics in which the nucleobases are attached to a neutral N-(2-aminoethyl)-glycine pseudopeptide backbone. If compared to the conventional oligonucleotide probes, PNAs have appeared particularly interesting for the development of electrochemical genosensing, the main reason being the drastically different electrical characteristics of their molecular backbone. Moreover, some reports described the synthesis and hybridization of a novel nucleotide termed LNA [68, 95]. LNA is a nucleic acid analogue of RNA, in which the furanose ring of the ribose sugar is chemically locked by the introduction of a methylene linkage between 2′-oxygen and 4′-carbon. The covalent bridge effectively ‘locks’ the ribose in the N-type (3-endo) conformation that is dominant in A-form DNA and RNA. This conformation enhances base stacking and phosphate backbone pre-organization and results in improved affinity for complementary DNA or RNA sequences, with each LNA substitution increasing the melting temperatures (T_m) by as much as 3.0–9.6 °C [96]. LNA bases can be interspersed with DNA bases, allowing binding affinity to be tailored for individual applications. Due to the very high affinity of the LNA molecules, it demonstrates that LNA probes hybridize with very high affinity to perfectly complementary targets, and at the same time shows an extraordinary specificity to discriminate the targets that differ by a single-base.

As well as specificity, sensitivity is also a key factor in the performances of a biosensor: sensitive detection of specific DNA/RNA sequence on the basis of the hybridization reaction can be achieved by increasing the immobilization amount and

controlling over the molecular orientation of the probes. At this purpose, nanomaterials have been increasingly introduced in the fabrication of biosensors in order to increase the immobilization amount of the probe and to magnify the detection signal and lower the detection limit [97-100]. Finally, the use of electroactive or enzymatic labels is a strategy widely performed to increase the sensitivity of the device, even if many examples of label free format have been reported.

1.4.3 Impedimetric genosensor

Impedimetric genosensor is a specific sub-class of genosensor that use impedance spectroscopy as transducer. A DNA biosensor based on EIS detection is a device that measures changes in interfacial properties between the electrode surface and the electrolyte solution induced by DNA hybridization, conformational changes, or DNA damages. In most electrochemical DNA biosensors, the target DNA must be labeled for its detection. On the contrary, DNA biosensors based on EIS detection can be label-free. Due to these properties, an impedimetric genosensor hold great promise for applications such as point-of-care diagnostics. As a result, the interfacial impedance, which is obtained upon application of a small AC voltage overlaid on a DC bias potential to the sensing electrode and the AC current obtained in the steady state, has been frequently employed for sensing various analytes [101, 102]. An electrode/electrolyte interface may be simplified by the schematic diagram in figure 1.3.

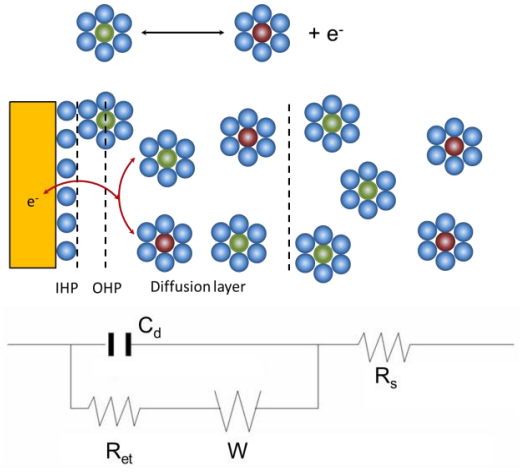

Figure 1.3 - Schematic diagram for an electrode/electrolyte interface in a faradaic sensor and its exemplary model circuit.

When an electrode is perturbated by an applied DC potential, solvated counter ions form an electrical double layer by aligning along the electrode surface, which is represented by the so-called double layer capacitor with a capacitance of C_d. The electron transfer to/from the electroactive species, which may approach the electrode as close as two solvent molecules away in the outer Helmholtz plane (OHP), takes place across the inner Helmholtz plane (IHP) by overcoming the activation barrier, R_p, which is termed a polarization resistance, and the solution resistance, R_s. Once the electron transfer gets started, the Warburg impedance (W) due to the mass transport begins to play a role in determining the electrode kinetics. In the non-faradaic EIS detection with no redox indicator added, the capacitance or the dielectric constant of the probe layer can be utilized as a main sensing signal. The electron transfer resistance (R_{et}), which is the polarization resistance at an equilibrium potential, is utilized as a main indicator in the faradaic EIS detection. A redox couple such as $[Fe(CN)_6]^{3-/4-}$ or $[Ru(NH_3)_6]^{2+/3+}$ is frequently used as a redox indicator for the electrode kinetics at the interface, which is modified by a substrate layer as well as probe and target DNAs on the electrode surface. Thus, the R_{et} values indicate how crowded the electrode surface is when it is modified by a functional molecule, which is capable of selectively capturing a given analyte. The R_{et} values are determined by how selective binding has taken place with the analyte and how much analyte is in the test solution. The changes in resistances or capacitances of the interface are induced by the DNA hybridization events with a single-stranded target DNA on a suitably designed probe platform. To improve the performance of the DNA sensor, the probe layer should be constructed using a well-defined surface chemistry preventing the non-specific binding as well as other side reactions so that it would exhibit high selectivity for a specific target DNA. As a result, various DNA sensors have been embodied on the electrodes modified with the various platforms such as self-assembled monolayers (SAMs), mixed SAMs, conducting polymer films, various nanomaterials such as gold nanoparticles, and peptide nucleic acids. The design of the probe layer depends on whether the sensor is of faradaic or non-faradaic nature. For example, a compact SAM or an insulating layer without a leakage current is needed for non-faradaic signal processing while a less-packed SAM or a conductive layer accessible to the redox species are more desirable for a faradaic sensor. Changes in electrical properties occurring at the DNA probe layer are usually extracted using a best fitting model. Each circuit element obtained by fitting impedance responses to an electrical circuit

can be utilized for analyzing the type and the amount of target DNA as well as its conformational changes [16,17]. In general, the changes in impedances are linearly related to the surface coverage by a target analyte in a low concentration region, but sometimes it is logarithmically related to the amount for the target analyte in the case of high concentration ranges or the heterogeneous binding between the probe and the target molecules. In a faradaic sensor, the charge-transfer resistance, R_{ct}, is associated with the energy barrier for electron transfer to/from the redox indicator approaching to the electrode surface, which is determined by the change in the crowdedness of the probe layer caused by its binding with target DNA. In a non-faradaic sensor, the capacitance of the probe layer is a main indicator exhibiting the conformational changes of double-stranded DNA due to its hybridization.

1.4.4 Electrochemical microRNA detection

Electrochemistry is an emerging technique for miRNA biosensing [58-60]. Electrochemical detection of miRNA was first reported by Gao and Yang in 2006 [103] using electrocatalytic nanoparticle tags (figure 1.4). The assay was based on a direct chemical ligation procedure involving a chemical reaction to tag miRNAs with OsO_2 nanoparticles. The nanoparticles catalyze the oxidation of hydrazine and enhance the detectability of miRNAs, thereby lowering the detection limit to femtomolar level.

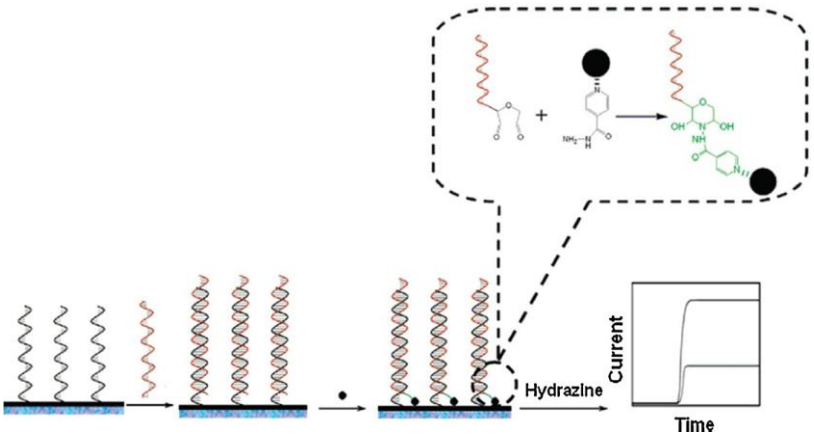

Figure 1.4 - Schematic illustration of miRNA assay using electrocatalytic OsO_2 nanoparticles. Reprinted with permission from [103]

Labeling of miRNAs for electrochemical assay is often necessary for miRNA sensitive detection. Gao and Yu reported a miRNA labeling procedure that utilizes a chemical ligation to directly label miRNA, via a covalent bond, to an isoniazid-substituted osmium complex [104]. In a separate attempt, the same group made use of the $Ru(PD)_2Cl_2$ (PD = 1,10-phenanthroline-5,6-dione) electrocatalytic moiety to monitor the oxidation of hydrazine [105]. Both these biosensors were applied to the quantitation of miRNA in total RNA extracted from HeLa cells.

Recently, it has been reported the use of ruthenium oxide (RuO_2) nanoparticles-initiated polymerization of 3,3'-dimethoxybenzidine and miRNA-templated deposition of an insulating poly(3,3'–dimethoxybenzidine) film [106]. In a separate work, RuO_2 nanoparticles tagged to target miRNA strands served as a catalyst for polymerization of aniline and the hybrid acted as templates for the deposition of polyaniline at the hybridized miRNA strands [107].

A biosensor based on palladium (Pd) nanostructured microelectrodes has been developed [108]. Differential Pulse Voltammetry (DPV) was used to monitor the electrochemical reduction current of Ru^{3+} accumulated on the electrode surface after hybridization with the target miRNA. The signals observed with this reporter system (Ru^{3+}) are amplified by the inclusion of ferricyanide, which can regenerate Ru^{3+} chemically after its electrochemical reduction. After a 30 min hybridization, the detection of 10 aM of target was reported and the RNA extracted in a panel of RNA samples tested.

Enzymes have been used as label in many biosensor formats. The use of such a label greatly amplify the hybridization signals, offering considerable promise for ultrasensitive electrochemical detection of DNA hybridization. An esterase as amplifier in a gap-hybridization assay format was used [109]. Another strategy for miRNA detection is through the use of an electrochemically activated glucose oxidase (GOx) tag/amplifer [110, 111]. A miRNA biosensor based on triple-signal amplification due to the immobilized graphene and dendritic gold nanostructure and subsequent monitoring of the reduction current as a result of the oxidation of hydroquinone by H_2O_2 and horseradish peroxidase was also reported[112].

A horseradish peroxidase (HRP)-modified LNA hairpin probe was used by Zhou's group in order to detect miRNA 21 [113]. The LNA incorporated hairpin probe was modified with biotin at its 5′-end and –SH at its 3′-end. After the probe hybridized with target miRNA-21, its loop-and-stem structure was unfolded to force the biotin

away from the electrode surface. Through the specific interaction between biotin and streptavidin-HRP, target can be quantified by electrochemical detection of the enzymatic product of benzoquinone in the presence of H_2O_2 and hydroquinone. Liu's group designed an enzyme-labelled amperometric genosensor based on streptavidin conjugated alkaline phosphatase (SA-ALP) [114]. The analytical procedure consisted of 6 steps: (a) immobilization of 3' thiolated DNA probe; (b) miRNAs were then captured forming an hybrid; (c) cis-diol group of ribose sugar at the end of the miRNAs chain allowed 3-aminophenylboronic acid (APBA)/biotin-modified multifunctional AuNPs (APBA–biotin–AuNPs) to be attached through the formation of a boronate ester covalent bond; (d) biotin in AuNPs facilitated the capture of SA–ALP via the biotin–streptavidin interaction; (e) addition of the 4-aminophenylphosphate (p-APP) substrate in presence of the enzyme produce the conversion from p-APP to p-aminophenol (p-AP) occurred. The resulting p-AP could be cycled by a chemical reducing reagent after its electro-oxidization on the electrode (known as p-AP redox cycling), thus enabling an increase in the anodic current, obtaining a detection limit of 3 fM (figure 1.5).

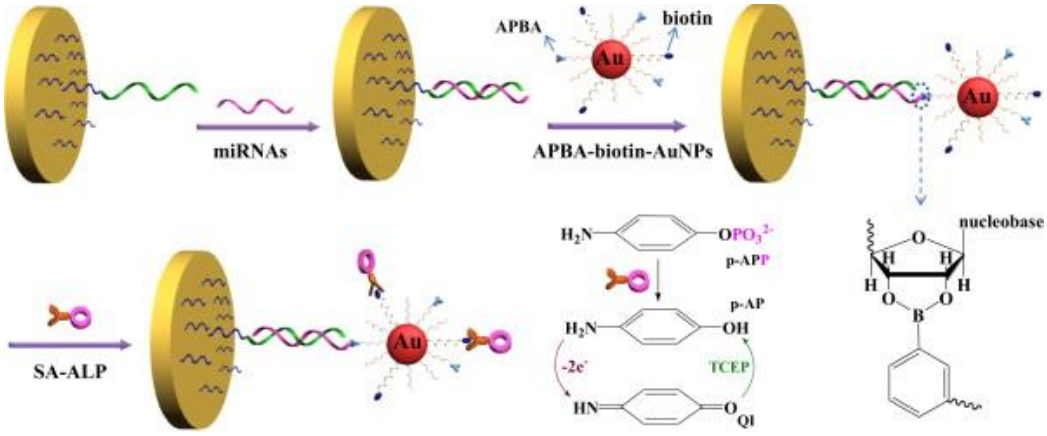

Figure 1.5 - Schematic representation of the label-free detection of miRNAs based on the triple signal amplification of APBA–biotin–AuNPs, SA–ALP and the p-AP redox-cycling reaction. Reprinted with permission from [114].

Bettazzi et al. were the first to report an electrochemical method based on paramagnetic beads and alkaline phosphatase amplification for miRNA detection [81]. Label free-detection schemes have been also reported. Such direct detection can be accomplished by monitoring the changes in some electrical parameter generated by the

hybridization event. This approach greatly simplify the sensing protocol, as they eliminate the use of indicators and labeling reaction in the real samples. Moreover, the assay safety is improved, since the indicators are usually toxic or carcinogenic compounds. The first indicator-free scheme in genosensors was described and consisted on the recognition of the hybridization event through the decrease of the guanine peak (that occur around 1.0 V vs SCE) of the immobilized probe [115]. However, this procedure is not applicable in most cases (e.g. for guanine containing targets). This limitation has been overcome by developing a new approach, based on the use of inosine-modified (guanine-free) probes [116, 117]. The inosine still forms a specific base-pair with the cytosine residue [118], but its oxidation signal is well separated from that of guanine. This approach was also used for miRNA detection [119]. A flat baseline (around +1.0 V) for the probe-modified electrode was observed. The hybrid formation was thus detected through the appearance of the guanine oxidation peak of the target sequence in differential pulse voltammetry. Detection limit of 1.4 μM of oligonucleotide target sequence were reported for an indicator-free hybridization biosensor based on magnetic beads coated with streptavidin and screen printed carbon electrode as transducer surface.

A different label-free approach, based on hybridized miRNA-templated deposition of an insulating polymer film and electrochemical impedance spectroscopic detection, was reported [120]. The biosensor described in this work was based on an indium tin oxide (ITO)-coated glass slide modified with a DNA morpholino capture probe. After hybridization, the neutral surface of the biosensor is converted to anionic by the hybridized miRNA strands. The deposition of the insulating polymer film, poly(3,3′-dimethoxybenzidine) (PDB), is then carried out by the horseradish peroxidase (HRP) catalyzed polymerization of 3,3′-dimethoxybenzidine (DB) in the presence of H_2O_2. Electron transfer resistance in presence of a $Fe(CN)_6^{4-}/Fe(CN)_6^{3-}$ equimolar solution increased with the miRNA concentration and used as analytical signal. This occurs because of negative hybrid nature that interact with DB producing a high density of monomer on the biosensor surface and, consequently, this facilitates DB polymerization and the deposition of PDB in the presence of HRP and H_2O_2. A detection limit of 2.0 fM was reported. In 2007, Fan and colleagues introduced a strategy for sensitive and label-free detection of miRNA based on conducting polymer nanowires [121]. In 2009 a miRNA biosensor based on PNA capture probes immobilized on silicon nanowire was proposed [122]. Resistance change measured

before and after hybridization correlates directly to concentration of the hybridized target miRNA. A detection limit of 1 fM was obtained.

In addition to the common hybridization-based strategies employed to detect and quantify miRNAs, several peculiar approaches have also been reported in the literature. Recently a three-mode electrochemical biosensor which exploited the strong and non- sequence specific binding of a p19 fused dimer protein to double-stranded miRNAs was proposed incorporating three modalities based on hybridization, p19 protein binding, and protein displacement [123]. Recently, an amperometric magnetobiosensors again involving protein p19 as a selective biorecognition element was reported [124, 125]. This p19-based magneto-sensors were able to detect 0.04 nm of a synthetic target and endogenous miR-21 (selected as a model for its role in a wide variety of cancers) in total RNA extracted from cancer cells and human breast-tumor specimens without PCR amplification and sample preprocessing.

1.5 Nanostructures and nanoarchitectures

Nanomaterials have dimension in the 1-100 nm range and can be obtained by different methods as illustrated in the next paragraphs. A wide variety of nanostructures have been reported in the literature for interesting analytical applications. Among them organic and inorganic nanotubes, nanoparticles and metal oxide nanowires have provided promising building blocks for the realization of nano-scale electrochemical biosensors due to their biocompatibility and technologically important combination of properties such as high surface area, good electrical properties and chemical stability. Moreover, the integration of nanomaterials in electrochemical devices offers the possibility of realizing portable, easy-to-use and inexpensive sensors, due to the ease of miniaturization of both the material and the transduction system. Nanowires, carbon nanotubes, nanoparticles and nanorods are merely some of the myriad objects that are emerging as candidates to become crucial elements of future biosensors [126, 127]. Over the last decade, this field has been widely investigated and a huge number of papers have been published. Many progress have been reported in the integration of nanomaterials such as nano vesicles, nanoparticles and polymer nanostructures, in electrochemical biosensing systems. In this thesis two different types of nanomaterials have been investigate for genosensor developing as described in the following paragraphs.

1.5.1 Liposomes

Liposomes are artificial spherical vesicles, which membranes contain one or more phospholipid bilayers. The lipid molecules consist of hydrophilic head groups and hydrophobic tails; in aqueous solutions they self-organize in order to increase their solubility in the surrounding medium and minimize the surface-to-volume ratio. In the final structure, they consist of a series of concentric bilayers of lipids with aqueous compartments within which soluble substances can be entrapped. Liposomes were discovered by Bangham et al. [128] and were initially used as drug carriers by Gregoriadis [129]. The name liposome is derived from two ancient greek words Lypos (fat) and Soma (body). Liposomes can be formed as uni-lamellar vesicles (ULV) or multi-lamellar vesicles (MLV) in different sizes that range from nanometers to micrometers [130]. Because of the similar structure and composition of cell membrane, one of the advantages in the use of liposome is the possibility to simulate and investigate cell phenomenon. They could be synthetized with a biological recognition element or label on the surface, or with various signal markers encapsulated on the inside cavity. The simplicity to conjugate the bilayer lipid with a variety of biorecognition elements ensures that liposomes are able to recognize various analytes for transduction of the signal: nucleic acids, antigen, enzyme, protein, biotin, etc. Another potential for liposomes is the simplicity to encapsulate different signaling molecules for biosensor development: colorimetric, fluorescent, chemiluminescent, electrochemical, etc. Phospholipids, that represent the main component of liposome, possess different advantages like relatively low cost, biocompatibility and lack of toxicity that make liposomes, with all the characteristics already mentioned, as versatile candidate for biosensor development. To the best of my knowledge, no work in literature report the use of liposomes in microRNA detection. Willner group developed a liposome-based electrochemical genosensor for detection of model nucleic acid sequence for the Tay-Sachs genetic disorder [131]. In particular, they synthetized HRP-tagged biotinylated liposome to bind directly to a biotinylated hybrid immobilized on a gold electrode through an avidin molecule. HRPs on liposomes were used to catalyze 4-chloronaphthol in the presence of H_2O_2 to form the insoluble product, which deposited on the gold electrode increasing the impedance signal. Sensitivity reported corresponds to 0.65 pM. Starting from this work, in this thesis

have been developed two different genosensors based on biotin-tagged liposomes coupled with an enzymatic detection scheme.

1.5.2 Nanoparticles

Nanoparticles (NPs) have been employed in an enormous variety of bioanalytical formats; in the last decade many papers have been published in the main international scientific journals, illustrating the versatile range of application of nanoparticles as quantification tags, immobilization substrates, signal amplifier and as carriers. This section will present only a brief overview of the fundamental characteristics which have made nanoparticles so interesting for biological sensing, with some examples in gold nanorods (AuNRs) such as electrodeposited gold. Depending on their composition (metal, semiconductor, magnetic), nano-size particles exemplify different functions in electroanayltical applications. Metal nanoparticles provide three main functions: enhancement of electrical contact between biomolecules and electrode surface, catalytic effects and, together with semiconductor ones, labelling and signal amplification [132]. They are typically obtained by chemical reduction of corresponding transition metal salts in the presence of a stabilizer, which give the surface stability and proper functionalization, in order to modulate charge and solubility properties [133]. Among metal nanoparticles, the most widely used have been gold nanoparticles (Au-NPs) because of their unique biocompatibility, structural, electronic and catalytic properties. The first scientific literature evidence of Au-NPs was reported by Michael Faraday in the middle of 19^{th} century [134]. The highly favorable properties, including the large surface to volume ratio, unique optical and electronic properties, and easy surface modification, have brought intensive focus on Au-NPs from both research and industry. The morphology, solubility, surface functionality and stability of Au-NPs can be controlled via different synthetic routes, such as Turkevich method [135] and Brust method [136]. An important use of nanoparticles in biosensing is their employment as platforms for the immobilization of biological elements. Their large surface area greatly increases biomolecule loading. Due to the ease of functionalization with thiol groups, gold nanoparticles have also been widely employed in this field.

Nanorods (NRs) represent one of the possible one dimensional nanoparticles. The optical properties, hydrodynamic behavior as well as phase behavior of Au-NRs,

unlike spheric nanoparticles, are influenced by their shape anisotropy [137]. A typical adsorption profile of these materials is reported in figure 1.6. It is possible to distinguish two absorption bands: one due to light absorbed along the short axis and the other due to absorption along the long axis.

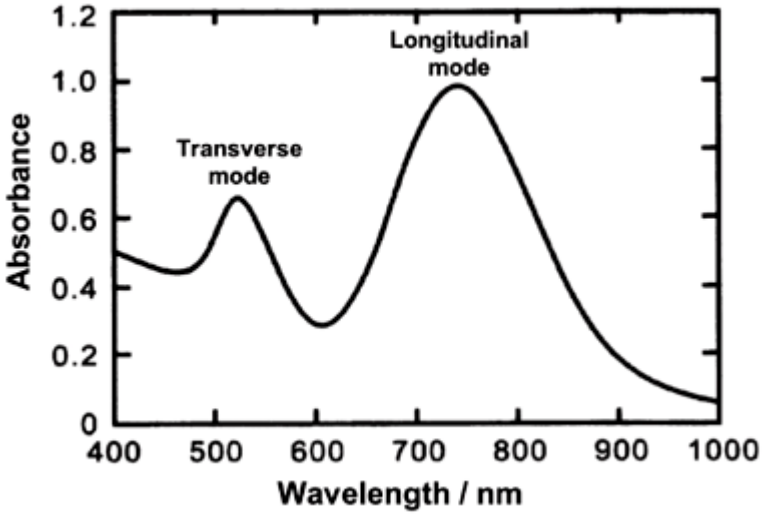

Figure 1.6 – Typical extinction spectra of Au-NRs from [138]

As the rod length increases, so does the longitudinal band red shift together with an increase in the extinction coefficient. As a result of this optical control and sensitivity to changes in local environment, gold nanorods are useful materials for sensing, photothermal therapy, and imaging [139].

There are three main methods for Au-NRs synthesis: a template method, an electrochemical method, and a seeded growth method. Chemical methods are characterized by reduction of an aqueous solution of chloroauric acid where reduced gold atoms initially can form a sub-nanometer cluster particle in the first nucleation stage, leading to growth. Particle aggregation is prevented through vigorous stirring and by adding appropriate stabilizing agents [137]. Template method was introduced by Martin in 1994 [140]. This method is based on the electrochemical deposition of gold within the pores of nanoporous polycarbonate or alumina template membranes. The diameter of the nanorod is determined by the pore diameter of the membrane, while the length can be controlled through the amount of gold deposited within the pores of the membrane. The electrochemical process for gold nanorods production was introduced by Wang´s group [141]. The synthesis is conducted with a two electrodes electrochemical cell: a gold plate as a sacrificial anode while the cathode is

platinum plate, both immersed in an electrolytic solution containing a cationic surfactant such as, hexadecyltrimethylammonium bromide (CTAB). The anode is initially consumed forming $AuBr_4^-$. These anions are complexed to cationic surfactants and migrate to the cathode where reduction occurs. An important factor for controlling the dimensions of gold nanorods is the presence of a silver plate inside the electrolytic solution. The redox reaction between gold ions generated from the anode and the silver metal leads to the formation of silver ions. The concentration of silver ions and their release rate determined the length of the nanorods.

The next advance was to replace the gold electrode as the source of gold and move to a chemical source, chloroauric acid [142]. Electrochemical reduction was replaced with chemical reduction using a weak reducing agent (ascorbic acid) and silver nitrate in presence of CTAB used during the synthesis as surfactant, although hexane and acetone were still added. The ascorbic acid is unable to reduce gold to the metallic state under the high CTAB concentration, but limit the reduction to Au(I) [143]. However, addition of small seed particles of about 3 nm in diameter into the Au(I) solution resulted in complete reduction to metallic gold, which is catalyzed by the surface of the seeds and leads to the gradual change in shape from quasi-spherical to rod-like crystal. It was determined that addition of less seed generally led to higher aspect ratio rods. However, the shape-yield of nanorods was still relatively low and a large amount of spheroidal shapes was present. Jana's group concluded that the formation of anisotropic nanoparticles was dependent on both, the nucleation rate as well as surfactant concentration, and also that their method is suitable for gram-scale synthesis of gold nanorods. Significant improvement of this method was achieved by El-Sayed [144] that introduced a modified seed-mediated method by using a cosurfactant mixture of CTAB and benzyldimethyl hexadecyllammonium chloride (BDAC), and concluded that the use of binary surfactant results in nanorods of fairly good uniformity, higher yield, and yet fewer byproducts. Another recent strategy in order to obtain Au-NRs with controlled aspect ratio in the presence of silver ions with a photochemical reduction was proposed by Kim and coworkers [145]. The synthesis allow the photoreduction of Au(III) to Au(0) starting from a gold chloride solution within a mixed CTAB and tetradodecylammonium bromide surfactant system with silver nitrate, acetone, and hexane additives. This solution is irradiated with a 254 nm UV light for more than 24 hours. A good yield of rods of different aspect ratio can be obtained by changing the silver concentration. It is possible to shorten the necessary

reaction time to less than 30 minutes by combining the chemical and photochemical techniques as proposed by Niidome and coworkers [146]. The method has the advantages of the photo-reduction and chemical reduction methods, making the process easier in a short time.

An electrochemical genosensor based on gold nanorods decorated graphene oxide sheets has been developed by Han et al. [147] obtaining a 3.5 fM of detection limit. In Congur et al. [148] is shown the increasing in sensitivity of a genosensor using a disposable graphite electrode modified with Au-NRs.

Despite chemical synthesis of Au-NPs is widely studied, with his own advantages and disadvantages, an interesting method for electrode modification with gold in order to obtain an immobilization route for DNA sensing is represented by electrodeposition starting from an Au(III) salt. Au-NPs modified electrodes can be prepared by potential-step or pulse-potential electrodeposition and the control of particle density and size distribution could achieved by adjusting the electrodeposition parameters [149]. Electrodeposition is a short version of electrolytic deposition. In this process an electrical current reduces cations of a desired material from a solution and deposes that material as a thin film onto a conductive substrate surface. Figure 1.7 shows a simple electrodeposition system for the deposition of metal from its salt solution.

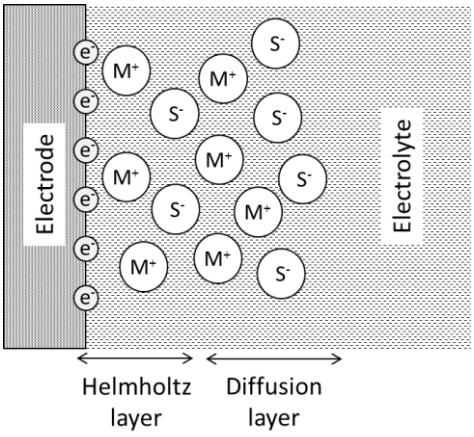

Figure 1.7 – Electrolysis scheme involved in electrodeposition

The electrolytic solution contains positively charged metal ions (cations) and anions. Under the applied external electric field, the cations migrate to the electrode where they are discharged and deposited as metallic particle.

$$M^+ + e^- \rightarrow M$$

Under the influence of an applied potential, rearrangement of ions near the electrode surface results in an electrical double layer called the Helmholtz double layer, followed by the formation of a diffusion layer as shown in figure 6. These two layers are referred as the Gouy-Chapman layer. The process is as follows:

- migration: the hydrated metal ions in the solution migrate towards the cathode under the influence of impressed current as well as by diffusion and convection;
- electron transfer: at the cathode surface, a hydrated metal ion enters the diffused double layer where the water molecules of the hydrated ion are aligned. Then the metal ion enters the Helmholtz double layer where it is deprived of its hydrate envelope. The dehydrated ion is neutralized and adsorbed on the cathode suface;
- the adsorbed atom then migrates or diffuses to the growth point on the cathode surface.

Thickness of the electrodeposited layer on the substrate is determined by the time duration of the process. In other words, the longer the time the object remains in the operating electrodeposition bath, the thicker the resulting electroplated layer will be. The key to electrodeposition of nanoparticles with controlled shape and size is the knowledge of the kinetics and mechanism of initial electrocrystallization stages in the particular electrochemical system. Electrodeposition of isolated metal nanoparticles can be achieved successfully in systems with weak metal–substrate interaction. No underpotential deposition (UPD) takes place in such systems and the electrocrystallization process starts in the overpotential deposition (OPD) range with the formation and growth of 3D metal nanoparticles (3D Me island formation) on an unmodified foreign substrate (Volmer–Weber growth mechanism) [150].

Several groups have used as electrolytes for electrodeposition of Au-NPs $AuCl_4^-$ salts in $HClO_4$ or H_2SO_4 aqueous solutions and investigated the influence of deposition conditions on the size, structure, morphology and electrochemical properties of electrodeposited nanoparticles [151-154]. Komsiyska and Staikov reported a study of the kinetics and mechanism of electrodeposition of Au-NPs using glassy carbon electrodes with 1mM $AuCl_4^-$ in 0.1M $HClO_4$ by means of cyclic voltammetry, chronoamperometry and scanning electron microscopy [155]. They demonstrate that gold electrodeposition follows the theoretical model for nucleation and 3D growth controlled by hemispherical diffusion. The potential dependences of the nucleation rate and the size of critical nuclei were determined from the analysis of initial parts of current transients at relatively positive electrode potentials. In order to study the

electrochemical behavior of $AuCl_4^-$ ions with glassy carbon electrode, O'Mullane and coworkers reported a cyclic voltammetry investigation [156]. The cyclic voltammogram shown in figure 1.8 illustrates the electrochemical process expressed by this reaction:

$$AuCl_4^- + 3e^- \rightarrow Au + 4Cl^- \quad (*)$$

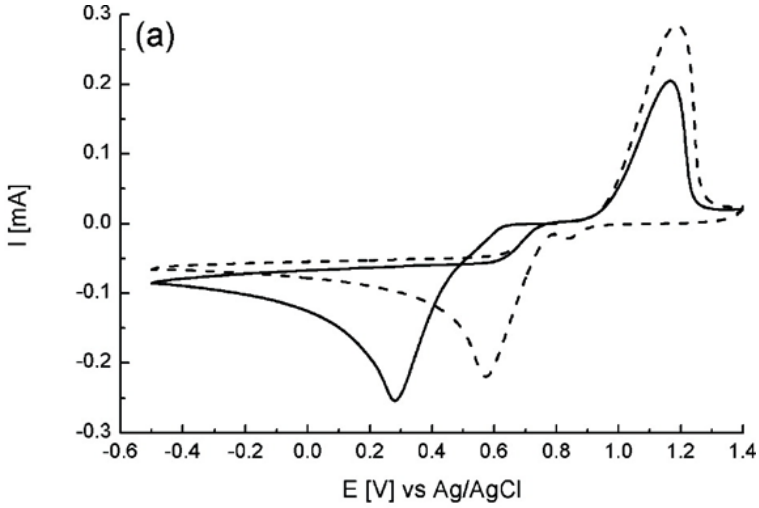

Figure 1.8 - Cyclic voltammograms obtained at a GC electrode at a sweep rate of 100 mV/s initiated at 0.70 V vs Ag/AgCl in the negative direction in 6.9 mM $HAuCl_4$. The second negative sweep is indicated as a dashed line. Reprinted with permission from ref [156].

On the chatodic sweep, a peak is observed at +0.28 V (vs. Ag/AgCl) corresponding to the reduction of $AuCl_4^-$ to metallic gold as outlined in equation (*). On the reverse sweep, a current crossover is observed at +0.49 V (vs. Ag/AgCl) which is indicative of nucleation growth kinetics as reported by [157] and [158]. This is followed by a large anodic peak due to electrodissolution of adsorbed Au(0) in chloride media generated through the reduction of the $AuCl_4^-$ salt in the first sweep and the formation of an oxide layer on the electrodeposited gold. On the second sweep, the cathodic peak observed at +0.28 V (vs. Ag/AgCl) shift to positive potential due to nucleation sites created on the first sweep. In other words, the higher potential required for gold reduction indicates that the deposition of gold on gold is easier than the nucleation of gold on GC.

An example in miRNA detection using elctrodeposited gold is reported in [100]. Developed genosensor is based on luminol anodic electrochemiluminescence (ECL) for the detection of microRNA-155 using H_2O_2 as a co-reactant and hemin as a catalyzer for signal amplification. The bare glassy carbon electrode (GCE) was first electrodeposited with AuNPs. The proposed biosensor showed a wide linear range from 5 fM to 50 pM with a relatively low detection limit of 1.67 fM for microRNA-155 detection.

In this thesis, gold was electrodeposited on graphite surface of a disposable screen printed carbon electrode and used as surface for immobilization of a thiolated DNA capture probe for the development of a genosensor for miRNA recognition with an enzymatic detection scheme.

1.5.3 Conductive polymer films

Another class of nanomaterials, which in the last few years has found a greatly increasing number of applications, is constituted by conductive polymer nanostructures. Conducting polymers are materials that can be employed as receptors as well as transducers or immobilization matrix in electrochemical biosensing. Before 1970, conventional polymers such as plastics, were considered dielectrics or insulators due to their significant resistance to electrical conduction. The discover by Alan J. Heeger, Alan G. MacDiarmid and Hideki Shirakawa of conductive polymers, culminated in 2000 with a Nobel Prize in Chemistry, gives new perspectives in the field of electronics and sensing [159, 160]. Conductive polymers are characterized by an extended π-conjugation along the polymer backbone which promotes an intrinsic conductivity. This conductivity is due to the formation of charge carriers upon oxidizing (p-doping) or reducing (n-doping) their conjugated backbone, because in neutral (uncharged) state they present no conductivity. They have the electrical properties like that of metals but with the characteristics of organic polymers such as light weight, resistance to corrosion, flexibility, lower cost and the added advantage that they can be simply modified in order to obtain the better structure or propriety for a specific application [161, 162]. Regarding sensing, conductive polymers assume further appealing properties: ease of preparation by chemical or electrochemical methods, sensitivity towards a wide range of analytes, great signal amplification due to their electrical conductivity and fast electron transfer rate. One of the widely used

method to synthetize polymers is the electropolymerization method. It consists in an electrochemical oxidation of opportune monomer, that is usually soluble only in organic media. Most of the polymer obtained through this method have alternative chemical synthesis, preferably by oxidation in organic media. However, chemical synthesis has the disadvantage that requires chemical oxidation that could result in pollution of the polymer product. Moreover, there is the problem to introduce the low-soluble polymerization product on the sensor layer. Instead, the use of electrolysis provides the formation of the polymer directly on the surface of the working electrode. One of the most useful advantages using electropolymerization for is represented by the possibility to introduce functional groups on the polymer film modifying the monomer with that group, or using copolymerization with different monomer units.

Regarding the development of genosensors, electropolymerization is surely an interesting technique, in order to covalently bind the capture probe to the electrode surface and to ensure a specific conductivity .

Generally, electropolymerization is initiated by the anodic oxidation of unsaturated monomer units followed by coupling cation radicals usually with the removal of the hydrogen ion. If the intermediate products are stable enough, the propagation stage can continue to form oligomeric and polymeric products with no additional electrochemical stimuli similarly to the ion-radical polymerization initiated by chemical oxidants. However, usually is preferable that the electrochemical stimuli continue until the end of the process, because of the low coupling efficiency of the neutral monomer. The propagation stage involves the formation of the cation radicals of intermediate products (dimers/oligomers) of the previous stages in which the electrochemical activity is similar to that of monomer. The so called termination stage can include a deeper oxidation of the intermediates, the formation of stable radicals and the reactions with molecular oxygen or nucleophilic substance present in solution (figure 1.9).

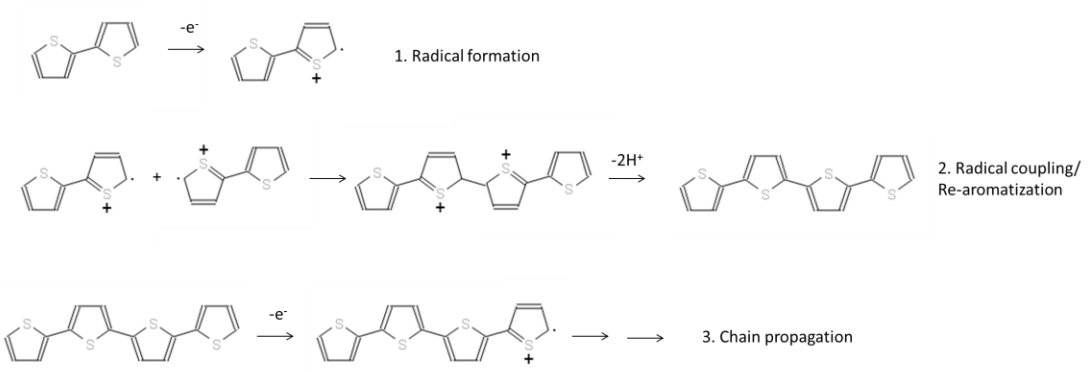

Figure 1.9 – Electropolymerization scheme for bithiophene monomer.

If the products of polymerization are electrochemically inactive and insoluble they precipitate on the electrode surface and hence suppress the electron transfer due to the electric insulation of the interface. In general, three types of electropolymerization products are used in the DNA sensor assembly:

- electroconductive polymers that exhibit semi-conductors behavior and participate in the effective electron transduction between the mediators or redox centers of biomolecules and electrodes. Three polymers are mostly investigated as DNA supports and components of the signal transduction systems of biosensors, i.e., polyaniline, polypyrrole and polythiophene [163-165];
- electrochemically active but non-conductive polymers which can mediate electron exchange only in a very narrow potential window near their standard redox potential and are quite effective as mediators. Polycyclic heteroaromatic systems obtained from phenazines, phenoxazines and phenothiazines belong to this group of polymers. Many of them are known under different names as dyes or redox indicators like Methylene Blue [166] based genosensor;
- non-conductive polymers that do not support electron transduction. Their use in the DNA sensor assembly is aimed at the mechanical protection of the biorecognition layer or the mechanical support for the immobilization of the DNA probes or mediators. They could be obtained by overoxidation of electroconductive materials like polypyrrole [167] or polyaniline [168].

There are two main strategies for the deposition of DNA on the electropolymerized surface.. The first one is performed in a polar organic solvent where the electrode is firstly modified and then transferred in an aqueous media in order to be covered with

the layer of a DNA probe and finally transferred into the aqueous media to record voltammograms and measure target analytes specifically bonded to DNA onto the electrode surface. The second approach involves electropolymerization in the aqueous solution of a monomer, in some cases containing the DNA oligonucleotides so that the immobilization can be performed simultaneously with the polymerization. The first strategy allows using monomers insoluble in water and results in formation of more dense and compact films with lesser permeability for ionic substances in comparison with the products of electropolymerization in aqueous media. Aqueous polymerization is more preferable for genosensor development due to its simpler realization and a better compatibility of the product with biopolymers bearing a sufficient amount of water and metal ions stabilizing the steric structure of the molecules and counterbalancing the negative charge of the phosphate skeleton of DNA and oligonucleotides. In this paragraph thiophene based polymer, which was one of the polymer investigated in this thesis, will be described.

Electropolymerization of thiophene usually occurs in organic medium. Electropolymerization in aqueous solutions is much more problematic than that of pyrrole and aniline. This is due to several reasons: (i) the solubility of thiophene in water is much smaller than that of pyrrole and aniline, (ii) the potential oxidation of thiophene is higher than that of both monomers (pyrrole and aniline) and of water and (iii) the thienyl cation radicals are more reactive with nucleophilic solvents than pyrrole and aniline cation-radicals [169]. Because of these features, the electropolymerization of thiophene and its derivatives is carried out generally in dry organic solvents [170, 171]. As mentioned before, the use of water medium is always preferable for biosensor development. Besides, it has been found that thiophene and its derivatives can also be electropolymerized in acid solutions [172], and polythiophene films have properties and structures similar to those formed in organic media. In order to increase the solubility of the monomer in aqueous medium, a small amount of organic solvents like methanol, ethanol and acetonitrile could be used. Although the importance of polypyrrole in electroanalysis, polythiophenes could be considered the conductive polymers preferred nowadays for electrode systems devoted to genosensing due to their intrinsic variety of possible functionalization of the thiophene monomer ring. This aspect can be exploited to impart specific physical properties to the electrode, such as conductivity and stability, or to give peculiar chemical characteristics in order to increase the specific affinity or reactivity towards a certain

analyte or molecule. Many different polythiophene derivatives have been proposed in electroanalysis. 2,2′-Bithiophene is widely used due to the very high potentials required to oxidize the unsubstituted thiophene, which may concurrently induce overoxidation of the polymer chains formed. Overoxidation implies the formation of chemical functionalities on the thiophene ring that either lower or interrupt the conjugation of the π electron system: an irreversible dramatic decrease of the conductivity of the polymer may occur. Chemical or electrochemical oxidative methods can be used to synthesize polythiophenes. Developing an electrochemical platform, it is evident that the electrochemical oxidation at a conductive support is the most spontaneous and most effective way to conduct the synthesis and the realization of polymer film. Many experimental factors chosen for the polymer electrogeneration affect not only the structural and morphological characteristics of the film produced, but also its chemical characteristics. In example, the polymerization is dependent by the concentration of the monomer, the nature of the solvent and the supporting electrolyte. Another important factor that influences the film characteristics is the electrochemical procedure chosen for the synthesis and coating, varying from potentiodynamic to potentiostatic and galvanostatic procedures. Anyway, in each procedure, it is important to avoid the potential values at which overoxidation of the deposited polymer occurs. In order to confirm the coating of the polymer on the electrode surface, some information concerning the resulting polythiophene coating can be obtained by combining electrochemical measurements with different techniques, like atomic force spectroscopy [173].

Recently, Kutner's group developed a genosensor based on a thiophene derivative biotinylated monomer [173]. Similar works based on polymer film bearing biotin on its backbone were reported for thiophene and pyrrole monomers, however pyrrole-based monomers are stable only in their doped state [174] and synthetic route of preparation of a monomer for thiophene based polymer was much more complicated and tedious if compared with the synthetic approach proposed by Kuter's group. The biotin-avidin binding is widely used in biosensor development. The reason is in the very high stability constant of the resulting complex (10^{15} M^{-1}) [175], making this non-covalent bind really strong. This high stability allows easy formation of stable assemblies of streptavidin or biotin conjugated substances. This approach was used, in this thesis, for miRNA detection in order to increase sensitivities and the possibility to obtain simple and portable and label free system.

1.6 Photoelectrochemical transducers

Recently, with the emergence of novel photo-electrochemically active species and new detection schemes, photoelectrochemistry has received increasing attention in the field of biosensors. In classical photoelectrochemical measurements, irradiation of an electrode with light that is absorbed by the electrode material causes the production of a current (a photocurrent). This photocurrent is dependent on the wavelength, electrode potential and solution composition. Since most of photoelectrochemical measurements occur at semiconductor electrodes, briefly the nature of semiconductor materials and their interfaces with solution will be described in the following paragraph. Indeed, photoeffects are also observed at metal electrodes [176], although the resulting photocurrent are much smaller. Furthermore, photoelectrochemical active species can be coupled to semiconductor or metallic electrodes to perform photoelectrochemical measurements. These photoelectrochemically active species act as the light-absorbing species. If injection of a photogenerated charge carrier into the electrolyte or electrode competes effectively with relaxation of the excited state of the species, a photocurrent might be observed. Some examples of these photoactive species are here reported. Finally, some examples of detection scheme are also shown.

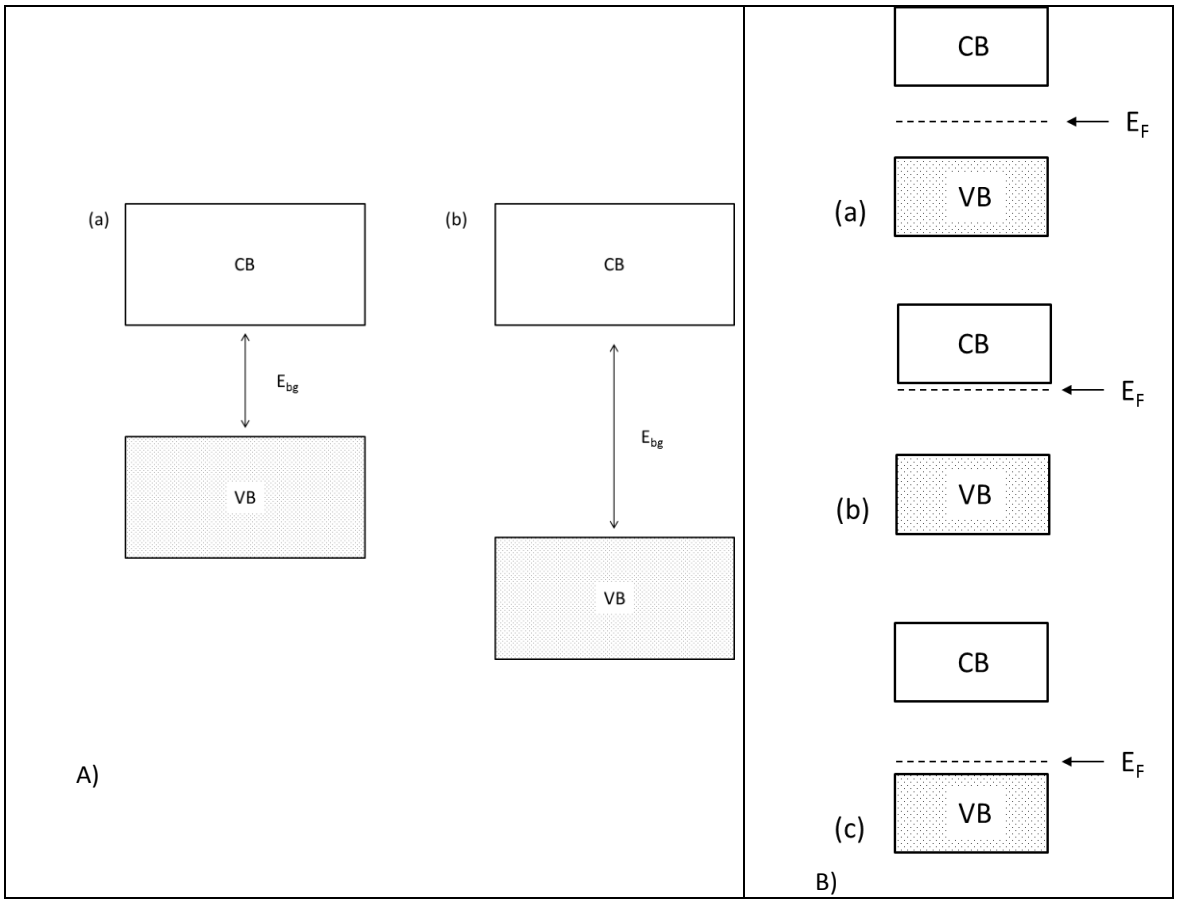

Figure 1.10 – A) Relative disposition of the CB and VB for a semiconductor (a) and an insulator (b). E_{bg} is the band gap energy. B) Relative disposition of the Fermi level (E_F) for an intrinsic semiconductor (n=p) (a), for an n-type semiconductor (b), and a p-type semiconductor (c)

.

The behavior of semiconductor materials in presence of light absorption can be described in term of the semiconductor energy band model. Of particular interest are the highest occupied (valence band, VB) and the lower empty (conduction band, CB) energy bands: if these two bands are well separated by a bandgap then the solid is a semiconductor or an insulator (figure 1.10A); if these two bands overlap then the solid is a conductor. An extremely important parameter is the bandgap energy defined as the energy unity separation between valence and conduction bands (E_{bg}, expressed in eV) [177]. Solids with E_{bg} lower than 3 eV are semiconductors and solid with bandgap larger than 3 eV are considered insulators [178]. In example, α-tin has a E_{bg} of 0.09 eV [177] and it is considered a metal; silica has a E_{bg} of 1.12 eV [179] and it is considered a semiconductor; carbon diamond has a E_{bg} of 5.48 eV [179] and it is considered an insulator. An important concept in the description of semiconductor electrodes is that of Fermi level (E_F), which

is defined as the energy for which the probability of electron occupancy is 50% (where it is equally probable that the level is occupied or vacant) [176].

Semiconductors can be made conductive by insertion of extra electrons in the free or partial free conduction band, or by removing electrons from the valance band. This could be generated in three different ways: thermal excitation, doping and photo-excitation. In general, the thermal excitation of an electron from VB to CB produces a free electron in the CB and a vacancy or hole in the VB. A material is called intrinsic semiconductor when the charge carriers, electrons and holes, exist in a dynamic equilibrium. Thermal excitation is important only for semiconductors with a E_{bg} lower than 0.5 eV [177]; doping is a process that introduce new energy levels into the bandgap by a partial reduction of the metal oxide, by adding impurity or, in general, by varying the stoichiometry. In these materials, E_F shifts closer to the band edges. In particular, when E_F shifts close to the VB, the semiconductor is termed p-type; instead, when E_F shifts close to the CB, the semiconductor is termed n-type (figure 1.10B). An electron could be also promoted from the valance to the conduction band with the absorption of light. The optical band gap of the semiconductor is an important parameter in defining its light absorption behavior. In this quantized process, an electron-hole pair is generated in the semiconductor when a photon of energy hν (ν = frequency, h = Planck constant, with hν > E_{bg}) is absorbed. Optical excitation thus results in a delocalized electron in the CB, leaving behind a delocalized hole in the VB; this is the band-to-band transition [180]. A plot of photocurrent versus the wavelength of irradiating light can be employed to determine E_{bg}.

When a semiconductor is immersed in a redox electrolyte solution, the E_F could be identified as the electrochemical potential of the electron ($\bar{\mu}_e$). If electrostatic equilibrium is attained, $\bar{\mu}_e$ in both phases (solid-liquid) must become equal, or equivalently E_F must become equal, and this can occur by a charge transfer between the phases. Indeed, when a semiconductor is immersed in solution, the electrochemical potential (Fermi level) is disparate across the interface. Equilibration of this interface thus necessitates the flow of charge from one phase to the other and a ‘‘band bending’’ ensues within the semiconductor phase [176]. This band-bending phenomenon occurs whenever two dissimilar phases are in contact (e.g. semiconductor-gas, semiconductor-metal) and it is an important point of distinction from metal electrodes. At a metal-electrolyte interface, the charge on the metal side is localized just at the metal surface, whereas, at a

semiconductor-electrolyte interface, the charge on the semiconductor side is distributed deep in the interior of the semiconductor, forming a wide space charge region.

Excellent reviews, book chapters, and research papers dealing with theory of photoelectrochemistry at semiconductor electrodes are available [176-180] and therefore, will be not described here in details.

In term of electrode materials, semiconductor photoelectrochemistry has evolved from the use of semiconductor single crystals to polycrystalline thin films and, more recently, to nm-size semiconductor particles (nanocrystalline films) (figure 1.11).

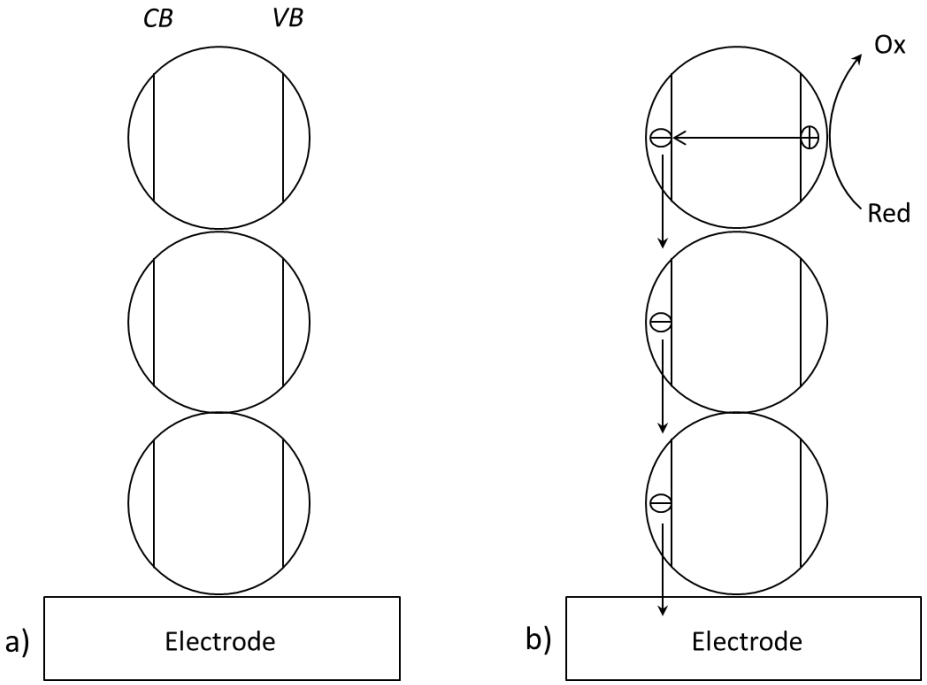

Figure 1.11 – Schematic representation of a nanocrystalline semiconductor-electrolyte interface: (a) in the dark, where no photocurrent is generated; (b) under illumination from the electrolyte side. Illumination induces an electron flux through the nanocrystalline interface.

Novel semiconductor nanoparticles (NPs) have been of special interest. Such small particles have properties that differ from those of larger dimension (μm) [176]. General properties and in particular the band structure of large particles are comparable with those of bulk material. However, when the particle dimension start to decrease to nm dimension band gap increases as the particle size decreases. Furthermore, such NPs have very large surface area/volume ratios, and electrodes formed from such preparations tend to have a high porosity and large roughness factors. Nanocrystalline TiO_2, for example, is an efficient electrode material for constructing photovoltaic devices, due to its high surface

area and porosity of the nanocrystal [181]. Similarly, SnO_2 is an important wide band-gap semiconductor, which is well-known for its excellent transparency and conductivity. SnO_2 NPs have been widely used in many fields such as dye-sensitized solar cells, transparent conductive electrodes and gas sensors [182]. SnO_2 has two main features compared to TiO_2: first, SnO_2 (E_{bg} 3.8 eV) shows a 0.6 eV larger band gap than that of TiO_2 (E_{bg} 3.2 eV) and creates fewer oxidative holes in the valence band under UV illumination; second, the mobility of charge carriers in SnO_2 is faster than that in TiO_2 [183]. ZnO is another semiconductor (E_{bg}=3.37 eV) extensively used for many applications such as piezoelectric transducers [184], gas sensors [185], and optoelectronic devices [186]. It can be grown in a variety of nanostructured morphologies, by low and high temperature methods [187-189]. Even copper(I) oxide (Cu_2O) is a well known p-type semiconductor with an E_{bg} value of 1.9 eV and a proper photochemical behavior [190-193].

In 1839 Becquerel was the first to discover that illuminating certain materials it is possible to generate an electric current. Starting from that discovery, interest in this phenomenon increased with particular attention to solar energy conversion. When photoelectrochemically active species are excited by light, charge separation and charge transfer will occur, generating a photocurrent [194]. With the development of new photoelectrochemically active species, photoelectrochemistry represents an intriguing approach also in the field of biosensor development.

Different nanomaterials have been used as photochemical active species for photoelectrochemical applications. Recently, Quantum Dots (QDs) have been extensively studied [195-198]. Photoexcitation of QDs produces the transfer of electrons from the valence band to the conduction band, yielding electron-hole pairs. This phenomenon is the primary event in the generation of a photocurrent. Ejection of the CB electrons to the electrode, in presence of an opportune donor in the electrolyte solution, generates an anodic photocurrent. In contrast, ejection of the CB electrons to an opportune acceptor in the electrolyte solution, with concomitant migration of an electron from the electrode to the VB, generates a cathodic photocurrent.

Moreover, as already mentioned, other semiconductor inorganic nanomaterials (like SnO_2, TiO_2, ZnO, etc.) have been widely used for developing photoelectrochemical nanostructured electrodes [199-203]. Even gold NPs (AuNPs) have been used for the nanostructuration of the electrodes because of the high surface area and high conductivity

of this material [133]. Lahav and coworkers [204] reported the fabrication of an ITO electrode modified by a layer-by-layer deposition process of a photosensitizer/electron acceptor molecular cross-linked AuNPs arrays. The irradiation of the crosslinked AuNPs multilayer results in a photocurrent that increased with the number of the layers. To enhance the photocurrent generated by semiconductors, the retardation of the recombination of the electron–hole species is essential. Moreover, the accumulation of the electrons allows extending the spectral response from UV to visible or near infrared region simplifying the analytical procedures and the costs of the processes. A possible way to enhance photocurrents is the coupling of semiconductors with other semiconductor NPs or with conductive nanomaterials [205-207]. For instance, the coupling of a large bandgap semiconductor with a narrow bandgap semiconductor extends the photoresponse to longer wavelengths and facilitates charge separation [205].
In figure 1.12 is reported an example of nanocrystalline semiconductor electrode, prepared by sequential deposition of SnO_2 and CdSe films onto an ITO-glass electrode. Upon illumination of ITO/SnO_2/CdSe electrodes with visible light, electron-hole pairs are generated in CdSe, as visible light is absorbed by CdSe only. Generally, the photogenerated electron-hole pairs recombine quickly in CdSe, resulting in loss of the charge carriers. On the contrary, in this coupled system the photogenerated electrons in CdSe (E_{CB} = -0.8V vs. SHE) quickly migrate to the lower lying conduction band of SnO_2 (E_{CB} = 0 eV vs. SHE). As a result, they escape recombination with photogenerated holes in CdSe, and are collected in greater number at the back contact ITO producing a larger photocurrent. Similarly, it was reported that TiO_2/CdS present highest photocurrent in comparison to CdS alone because of the enhanced charge separation [208]. Wang and coworkers [209] reported a nanocomposite system based on TiO_2/CdS modified ITO electrodes with alternately dipping the TiO_2 modified ITO electrode into $[Cd(NH_3)_4]^{2+}$ and S^{2-} solution repeatedly.

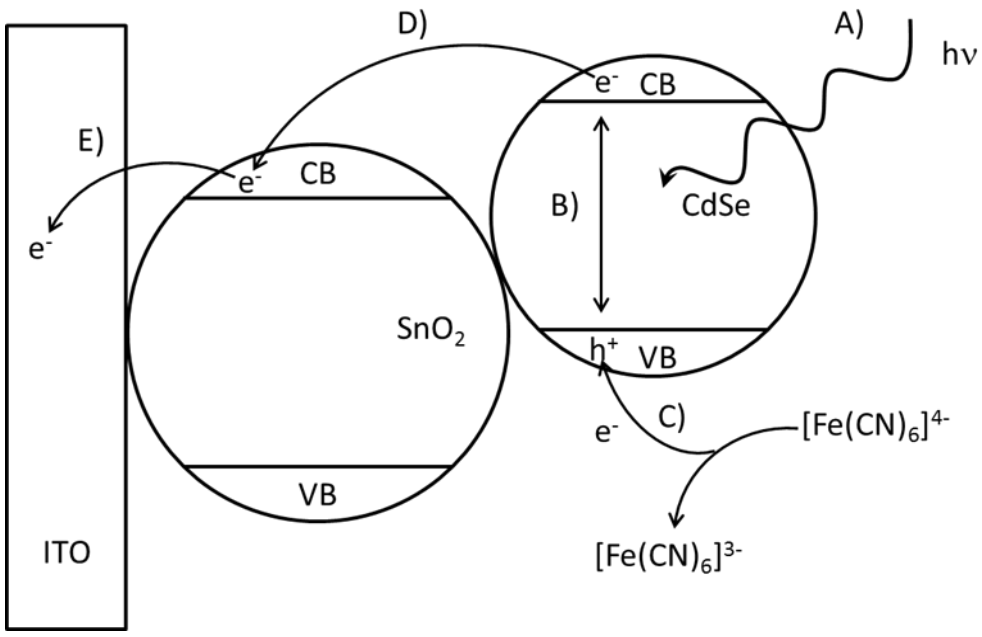

Figure 1.12 – Schematic model of quantum dots coupling. Upon illumination of the ITO/SnO_2/CdSe electrodes with visible light, electron-hole (e^--h^+) pairs are generated in CdSe, as visible light is absorbed by CdSe only. The photogenerated electron-hole pairs can recombine, resulting in loss of the charge carriers, or the holes can be captured by the electrolyte $[Fe(CN)_6]^{4-}$ leaving the electrons in CdSe. The electrons in CdSe are then collected at the back ITO contact to produce an anodic photocurrent. The charge recombination is much more important in the simple CdSe electrode than in the coupled system. The reason is that in the coupled system the photogenerated electrons in CdSe quickly migrate to the lower lying conduction band of SnO_2. As a result, they escape recombination with photogenerated holes in CdSe, and are collected in greater number at the back contact ITO producing a larger photocurrent. Modified from Ref. [205] Copyright © 1997, Elsevier.

In order to increase photoresponse of CdS, Willner and coworkers developed a AuNPs/CdS nanoparticle system [210]. The enhanced photocurrent was attributed to the effective charge separation of the electrode hole pair by the injection of conduction-band electrons from CdS to AuNPs. Furthermore, the coupling of semiconductor materials such as TiO_2 with AuNPs are expected to decrease the overvoltage that is necessary for the hole transfer to the redox couple in the electrolyte [211, 212]. By promoting the interfacial hole transfer to the redox couple, the adsorbed AuNPs should facilitate charge (electron) stabilization within the nanocrystalline TiO_2 films.

1.6.1 Detection of Nucleic Acid by Photoelectrochemical Genosensors

It is well known that plant cells and photosynthetic bacteria exert photoelectric behavior. Photoelectrochemistry has also been applied to investigate specific phenomena in mammalian cell such as the apoptosis process [213]. Nucleic acids are also claimed to be photoelectroactive. In other words, some analytes (including nucleic acids) can generate photocurrent by themselves, on the basis of which quantitative determination can be performed. In addition, the interaction between the analytes and the photoelectrochemical materials (semiconductor electrodes or photoactive species) can induce the changes of the photocurrent, which can also be used as the signal for photoelectrochemical detection.

Starting from these considerations different sensing schemes can be developed and different analytical strategies have already been reported in literature for the detection of nucleic acids using photoelectrochemistry. In the following sections some examples of qualitative and quantitative analysis of nucleic acids are reported. The paragraph is organized considering label free strategies, namely sensing scheme based on the interaction of nucleic acid with the light and the electrode material, and label-based method. In the case of label-based methods, both photoactive materials and classical labels such as enzyme or particles that can cause or alter a photocurrent are described.

1.6.2 Label-free genosensors

It is generally accepted from the scientific community [214] that π-stacked double strand DNA (dsDNA) molecule is a one-dimensional electrical conductor comparable to that of conventional conducting polymers [215, 216]. However, debates on the exact mechanisms of conductivity and particularly on the electron transfer (ET) properties of dsDNA are ongoing, and it is still not completely clear how efficiently DNA can transport electrons over long distances [214, 217, 218]. Photoelectric behavior of nucleic acid has also been reported in literature [219, 220]. This behavior has been exploited for analytical purposes, using different electrode materials. Qingwen et al. reported, in 2000, an analytical attempt [221] for the detection of the hybridization reaction using a metal electrode. A gold electrode was modified with a thiolated DNA probe and a photocurrent was measured. In order to demonstrate that photoelectric activity of DNA was due to Guanine base (G), two different sequences

have been tested: one reach in G denoted as probe 1 and the other, total free of G, denoted as probe 2. Both these probes were hybridized with a complementary target. The authors reported that when probe 1 modified electrode was illuminated, the observed photoelectric behavior resulted from the electrons hoping from G to the substrate electrode mediated by the DNA helix. When it is hybridized with its complementary part, the photocurrent of the dsDNA modified electrode decreased. The authors ascribed this behavior to the decreased activity of G when specifically bound with cytosine (C). In order to further confirm the accuracy of this assumption, another probe containing only adenine (A) and timine (T) was tested. When probe 2 modified electrode was hybridized with its complementary part, the photoelectric current of the dsDNA electrode decreased as well. The conclusion of the authors was that the observed photoelectric phenomenon did not merely come from G base in the DNA helix but reflected the total interfacial properties of the modified electrodes. The self-assembly of negatively-charged single stranded DNA (ssDNA) and specifically formed dsDNA molecule would alter the double-layer potential at the electrode surface, and further the Fermi energy difference at the electrode/solution interface.

Lu and coworkers in 2006 [222] reported a label free genosensor using a semiconductor TiO_2 film electrode deposited onto a conductive F-SnO_2 electrode. Hairpin DNA was bound to TiO_2 film electrode. After hybridization with the complementary target a decrease of photocurrent was observed. The authors attributed the photocurrent change to the oxidation of G and, consequently, to the charge transfer rate in the interfacial layer between the TiO_2 surface and electrolytes. The photophysical process was elucidated by the authors as follows: an electron(e^-)/hole(h^+) charge pair was first generated when the excited light was absorbed by TiO_2, instantaneously the charge separation occurred, and consequently e^- migrated to the F-SnO_2 electrode while h^+ migrated to the electrolyte, which simultaneously underwent undesired recombination. These processes led to the generation of an anodic photocurrent. Next, G of the hairpin DNA probes were oxidized into guanine radical cations (G^+) by the photoinduced hole carriers (h^+) and OH^- in the electrolyte. In the process, the hole trapping action of guanine served as a hole scavenger or as an electron donor, resulting in the significant increase of photocurrent. After hybridization with the complementary target, a decrease in the photocurrent was observed. The authors reported two possible reasons for photocurrent reduction after hybridization: 1) the charge transfer rate was inhibited due to the introduction of target

DNA molecules because the charge transfer efficiency of DNA is dependent on its sequence and on the distance. The lower charge transfer rate enhanced undesired recombination, and thus caused the photocurrent decrease; 2) the G base of the target DNA cannot interact with the oxidizer directly because of steric hindrance in the DNA helix, which diminished its hole trapping capacity and thus led to the lower photocurrent. Two years later, in 2008, the same group [223] optimized another genosensor based on the same electrode used in the previous work, but coupled with the use of AuNPs. The AuNPs served as a charge sink, reducing bulk recombination via band gap states and promoting the charge separation rate and transfer rate, resulting in a higher photocurrent compared with TiO_2. A detection limit of 1 nM was reported.

1.6.3 Label-based genosensors

Different photosensitizers have been reported in literature for the detection of nucleic acids. Among them organic compounds known to be as intercalators of the DNA double helix have been extensively used. Liu and coworkers [224] developed a photoelectrochemical biosensor using a ruthenium bipyridine derivative as photosensitizer, a SnO_2 electrode, and oxalate as electron donor. Ruthenium 2,2'-bipyridine - dipyrido[3,2-a:2'3'-c]phenazine [$Ru(bpy)_2dppz$] generate an anodic photocurrent if irradiated with a 470 nm light. In presence of hybrid dsDNA, the photocurrent is reduced and this reduction was attributed to the intercalation of $Ru(bpy)_2dppz$ into DNA helix. Three possible reasons for the reduction of photocurrent were reported by the authors: (a) impeded electrode reaction of Ru-dppz after intercalating into DNA; (b) reduced mass diffusion due to the increased size of the DNA/Ru-dppz adduct; and (c) electrostatic repulsion between DNA phosphates and oxalate anion, which interferes with the catalytic reaction between intercalated Ru-dppz and oxalate. Even bisintercalator molecules have been used. The term bisintercalator is derived from the ability of these molecules to directly bind to duplex DNA through two planar intercalating moieties. Gao and Tansil [225] reported the use of a novel bisintercalator the N,N'-bis(3-propyl-imidazol)-1.4.5.8-naphtalene diimides (PIND) linked by $Ru(bpy)_3$ complex (PIND-Ru-PIND). Using PIND-Ru-PIND as photosensitizer and a modified ITO electrode, a detection limit of aproximatevely 20 fM, with a dynamic range of 50 fM - 1 nM and a RSD% of 13%, was obtained. The

biosensor was tested directly on genomic samples. In particular, a full-length TP53 cDNA was analysed (the TP53 cDNA refers to the copy DNA of the Human tumor protein p53).

However, photoactive species, like organic dyes or NPs, can also be bound covalently to the target DNA or RNA, instead of being intercalated within the helix. As an example, Tokudome et al. [226] reported a genosensor based on photoelectrochemical DNA detection with rhodamine B dye as photosensitizers. In particular, the DNA probe was chemically adsorbed on nanoporous crystalline TiO_2 particles (through the affinity of phosphate groups condensed to OH groups of titanium dioxide), coated onto a transparent conducting oxide glass (TCO). After the hybridization between the probe and target DNA molecules, labeled with rhodamine B, light irradiation generates electrons in the dye molecules, and these electrons are injected into the TiO_2 electrode. The photocurrent generated was associated to target concentration. A detection limit of 100 pM was reported. One of the interesting aspect of this biosensor is the mechanism that allow to have simultaneous detection of different sequences. Varying the dye bound to a specific target sequence (i.e. Alexa Fluor^{TM} 647 and rhodamine B), different photocurrent spectra were obtained.

Willner and coworkers demonstrated the possibility to use inorganic semiconductor NPs as labels in photoelectrochemical DNA sensing [196]. They described an interesting nanoarchitecture of DNA-cross-linked CdS nanoparticle on gold electrode and the structurally controlled generation of photocurrents upon irradiation of these systems. The array of CdS NP layers was constructed by layer by layer hybridization process using CdS NPs modified with thiolated DNA. The photocurrents were generated by the DNA-cross-linked CdS arrays that contained different generations of NPs. The mechanism of photocurrent generation probably involves the photoejection of conduction-band electrons of CdS particles in contact with or at tunneling distances from the electrode. However, some of the cross-linked NPs do not participate in the development of the photocurrent. To assist the generation of the photocurrent by inactive CdS particles, the arrays were treated with $[Ru(NH3)_6]^{3+}$. In the presence of $[Ru(NH3)_6]^{3+}$, which is electrostatically bound to the DNA, the photocurrents were two times higher. $[Ru(NH3)_6]^{3+}$ acts as an electron acceptor for the conduction-band electrons, and could thus mediate electron transfer from inactive CdS particles to the electrode. A similar work was proposed in 2011 by Guo and coworkers [227] using methylene blue as the intercalator molecule with target DNA modified with CdS NPs.

Increasing the concentration of target DNA, the photocurrent increased lineary in the range of 1 fM to 20 fM with a detection limit estimated to 1 fM and a reproducibility of 4.5%. A step further in the use of QD-DNA assembly was that proposed by Willner and coworkers [228]. These authors reported the organization of semiconductor NP/relay or photosensitizer/ electron-acceptor structures on electrodes modified by DNA sequences.

Metal NPs are common labels in many biosensor formats. Recently, Xu and coworkers explored the possibility to use AuNPs and silver nanoparticles (AgNPs) as labels in photoelectrochemical genosensors. In particular they focused their studies on the energy transfer between CdS QDs and metal NPs [229, 230]. The probe was immobilized onto the QDs and the Ag NP was the label on the target sequence. Due to the overlap of the absorption spectra, the exciton and the plasmon could be induced simultaneously, resulting in the photoresponse of the QDs greatly attenuated by the stimulated exciton-plasmon interactions (EPI). The EPI resonant nature enabled manipulating photoresponse of the QDs via tuning inter-particle distances. With a light source of 420 nm and a potential of 0 V the lowest DNA concentration detected was 2 fM.

Enzymes are frequently used labels in both electrochemical and optical DNA-based biosensors. They have been proposed as labels also in photoelectrochemical assay schemes. As an example, an enzyme-based approach coupled to a Bi_2S_3 nanorods modified ITO electrode for sensitive and specific detection of microRNA was proposed in [231]. Using alkaline phosphatase and L-ascorbic acid 2-phosphate (AAP) as enzymatic substrate, ascorbic acid (AA) was in situ generated and used as electron donor for photocurrent amplification. A low detection limit of 1.67 fM was reported. This high sensitivity is attributed, also, to the use of immunogold labeled streptavidin nanostructures that could bind more enzyme molecules inducing a highest catalytic activity in the in situ production of the AA electron donor. The same group reported a similar approach based on ascorbic acid loaded apoferritin and Trypsase [232]. In conclusions many different labels can be used in photoelectrochemical-based genosensors.

Electrode materials	Label	LOD [Ref]
SiO_2	$Ru(bpy)_2dppz$	180 pM [224]
ITO	PIND-Ru-PIND	20 fM [225]
TCO/TiO_2	Rhodamine B	100 pM [226]
FTO/TiO_2	-	2.5 nM [222]
FTO/TiO_2/AuNPs	-	1 nM [223]
ITO/CdS	AgNPs	2 fM [230]
Au	CdS	1 fM [227]
ITO/Bi_2S_3/AuNPs	Alkaline phosphatase	1.67 fM [231]
ITO/Bi_2S_3/AuNPs	Ascorbic acid loaded apoferitin + trypsase	0.35 fM [232]

Table 1.3 - Examples of different electrode materials and labels for quantitative analysis of nucleic acids using photoelectrochemical genosensors.

In Table 1 are summarized some examples of different assay schemes for the quantitative analysis of nucleic acid. The materials used for the electrode development as well the employed labels are reported together with the limit of detection (LOD).

1.7 Aim and objectives

Starting from the initial discovery in the early 90's, over the last decade has become more clear that miRNAs play important role in many biological process as modulator of gene expression. An abnormal miRNA expression could be linked to many diseases, like cancer. For this reason, miRNAs represent good candidates as diagnostic and prognostic tumor biomarkers. Lung cancer is the tumor with the highest mortality according to WHO, and miRNA-221 and miRNA-222 resulted overexpressed in patients affected by this particular disease. One of the most used standardized methods for detection of miRNAs, due to the inherent sensitivity and reliability, is RT-PCR. However, this method is laborious and require the use of a well-equipped laboratory with specialized and well-trained personnel, and is neither feasible for routine determination of miRNAs nor applicable for point-of-care (POC) testing. Electrochemical biosensors represent good options for miRNA detection. Despite the attractive analytical performances of the

genosensing schemes described in the literature for electrochemical miRNA diagnostic, most of them are unlikely to be applicable to routine analysis. Typical levels of circulating miRNAs in serum were estimated to be in the aM to pM range [58-60].

The present work was focused on the investigation of different types of nanomaterials (liposomes, gold nanoparticles, polymer films and titania films) and their application in highly sensitive genosensing systems. In particular, miRNA 221 and 222, considered as potential candidates for biomarkers of lung cancer, were detected. The choice of these particular materials and specific applications for each of them derived from the necessity to develop simple and low cost platforms for miRNAs subpicomolar detection.

In a first part of the work EIS was used as electroanalytical technique due to the its intrinsic propriety that allow a label free genosensor development. Firstly, a label-free detection scheme based on the recognition of the hybridization event through the enhancement of the electron transfer resistance was investigated with screen printed gold electrodes (SPGEs). Moreover, in order to increase the sensitivity of the assay, an enzyme amplification route was investigated. In this case, the hybrid formed on the electrode surface was labeled using the enzyme Alkaline-Phosphatase. The electrochemical transduction of the hybridization process was performed by means of EIS, after a biocatalyzed conversion of a soluble substrate into an insoluble and insulating product. Enzyme-decorated liposomes were then tested as labels in order to amplify the miRNA-electrochemical sensing. The possibility to further increase the sensitivity of the assay by nanostructuration of the working electrode surface was also investigated using carbon screen printed electrodes modified with gold nanoclusters through electrodeposition, obtaining a detection limit in the picomolar range.

In another approach, an electroconductive polymer film was investigated in order to obtain a label-free assay. In particular, a biotinylated bisthiophene monomer was potentiodynamically polymerized to form films on the SPGEs surface. On top of these films, streptavidin was immobilized by complexing the biotin moieties of the polymer. Finally, biotinylated oligonucleotide capture probe was immobilized by complexing the surface-immobilized streptavidin. This structure served as recognition element of the complementary miRNA sequence via hybridization event. EIS was chosen as electroanalytical technique. The use of conductive polymer resulted in a label-free assay with sensitivity in the picomolar range.

The last part of the thesis was focused on the development of a photoelectrochemical system for miRNAs detection.

Recently, with the emergence of novel photo-electrochemically active species and new nanomaterials, photoelectrochemistry has received increasing attention in the field of biosensors. Commercial ITO-nanoTiO_2 electrodes were modified with gold nanorods and characterized in order to develop an enzyme-based genosensor. A white LED was used as a light source. Finally, hairpin capture probes were designed and applied for the genosensing.

Papers published from this research were:

1) RNA and DNA Diagnostics, Ed: Volker A. Erdmann, Stefan Jurga and Jan Barciszewski, Springer series RNA Technologies, Springer Verlag. Chapter title – Electrochemical biosensors for miRNA detection by Diego Voccia and Ilaria Palchetti. *In press*.
2) D. Voccia, I. Palchetti, Photoelectrochemical Biosensors for Nucleic Acid Detection, Journal of Nanoscience and Nanotechnology, Vol. 15, 3320–3332, 2015.
3) D. Voccia, F. Bettazzi, G. Baydemir, I.Palchetti, Enzyme-based nanoarchitectures for the electrochemical biosensing of microRNAs, Journal of Nanoscience and Nanotechnology, Vol. 15, 3378–3384, 2015.

Chapter 2 – Modified Screen Printed Gold Electrodes for Enzyme Amplified Impedimetric Sensing of microRNA

This chapter describes the development of an enzyme-based genosensor using screen printed gold electrodes. Enzyme labels are herein investigated for signal amplification in the electrochemical detection of nucleic acids and in particular of has-miRNA-222. An enzyme amplification of the analytical signal is accomplished by the use of streptavidin conjugated alkaline phosphatase. Moreover, biotin-tagged liposomes are tested as functional tethers of multiple enzyme molecules. Owing to their dimension in the nanoscale and thus to their large surface area they are capable of carrying a large number of enzyme molecules.

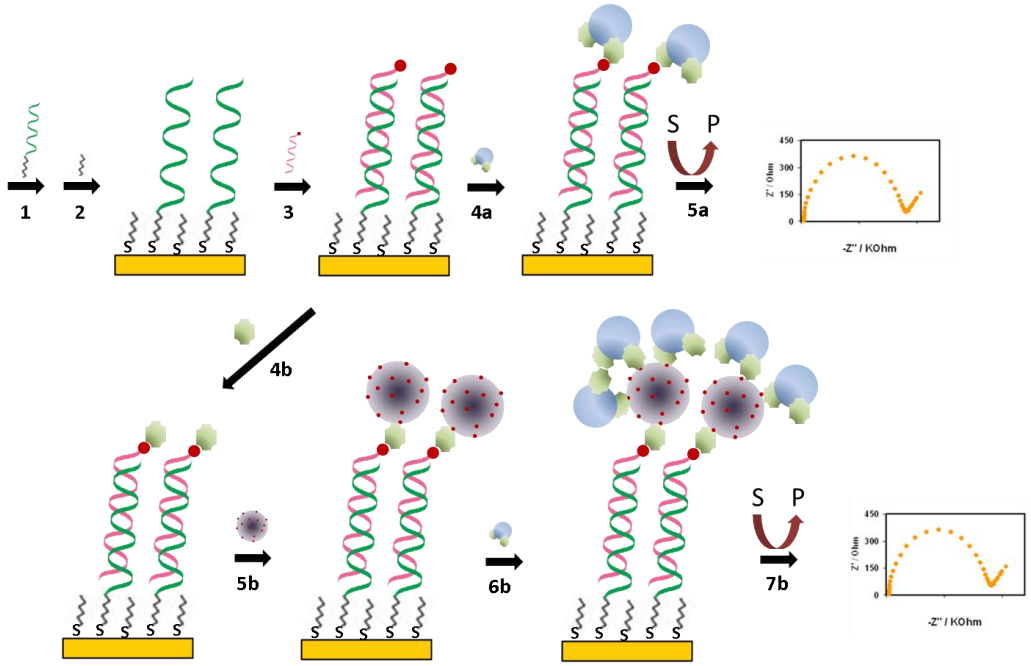

Figure 2.1 - Illustration of the different assay schemes. The biotinylated hybrid is formed on the gold electrode surface (1,2,3). Streptavidin-Alkaline Phosphatase is added (4a). After incubation of the proper substrate, enzymatic product is revealed by EIS (5a). Otherwise, streptavidin (4b) and biotinylated liposomes (5b) are added. The liposome-modified hybrid is then exposed to streptavidin-Alkaline Phosphatase (6b). After incubation of the substrate, the enzymatic product is revealed by EIS (7b).

These enzyme-rich nanoarchitectures are used as labels to amplify the miRNA-sensing events by their association to the probe-miRNA hybrid generated onto a gold transducer. Faradaic impedance spectroscopy was applied to characterize these amplification routes.

Immobilization of the thiol-tethered DNA probe was qualitatively and quantitatively investigated by means of faradic impedance spectroscopy and chronocoulometry, respectively. Electrochemical transduction of the hybridization process was also performed by means of faradic impedance spectroscopy with an enzyme-amplified detection scheme, based on the coupling of a streptavidin-alkaline phosphatase conjugate and biotinylated target sequences (figure 2.1). Streptavidin-alkaline phosphatase conjugate catalyzes precipitation of an insoluble and insulating product onto the sensing interface increasing the resistance to the electron transfer, used as analytical signal. In a first approach a direct streptavidin-conjugated-enzyme binding to the biotinylated hybrid formed on the sensor surface was used. In a second approach, biotin-tagged liposomes were used as functional tethers for streptavidin- enzyme conjugates.

The two strategies have been characterized in term of analytical parameters and results, here, reported.

2.1 Material and methods

2.1.1 Reagents

Dithiothreitol (DTT), 6-mercapto-1-hexanol (MCH), streptavidin–alkaline phosphatase (S2890, Strept-AP, 2:1 conjugation stoichiometry), streptavidin (S4762, Strept), diethyl pyrocarbonate (DEPC), 5-bromo-4-chloro-3- indolyl phosphate (BCIP), BCIP/nitro blue tetrazolium mixture [BCIP/NBT (cat. no. B-1911)], bovine serum albumin (BSA), Tris–HCl, diethanolamine (DEA), dimyristoylphosphatidylethanolamine (DMPE), distearoylphosphatidyl choline (DSPC) and cholesterol were obtained from Sigma–Aldrich (Milan, Italy). Biotin-XDHPE was obtained from Invitrogen Molecular Probes (Eugene, OR). Disodium hydrogenphosphate, potassium hexacyanoferrate (III and II), sulphuric acid, magnesium and potassium chloride were purchased from Merck (Milan, Italy). NAP-10 columns of Sephadex G-25 were obtained from Amersham Pharmacia Biotech (Uppsala, Sweden). MilliQ water (DEPC treated for RNA analysis) was used

throughout this work. Synthetic oligonucleotides were obtained from MWG Biotech AG (Germany):

Probe (DNA-SH): 5’ GAG-ACC-CAG-TAG-CCA-GAT-GTA-GCT – SH 3’

Target hsa-mir-222: 5’ AGC-UAC-AUC-UGG-CUA-CUG-GGU-CUC –biotin 3’

Non-complementary hsa-mir-16 : 5′ UAG-CAG-CAC-GUA-AAU-A-biotin-3′

Prior to use, the thiol-modified oligonucleotides were treated with DTT. This reagent allowed reduction and cleavage of oligo dimers eventually obtained by oxidative coupling of two DNA-SH molecules (i.e. DNA-S-S-DNA). The lyophilized oligonucleotides were dissolved in a 10 mM Tris-HCl buffer solution (pH 8.3) containing 20 mM of DTT. The reaction was allowed to proceed for 2 h at room temperature. The thiolated DNA was then purified by elution through a NAP-10 column of Sephadex G-25 using 0.5 M phosphate buffer (pH 7.4). DNA-SH stock were prepared in the same buffer and stored frozen.

2.1.2 Liposome preparation and characterization

Liposomes containing DSPC/cholesterol/DMPE/DHPE-X-Biotin in molar ratio 40:40:19.5:0.5 were prepared by extrusion through polycarbonate membranes as described by Alfonta et al. [131]. Extrusion was carried out using a manual liposome extruder (LiposoFast-Basic, Avestin Inc., Canada). The dry lipids were dispersed in 20 mM HEPES, pH 7.4, 0.15 M NaCl with vortex mixing. The solution containing the mixture was passed 20 time through a polycarbonate membrane of 100 nm pore size and 19 mm diameter (Avestin Inc., Canada), by pushing the sample back and forth between two syringes. The liposome solution was stored at 4°C until further use.

Hydrodynamic diameters of liposomes were estimated by dynamic light scattering (DLS) using a commercial device (Zetasizer Nano ZS90, Malvern). Samples for size measurement were prepared by addition of 25 µl L of liposomes to 2 mL of 10 mM phosphate buffer, pH 7.4. The solution was filtered using 0.2 µm syringe filter and dispensed into a clean plastic cuvette.

In order to confirm the presence of biotin on the surface of liposomes, hydrodynamic diameters of liposome aggregates were estimated by dynamic light scattering (DLS) using a Brookhaven Instruments apparatus (BI 9000AT correlator card and BI200SM goniometer). The light source was the second harmonic of a diode-pumped Coherent Innova Nd:YAG laser (λ = 532 nm), linearly polarized in the vertical direction and impinging on the sample with 60 mW power. The signal was detected by an EMI 9863B/350 photomultiplier. To obtain the size distribution of the scattering objects, the autocorrelation functions were Laplace inverted using the CONTIN routine. Samples for aggregations test for liposome were prepared by addition of 25 μL of a 1:1 mixture of liposomes and streptavidin (0.5 mg/L in PB) or liposomes and streptavidinalkaline phosphatase (8 U/mL in DEA) incubated in a vial for 20 minutes under mixing to 2 mL of 10 mM phosphate buffer, pH 7.4. A sample with only liposomes was used as negative control. The solution was filtered using 0.2 μm syringe filter and dispensed into a clean glass cuvette.

2.1.3 Electrode pretreatment and modification

Materials and procedures to screen-print the electrode transducers are described in previously published papers [84, 233].

Prior to immobilization of the thiol-tethered DNA probe, a multiple-pulse amperometric pretreatment of the gold surface was carried out in a stirred 0.5 M H_2SO_4, 10 mM KCl solution. The following triple-potential pulse sequence: −0.3 V for 0.30 s; 0.0V for 0.30s and +1.0V for 0.15s (150 cycles) was applied.

The gold working electrode surface of these planar sensors was then exposed to the thiolated oligonucleotide solution (10 μL, 1 μM in 0.5 M phosphate buffer, pH 7). Chemisorption was allowed to proceed overnight (≈16 h) with electrodes stored in Petri dishes to protect the solutions from evaporation. The immobilization step was followed by treatment with a spacer thiol. A 10 μL drop of 1 mM aqueous solution of MCH was placed onto the probe-modified surfaces for 30 min. Prior to the hybridization reaction, the modified electrodes were washed twice with 15 μL of phosphate buffer.

2.1.4 Hybridization procedure

Hybridization experiments were carried out using biotinylated target sequences in a direct format. Probe-modified gold electrodes were exposed to a 10 µL drop of the biotinylated target sequence solution (in 0.5 M phosphate buffer) for 20 min. A biotinylated non-complementary sequence was used as the negative control. After hybridization, the sensors were washed twice with 15 µL of DEA buffer (diethanolamine 0.1 M, $MgCl_2$ 1 mM, KCl 100 mM; pH 9.6) in the case of strept-AP assay or with 0.5 M phosphate buffer in the biotin-tagged liposome assay scheme.

2.1.5 Labeling and EIS Detection

Strept-AP-Based Assay: the biotinylated hybrid obtained at the electrode surface was reacted with a 10 µL drop solution containing 1 U/mL of the strep–AP conjugate and 8 mg/mL of BSA in DEA buffer. After 20 min, the genosensors were washed twice with 15 µL of DEA buffer. The enzyme-modified surfaces were then incubated with 30 µL of the BCIP/NBT mixture for 20 min. After precipitation of the insoluble and insulating product and prior to impedimetric measurements, the sensors were washed with 0.1 M KCl for 10 s.

Biotin-tagged Liposome Assay: The biotinylated hybrid obtained at the electrode surface was reacted with a 10 µL drop solution containing 0.05 mg/L of streptavidin in 0.5 M phosphate buffer. After 20 min, the genosensors were washed twice with 15 µL of HEPES buffer and were then reacted with liposome solution (20 min, room temperature).

The final configuration was reacted with a 10 µL drop solution containing 4 U/mL of the streptavidin–alkaline phosphatase conjugate and 8 mg/mL of BSA in DEA buffer. After 20 min, the genosensors were washed twice with 15 µL of DEA buffer. The enzyme-liposome-modified surfaces were then incubated with 30 µL of the BCIP/NBT mixture for 20 min. After precipitation of the insoluble and insulating product and prior to impedimetric measurements, the sensors were washed with 0.1 M KCl for 10 s.

Each result is the mean and standard deviation of at least three measurements.

2.1.6 Electrochemical measurement

All electrochemical measurements were performed with an AUTOLAB PGSTAT 10 digital potentiostat/galvanostat. The GPES 4.9004 software (Eco Chemie BV, Utrecht, The Netherlands) was used for cyclic voltammetry (CV), chronocoulometry (CC) and multi-pulse amperometry (MPA); the FRA2 module was used for faradaic impedance experiments. All potentials were referred to the screen-printed silver pseudo-reference electrode; the experiments were carried out at room temperature.

Faradaic impedance measurements were carried out in the presence of 5 mM $[Fe(CN)_6]^{3/4-}$ redox probe (equimolecular mixture in 0.1 M KCl). An alternate voltage of 10 mV in amplitude (peak-to-peak), within the frequency range 100 kHz–10 mHz, was superimposed to the applied bias potential. The dc potential was set up at +0.13 V, the formal potential of the $[Fe(CN)_6]^{3/4-}$ redox probe. Experimental spectra, presented in the form of complex plane diagrams (i.e., Nyquist plots), were fitted with proper equivalent circuits using the facilities of the FRA2 software 4.9004 (EcoChemie). Both charge transfer resistance and Δ charge transfer resistance values were taken as analytical signals. The "Randles equivalent circuit" was successfully applied to fit data acquired.

2.2 Results

2.2.1 Electrochemical characterisation of the screen printed gold electrodes

The screen-printed gold electrodes were firstly characterized by CV in 0.5 M H_2SO_4. Characteristic gold oxidation and reduction peaks were found near +1.11 V and +0.61 V vs. silver pseudo-reference electrode, respectively (figure 2.2a). A characterization of bare screen printed gold electrode was also performed, showing a quasi-reversible voltammogram, indicating that a pretreatment was needed (figure 2.2b solid line).

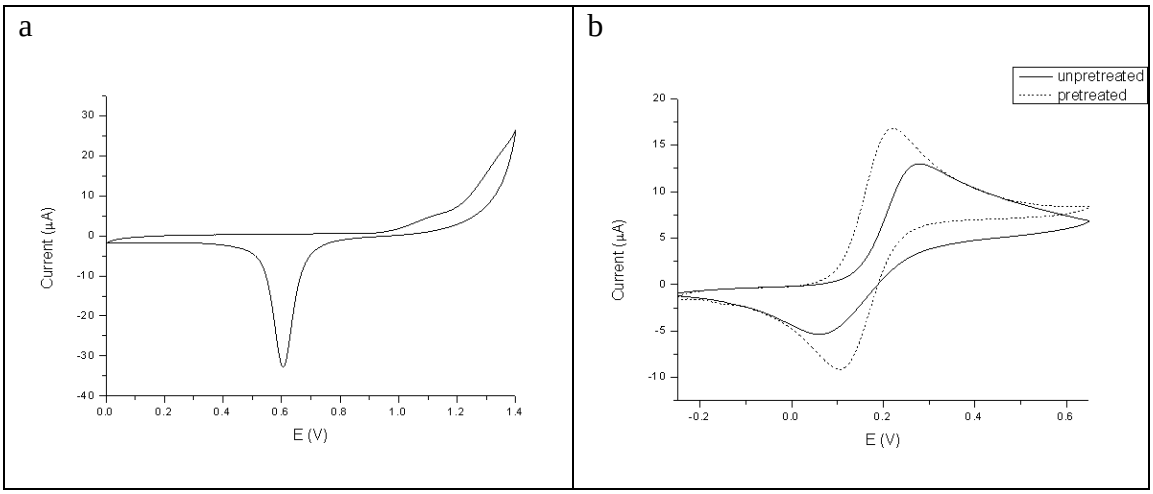

Figure 2.2 – a) Cyclic voltammetric signal of a screen printed gold electrode in 0.5 M H_2SO_4. Potential scan: from 0.0 to +1.4 V; step potential = 2.44 mV; scan rate = 100 mV/s. b) Cyclic voltammetric signal of an unpretreated (dash line) and pretreated (solid line) screen printed gold electrode in 5 M $Fe(CN)_6^{4-}$ (0.1 M KCl supporting electrolyte). Potential scan: from –0.25 to +0.65 V; step potential = 2.44 mV; scan rate = 10 mV/s.

Mechanical or electrochemical cleaning of the gold surface is usually recommended and thiol-tethered DNA probe immobilization was found to be significantly affected by surface pretreatments. Two different pretreatment were performed: CV in 0.5 M H_2SO_4 (6 cycles) and MPA in a stirred 0.5 M H_2SO_4 and 10 mM KCl solution. A set of electrodes pretreated with both technique was modified with a 1 µM DNA-SH in phosphate buffer overnight followed by incubation with 1 mM MCH solution for 1h. and compared with bare electrodes in order to determine the best surface for DNA immobilization. A set of unpretreated electrodes was used as control. Results are summarized in figure 2.3 and show that the highest signal ratio (DNA/MCH:bare) is obtained for MPA pretreatment. Thus, MPA pretreatment was used in all subsequent experiments.

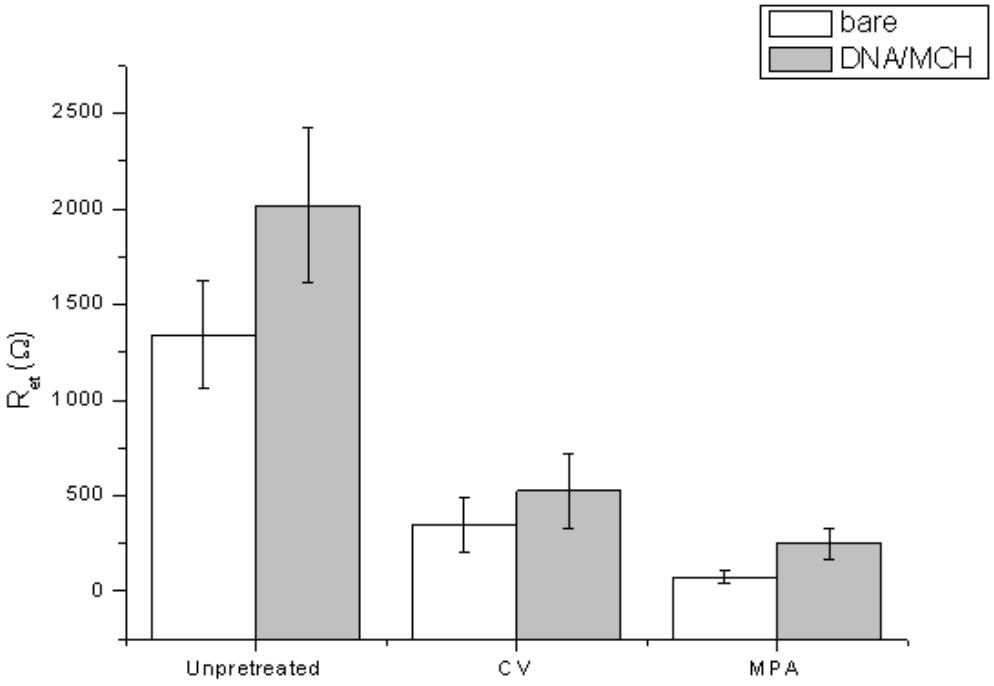

Figure 2.3 – Electron transfer resistance evaluated through EIS in 5 mM $[Fe(CN)_6]^{3/4-}$ redox probe (equimolecular mixture in 0.1 M KCl) in the condition described in paragraph 2.1.6 for bare and DNA modified screen printed gold electrodes with different pretreatment.

The electrochemically active surface of pretreated screen printed gold sensors was then evaluated by CV, in presence of 5 mM ferrocyanide solution in KCl 0.1 M (figure 2.2b dash line) and compared with unpretreated electrodes.
The Randles-Sevcik equation:

$$i_p = (2.687 \cdot 10^5)\, n^{3/2}\, A\, D^{1/2}\, C\, \nu^{1/2}$$

was used for the calculations of the active surface of the electrode. In the equation i_p (A) is the ferrocyanide peak current, (experimentally determineted by CV), n the number of electrons involved, A the electrode area (cm^2), D the diffusion coefficient ($=6.50 \cdot 10^{-6}$ cm^2/s [234]), C the concentration (mol/cm^3) and ν the scan rate (V/s). An electrochemically active surface of 5.55 ± 0.06 mm^2 was calculated from the results with pretreated electrodes and an active surface of 2.95 ± 0.65 mm^2 for unpretreated electrodes (geometrical area = 7.07 mm^2). The small relative standard deviation found for these measurements on pretreated electrodes (1.14 % [n = 5]) against unpretreated electrodes (22.1% [n=5]) confirmed that a pretreatment was necessary in order to

obtain high reproducibility.

Morover, the true area of a gold electrode was also evaluated from the charge needed to reduce a layer of adsorbed oxygen [176]. Gold oxide reduction peaks were measured in 0.5 M H_2SO_4 solution by CV (figure 2.2a). Assuming 482 μC/cm^2 to be the charge required for the reduction of a monolayer of oxides on polycrystalline gold electrodes [235] an electrochemically active area of 7.96 ± 0.66 mm^2 was calculated (n= 5). This value was in agreement with that previously evaluated and much closer to the geometrical area.

2.2.2 Chronocoulometric quantification of probe surface density and of hybridization efficiency

Qualitative information extracted from impedance spectra was integrated with the quantitative measurement of probe surface densities, according to the method developed by Steel et al. [92]. Briefly, this method relies on the CC measurement of a highly charged cationic redox marker, $[Ru(NH_3)_6]^{3+}$. In low ionic strength buffers, this metal complex exchanges with cations naturally compensating the polyanionic backbone of the oligonucleotides. Therefore, at equilibrium conditions, the amount of $[Ru(NH_3)_6]^{3+}$ electrostatically associated to the phosphate groups is directly proportional to the number of immobilized probe molecules. A series of sensors was exposed to thiolated oligonucleotide solutions (0.1 and 1 μM in 0.5 M phosphate buffer) with chemisorption allowed to proceed overnight. After treatment with MCH, each subset of modified sensors was exposed to the biotinylated complementary sequence (2.5 nM), while the phosphate buffer and non-complementary target were used as negative control. The results of CC measurements are displayed in table 2.1. Clear signals were obtained at 0.1 and 1 μM DNA-SH/MCH modified electrodes. Calculated probe surface densities were found to be similar to those reported for analogous immobilization accomplished onto evaporated gold films by Steel et al. [92]. Hybridization of the surface-tethered probes with the corresponding target sequence increases the number of $[Ru(NH_3)_6]^{3+}$ binding sites (nucleotide phosphates) at the electrode interface. Therefore, the number of hybridized target molecules can be conveniently evaluated from the excess of $[Ru(NH_3)_6]^{3+}$ found when comparing hybrid and probe-modified electrodes. Figures 2.4 shows typical CC signals obtained at 0.1 and 1 μM DNA-SH modified electrodes, respectively.

	Oligonucleotide molecules (10^{12} molecules/cm^2)	Hybridization efficiency (%)	R_{et} (kΩ)
0.1 µM DNA probe	1.97 ± 0.4		1.3 ± 0.2
Hybridization	1.99 ± 0.01	101	3.1 ± 0.6
1 µM DNA probe	2.4 ± 0.2		1.6 ± 0.2
Hybridization	1.97 ± 0.4	82	4.1 ± 0.7

Table 2.1 - Chronocoulometric experiments were carried out in 10 mM Tris buffer (pH 7.4) in presence of 50 µM of $[Ru(NH_3)_6]^{3+}$. Prior to measurements the solutions were deoxygenated via purging with N_2 for at least 10 min; the electrochemical cell was blanketed with N_2 during the experiments. Initial and final potentials were +0.1 and –0.4 V, respectively; a pulse duration of 2 s was applied. Faradic impedance spectra were recorded according to the conditions described in materials and methods. Each measurement was repeated at least three times.

According to the literature, the hybridization efficiency (i.e. the percentage of surface bound probes undergoing hybridization) increased as the probe density was diminished. Such a behavior reflected the lower steric hindrance and electrostatic repulsion experienced by the target molecules at less tightly packed probe monolayers. Because of the non-destructive characteristics of CC measurements, the same batch of electrodes was further processed. Probe-modified sensors were exposed to the streptavidin-alkaline phosphatase conjugate and then incubated with the enzymatic substrate solution. The precipitation of an insoluble product, obtained through the catalyzed oxidative hydrolysis of the BCIP/NBT mixture, generated an insulating layer which inhibited the interfacial electron transfer of the $[Fe(CN)_6]^{3/4-}$ redox probe. The resulting electron transfer resistance values, detected by means of faradic impedance spectroscopy, were taken as the analytical signals. Such values are displayed in the last column of table 2.1 as a function of the DNA-SH concentration. The impedimetric results confirmed the CC experiments. Furthermore, comparable responses were observed for the 0.1 and 1 µM DNA-SH/MCH modified sensors.

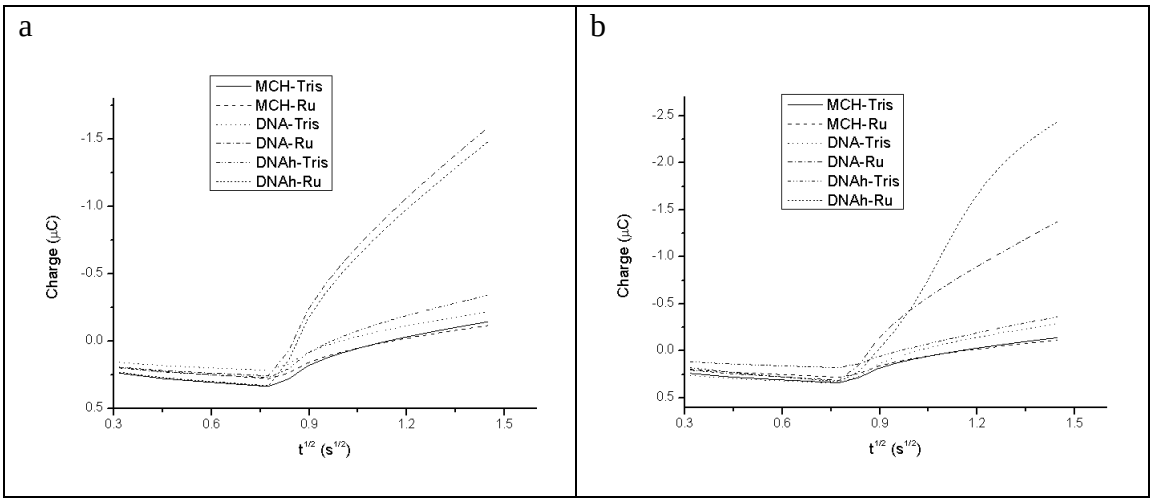

Figure 2.4 - Typical chronocoulometric signals obtained at MCH-modified and 0.1 (a) and 1 μM (b) probe-modified electrodes, before and after hybridization and in presence of $[Ru(NH_3)_6]^{3+}$ complex (Ru in figures) and in Tris buffer only (Tris in figures). Other experimental conditions as described in table 2.1.

Despite the difference in the hybridization efficiencies (100 and 82 %, respectively), the actual number of hybridized target molecules at these surfaces was, in fact, rather similar (1.8 vs. 2.4) · 10^{12} molecules/cm^2.

2.2.3 Liposome characterization

These biotinylated liposomes were characterized by DLS, and a hydrodynamic diameter of 146 ± 9 nm was calculated as reported in figure 2.5a. Average diameters of prepared liposomes were determined at the day of preparation and compared with those after store for 30 days at 4°C (stability test). Aggregation of liposomes during the stability test was negligible (figure 2.5b).

a

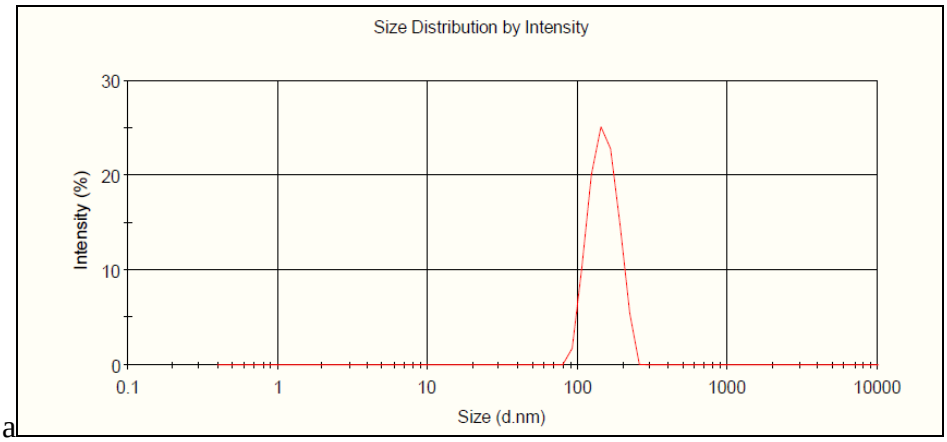

b

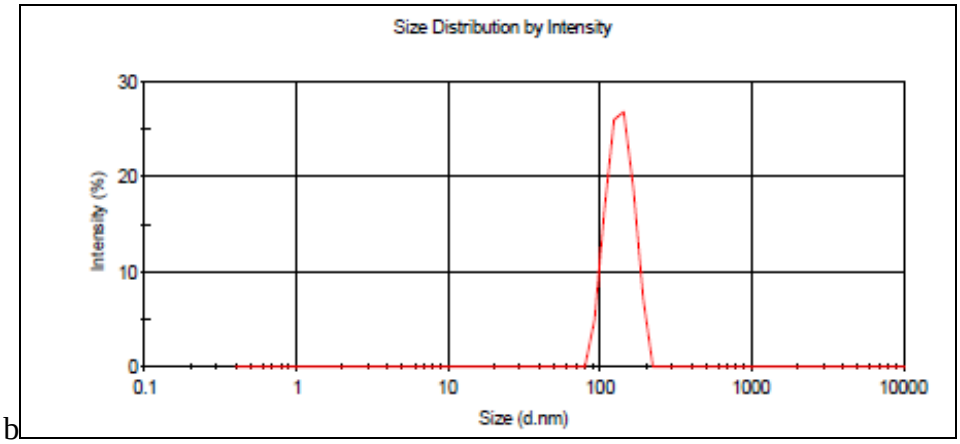

Figure 2.5 – Size distribution intensity obtained with DLS with 25 µl L of liposomes preparative in 2 mL of 10 mM phosphate buffer, pH 7.4 a) at the day of preparation and b) after store for 30 days at 4°C .

In this section, DLS was also used in order to confirm the presence of biotin in the structure through the ability of the biotin molecules to bind with streptavidin. The increase of particle size due to liposome aggregation in presence of streptavidin can be observed by DLS. Thus in the dispersions of biotinylated liposomes a known concentration of streptavidin was introduced (0.5 ppm) and after a proper incubation time under mixing condition at room temperature (20 min), the average hydrodynamic diameter was evaluated by DLS.

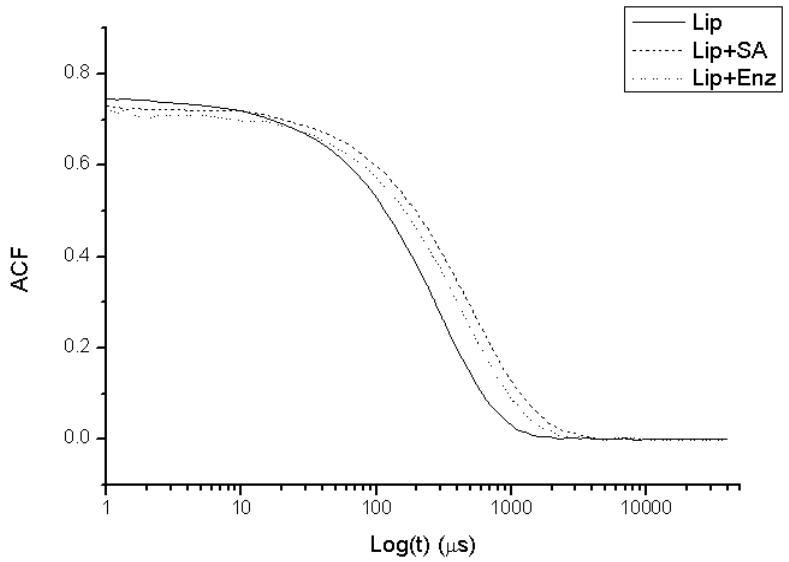

Figure 2.6 – Auto correlation function registered under a green laser in DLS in presence of free liposome dispersion (solid line), in presence of liposome and streptavidin dispersion (dot line) and liposome and streptavidin alkaline phosphatase dispersion (dash line).

In all the experiments, the concentration of biotinylated liposomes and total volume of the solution were kept constant to allow for direct comparison. Because streptavidin has four biotin binding sites, it can act as a biological cross-linking agent and initiate the formation of liposome aggregates. Indeed, the hydrodynamic radius of the liposome population increases in presence of the streptavidin. However, the measured diameter is around the double of the diameter found in absence of streptavidin. The same experiment was performed using streptavidin alkaline phosphatase enzyme. This enzyme is conjugated with two streptavidin, permitting to this molecule to work in the same way of free streptavidin. Thus in the dispersions of biotinylated liposomes a known concentration of streptavidin alkaline phosphatase was introduced (8 U/mL) and after a proper incubation time under mixing condition at room temperature (20 min), the average hydrodynamic diameter was evaluated by DLS. Also in this case an increasing of the hydrodynamic radius of the liposome population is observed. Auto correlation functions (ACF) of the DLS experiments are showed in figure 2.6. Hydrodynamic diameters calculated (D_h) are summarized in table 2.2.

	D_h (nm)
Liposome	140
Liposome + Streptavidin	250
Liposome + Enzyme	214

Table 2.2 - Hydrodynamic diameter of liposome formulations

2.2.4 Liposome assay optimization

In order to further optimize the analytical assay, the influence of the streptavidin, liposome and enzyme concentrations on electrochemical signals were investigated.

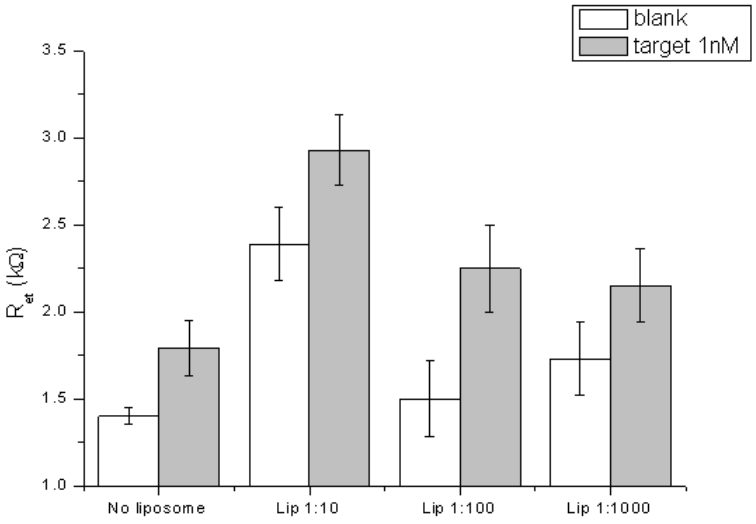

Figure 2.7 - Influence of liposome dilution on the analytical signals registered in enzyme-decorated liposome assay. A comparison with the enzymatic assay is also showed. Probe-modified sensors were exposed to a 10 µL drop of phosphate buffer (blank) and biotinylated complementary target sequence solutions (target 1 nM in phosphate buffer) for 20 min. Biotinylated hybrid was then exposed to a 0.5 mg/L streptavidin solution in phosphate buffer for 20 min. Different liposome dilutions (1:10, 1:100 and 1:1000 in HEPES buffer) were incubated for 20 min. After labelling with the streptavidin-alkaline phosphatase conjugate (0.8 U/mL), the sensors were exposed to 30 µL of BCIP/NBT mixture for 20 min. Further details are available in the Materials and Methods section. The bars are the average of at least three measurements and the error bars the corresponding standard deviation.

A series of sensors was exposed to increasingly liposome dilutions (1:10, 1:100,

1:1000 in HEPES buffer) while keeping constant streptavidin and enzyme concentration. Experimental data, summarized in figure 2.7, show how both the signal due to the nonspecific adsorption of the liposome and that due to its specific coupling with the biotinylated hybrid changed with the dilution. These results suggested that optimal analytical signal (compatibly with minimal aspecific signal) could be achieved using 1:100 dilution. This value was used for all subsequent experiments.

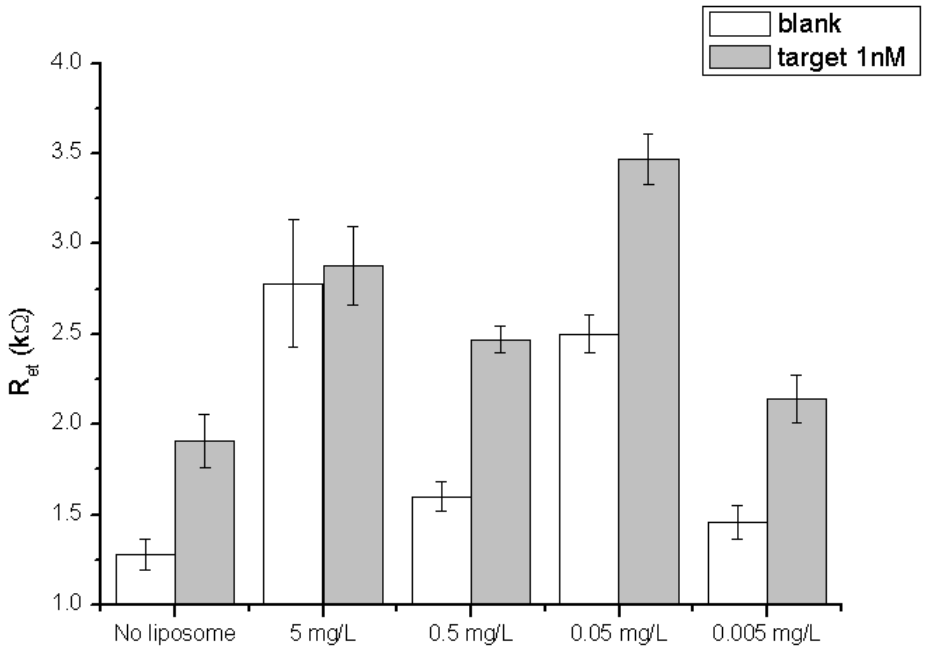

Figure 2.8 - Influence of streptavidin concentration on the analytical signals registered in enzyme-decorated liposome assay. A comparison with the enzymatic assay is also showed. Probe-modified sensors were exposed to a 10 µL drop of phosphate buffer (blank) and biotinylated complementary target sequence solutions (target 1 nM in phosphate buffer) for 20 min. Biotinylated hybrid was then exposed to different streptavidin concentrations (0.005, 0.05, 0.5 and 5 mg/L in phosphate buffer) for 20 min. Liposome 1:100 dilution in HEPES buffer was incubated for 20 min. After labelling with the streptavidin-alkaline phosphatase conjugate (0.8 U/mL), the sensors were exposed to 30 µL of BCIP/NBT mixture for 20 min. Further details are available in the Materials and Methods section. The bars are the average of at least three measurements and the error bars the corresponding standard deviation.

Then, a series of sensors was exposed to increasingly amounts of streptavidin (0.005, 0.05, 0.5 and 5 mg/L in 0.5 M phosphate buffer) while keeping constant liposome and enzyme concentration.

Experimental data, summarized in figure 2.8, shows a high non-specific signal at high concentration. At lower concentrations of streptavidin, ΔR_{et} showed its highest result at 0.05 mg/L. These results suggested that optimal analytical signal (compatibly with minimal non-specific signal) could be achieved using the 0.05 mg/L concentration. This value was used for all subsequent experiments.

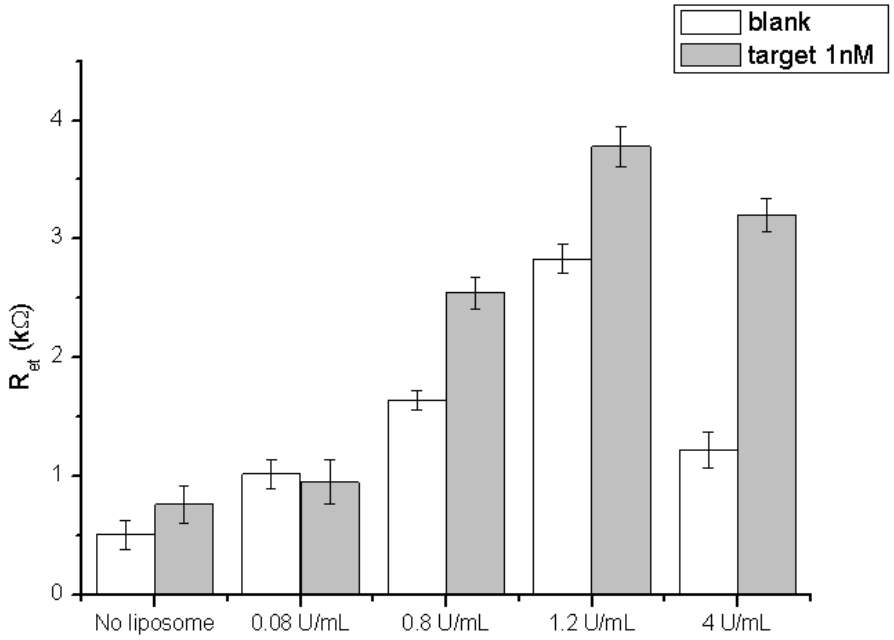

Figure 2.9 - Influence of enzyme concentration on the analytical signals registered in enzyme-decorated liposome assay. A comparison with the enzymatic assay is also showed. Probe-modified sensors were exposed to a 10 µL drop of phosphate buffer (blank) and biotinylated complementary target sequence solutions (target 1 nM in phosphate buffer) for 20 min. Biotinylated hybrid was then exposed to a 0.05 mg/L streptavidin solution in phosphate buffer for 20 min. Liposome 1:100 dilution in HEPES buffer was incubated for 20 min. After labelling with the streptavidin-alkaline phosphatase conjugate (0.08, 0.8, 1.2 and 4 U/mL), the sensors were exposed to 30 µL of BCIP/NBT mixture for 20 min. Further details are available in the Materials and Methods section. The bars are the average of at least three measurements and the error bars the corresponding standard deviation.

Finally, the influence of the enzymatic conjugate concentration on electrochemical signals was also investigated. A series of sensors was exposed to increasingly amounts of streptavidin-alkaline phosphatase (0.08, 0.8, 1.2 and 4 U/mL in a 8 mg/mL BSA in DEA buffer solution) while keeping constant streptavidin and liposome concentration.

Experimental data, summarized in figure 2.9, show how both the signal due to the nonspecific adsorption of the conjugate and that due to its specific coupling with the biotinylated hybrid increased with the streptavidin-alkaline phosphatase concentration (except for the highest concentration tested). These results suggested that optimal analytical signal (compatibly with minimal non-specific signal) could be achieved using 4 U/mL enzyme concentration. This value was used for all subsequent experiments.

2.2.5 Calibration plot for synthetic oligonucleotides

To demonstrate the analytical performances of the impedimetric assay a calibration experiment was designed (figure 2.10 and 2.11). When analyzing synthetic target solutions whose concentration was increased by orders of magnitude, a linear response were observed until a plateau was achieved.

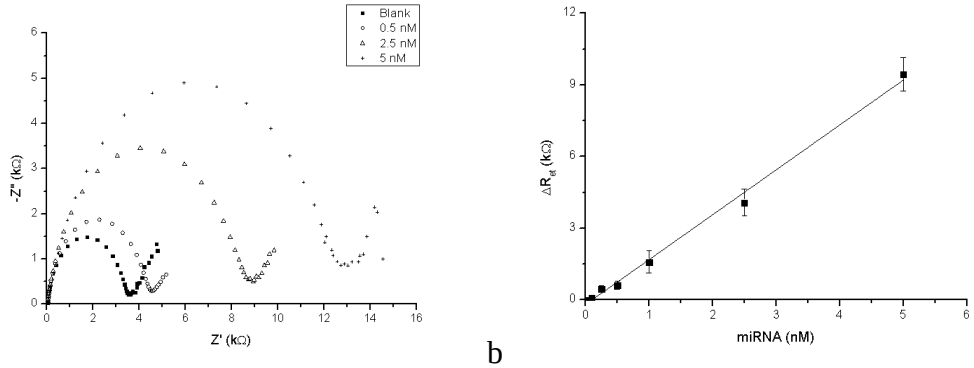

a b

Figure 2.10 – a) Faradaic impedance spectra (in the form of Nyquist plots) for the measurements corresponding to increased concentration of miRNA target (0, 0.5, 2.5, 5 nM in phosphate buffer). Data are recorded in 0.1 M KCl in the presence of $Fe(CN)_6^{3-/4-}$*, 5 mM (molar ratio 1:1). Further details are reported in the material and methods section. b) Calibration plot for synthetic oligonucleotides in enzymatic assay. Probe-modified sensors were exposed to a 10 µL drop of the biotinylated target sequence solution (0, 0.1, 0.25, 0.5, 1, 2.5, 5 nM) for 20 min. Each point represents the mean of at least three measurements and the error bars the corresponding standard deviation.*

In the enzymatic assay, the analytical signals varied linearly (R^2 = 0.995) with the target concentration from 0.1 to 5 nM (figure 2.10). Signals leveled off for higher concentrations, indicating that saturation of all available probes was achieved;

moreover, the non-specific signal of biotinylated non-complementary oligomers was negligible up to 5 nM (data not shown). Within the linear analytical range, the sensitivity was 1.89 kΩ/nM, with an estimated detection limit of 180 pM and an average RSD of 14%.

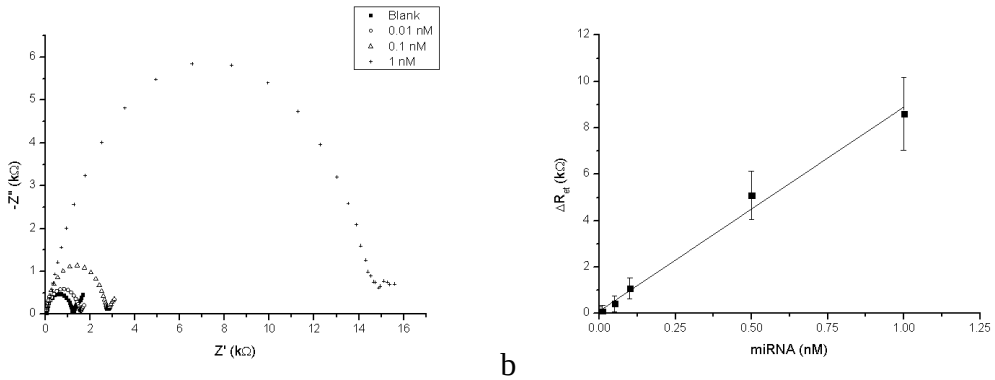

a b

Figure 2.11 - a) Faradaic impedance spectra (in the form of Nyquist plots) for the measurements corresponding to increased concentration of miRNA target (0, 0.5, 2.5, 5 nM in phosphate buffer). Data are recorded in 0.1 M KCl in the presence of $Fe(CN)_6^{3-/4-}$*, 5 mM (molar ratio 1:1). Further details are reported in the material and methods section. b) Calibration plot for synthetic oligonucleotides in the enzyme-decorated liposome assay. Probe-modified sensors were exposed to a 10 µL drop of the biotinylated target sequence solution (0.1, 0.25, 0.5, 1, 2.5, 5 nM) for 20 min. Further details are available in the Materials and Methods section. Each point represents the mean of at least three measurements and the error bars the corresponding standard deviation.*

In enzyme-decorated liposome assay, the genosensor response varied linearly (R^2 = 0.998) with the target concentration between 50 pM to 1 nM (figure 2.11). Signals leveled off for higher concentrations, indicating that saturation of all available probes was achieved; moreover, the non-specific signal of biotinylated non-complementary oligomers was negligible up to 1 nM (data not shown). Within the linear analytical range, the sensitivity was 10.3 kΩ/nM, with an estimated detection limit of 37 pM and an average RSD of 15%.

2.3 Discussion

The features of the DNA probe immobilization process and the formation of DNA-SH/MCH mixed monolayers with different pretreatment of screen printed gold

electrodes were qualitatively investigated by faradic impedance spectroscopy, using the $[Fe(CN)_6]^{3/4-}$ mixture as the redox probe and cyclic voltammetry using $[Fe(CN)_6]^{4-}$ and H_2SO_4. Results show how pretreatment is necessary in order to obtain impedimetric reproducible signals. Electrochemical impedance spectroscopy (EIS) is the electrochemical technique where the electrode impedance is monitored as a function of the frequency of an applied alternate voltage [176]. The use of both electrochemical and faradic impedance spectroscopy to probe the interfacial properties of surface-modified electrodes and thus for monitoring biorecognition processes was proposed by Willner and co-workers [131, 236]. Compared to other electrochemical methods, faradic impedance spectroscopy is considered to be a gentle electrochemical method. The features of bio-modified electrodes can be studied by applying a small perturbation, so that the systems are investigated nearly in their steady-state. A combination of physical coverage by the oligonucleotides and electrostatic repulsion between the negatively-charged redox ions and the polyanionic backbone of the oligos [237] was considered responsible for the enhanced electron transfer resistance measured at the modified electrodes. Amines are known to chemisorb weakly on gold. According to the literature [238], in order to avoid a non-specific adsorption of sequences on the electrode surface through a direct interaction of the nitrogen-containing purine and pyrimidine bases with the gold surface, a treatment with MCH is necessary.

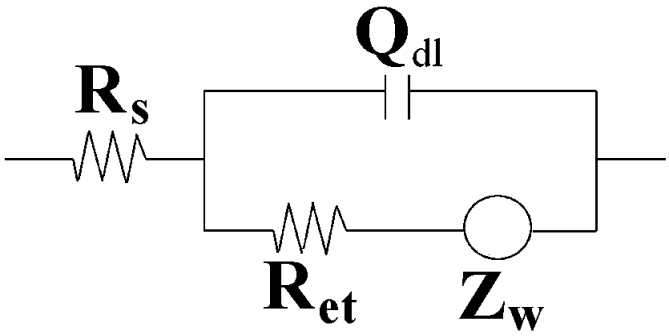

Figure 2.12 – Randles equivalent circuit modified with constant phase element Q_{dl}.

The equivalent circuit required to fit experimental impedance spectra is showed in figure 2.12. The constant phase element, Q_{dl}, was always used instead of pure capacitive elements to take into account the roughness of the modified sensor surfaces [239]. This circuit, better known as the "Randles equivalent circuit" [176] was successfully applied to fit data acquired at modified sensors. The Warburg impedance (Z_W) usually is registered at low frequencies and correspond to the diffusion to the electrode surface.

The amount of thiol-tethered DNA probe immobilized at the sensor surface was quantified through chronocoulometric measurements, in the presence of $[Ru(NH_3)_6]^{3+}$. This complex exchanged with K^+, the cation natively compensating the polyanionic backbone of the oligonucleotides. At saturation coverage of $[Ru(NH_3)_6]^{3+}$, the surface density of the probe was calculated assuming complete charge compensation by these redox cations. The validity of this approach also relied upon the following assumptions:bthe redox marker associates with DNA strictly through electrostatic interactions;ball redox molecules are electrochemically accessible. The ruthenium complex was quantified using chronocoulometry. This method was selected because of its ability to differentiate between the double-layer charge, the charge due to reaction of species adsorbed at the interface and that due to diffusing species. Therefore, measurements of the surface-confined complex could be made in the presence of solution redox marker, so that the system was observed under equilibrium conditions. The measured charge (Q) as a function of time (t) is expressed by the integrated Cottrell equation:

$$Q = \frac{2nFAD_0^{\frac{1}{2}}C_0^*}{\pi^{\frac{1}{2}}} t^{\frac{1}{2}} + Q_{dl} + nF\Gamma_0$$

where n is the number of electrons involved; F the Faraday constant (Coul/equiv); A the electrode area (cm^2); D_0 the diffusion coefficient (cm^2/s); C_o* the bulk concentration (mol/cm^3); Q_{dl} the capacitive charge and ($nFA\Gamma_0$) the charge for the reduction of Γ_0 (mol/cm^2) of adsorbed redox marker. The term Γ_0 (“surface excess”) expresses the amount of ruthenium hexaammine confined near the electrode surface. The chronocoulometric intercept for t = 0 is the sum of the double-layer charge and the charge due to reduction of adsorbed species. The latter term was then determined from the difference in chronocoulometric intercepts for identical potential step experiments in the presence and absence of the redox marker. The saturated surface excess of ruthenium hexaammine was converted to DNA probe density using the following relationship:

$$\Gamma_{DNA} = \Gamma_0(z/m)N_A$$

where: Γ_{DNA} is the probe surface density (molecules/cm^2); m the number of bases in the DNA probe; z the charge of the ruthenium complex and N_A the Avogadro's number. Interestingly, these measurements are insensitive to both base composition and chain order (single stranded vs. double stranded DNA).

In this chapter, liposomes were used to tether multiple molecules of enzyme in order to increase sensitivity of enzyme label biosensor. Liposomes are spherical vesicles, which membranes contain one or more phospholipid bilayers. The lipid molecules consist of hydrophilic head groups and hydrophobic tails; in aqueous solutions they self-organize in order to increase their solubility in the surrounding medium and minimize the surface-to-volume ratio. As mentioned in the introduction, liposomes are promising for the development of sensitive bioanalytical methods [240] because they can carry a large number of receptor molecules or can be loaded with an appreciable amount of markers due to their large surface area and internal volume. Herein, a procedure to obtain biotin-tagged liposomes has been adapted starting from procedure reported in literature [131]. These biotinylated liposomes were characterized by DLS, showing a hydrodynamic diameter of ≈150 nm. Average diameters of prepared liposomes were determined at the day of preparation and compared with those after incubation for 30 days at 4°C (stability test). Aggregation of liposomes during the stability test was negligible.
In order to confirm the presence of biotin on the vesicle surface, free streptavidin and streptavidin conjugated alkaline phosphatase were used to allow the aggregation of liposomes through biotin-streptavidin binding. Results show how hydrodynamic diameter increase in presence of both molecules. However, the measured diameter is around the double of the diameter found in absence of both molecules. This suggests that only a small fraction of the biotin binding sites of streptavidin are available to biotinylated liposomes. This may be because the size of the streptavidin is 5-6-nm, thus small if compared with the size of the liposomes. Surface geometry prevents binding of liposomes into more than one or two sites on streptavidin, giving only a dimerization instead of an aggregation. Moreover, has been reported in literature that liposomes are negatively charged, so aggregation could be limited by electrostatic repulsion of the vesicles.

As reported in figure 2.1, the assay consists in the incubation of the biotynilated hybrid immobilized on the electrode surface with streptavidin, then with the biotin-taged liposomes. The enzymatic conjugate (strept-AP) was, then, anchored trough biotin tags

present on the liposome.

It is important to note that, due to their chemical composition, the giant liposome micromembrane alters the interfacial properties of the electrode. Indeed, this alteration can be successfully followed by impedance spectroscopy. However, in order to increase the sensitivity of the assay, the liposome-modified biosensor were incubated with enzyme molecules and then with a proper enzymatic substrate. Thus, BCIP/NBT mixture was used as enzymatic substrate, since Alkaline Phosphatase stimulate the oxidative hydrolysis of the BCIP/NBT mixture to an insoluble product (figure 2.13).

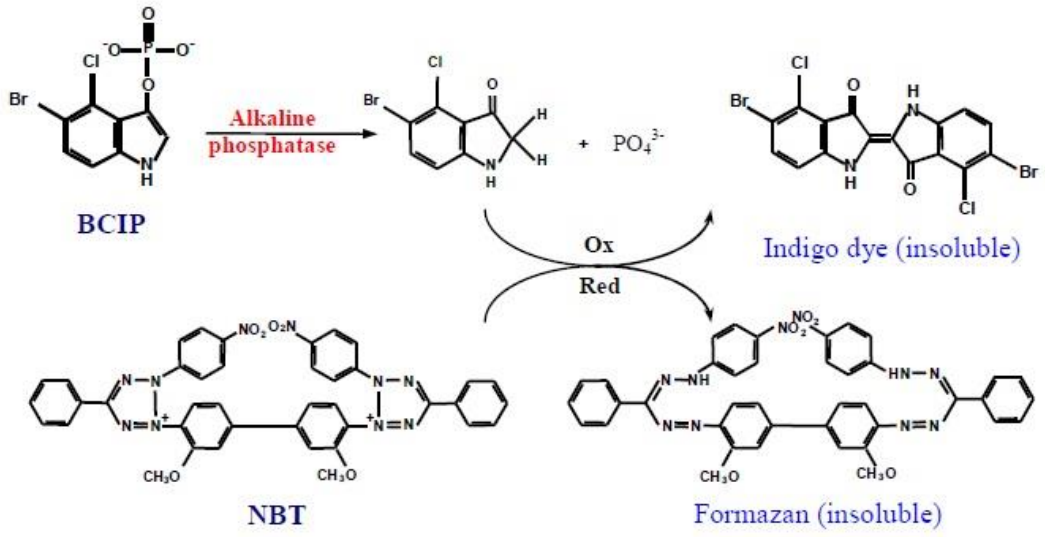

Figure 2.13 - BCIP/NBT mixture: enzymatic hydrolysis of BCIP and subsequent coprecipitation of two insoluble products.

The precipitation of this insoluble product generated an insulating layer which inhibited the interfacial electron transfer of the redox probe ($[Fe(CN)_6]^{3/4-}$) in impedance measurements. The resulting charge transfer resistance values were taken as the analytical signals. In figure 2.14 are reported the electron transfer resistances for the different steps of the assay.

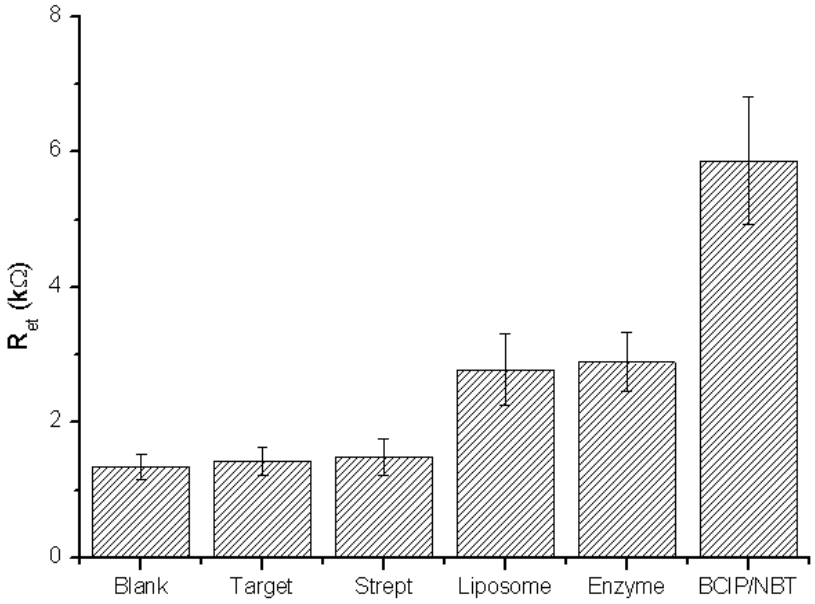

Figure 2.14 – Electron transfer resistances for the measurements corresponding to 1) probe functionalized electrode (blank); 2) after interaction with 1 nM miRNA target; 3) after treatment with streptavidin; 4) after interaction with liposome; 5) after interaction with strept-AP; 6) after interaction with the substrate. Data are recorded in 0.1 M KCl in the presence of $Fe(CN)_6^{3-/4-}$*, 5 mM (molar ratio 1:1).*

The hybridization event is accompanied by a relatively small increase of the electron-transfer resistance at the electrode. These results are consistent with the fact that the formation of the duplex on the surface electrostatically repels the redox probe, $[Fe(CN)_6]^{3/4-}$, and thus the interfacial electron transfer resistance gradually increases upon the buildup of the assembly. The association of the streptavidin, slightly increases the interfacial electron-transfer resistance, as a result of the partial hydrophobic insulation of the electrode support. On the contrary, the association of the biotin-tagged liposome substantially increases the electrode transfer resistance due to the electrostatic repulsion of the redox label with the negatively charged liposomes [131] as well as due to the hydrophobic insulation of the electrode. Furthermore, the biocatalyzed precipitation of the insulating product determines an important increase of the electron-transfer resistance.

2.4 Conclusions

Both the enzymatic assay demonstrate the possibility to increase the sensitivity of the assay in comparison with the label free scheme. In the first strategy, streptavidin conjugated alkaline phosphatase was used as enzymatic label. A sensitivity of 1.89 kΩ/nM, with an estimated detection limit of 180 pM and an average RSD of 14% was obtained. Liposomes, owing to their large surface area, are capable of carrying a large number of streptavidin conjugated alkaline phosphatase. The biotin tags provides an anchoring site that links the liposome probe to the biorecognition assembly and to enzyme molecules. Compared to the enzyme assay, the enzyme-decorated liposome assay allows a 10-fold enhancement of the electroanalytical signal using impedance spectroscopy.

Moreover, it is important to note that this method is not limited to only the hybridization assay systems, but can also be extended other applications and other enzyme linked affinity assay.

Chapter 3 – Gold Modified Screen Printed Carbon Electrodes for Enzyme Amplified Impedimetric Sensing of microRNA

Chapter 3 is an extension of the work described in Chapter 2 and reports on the complete characterization and further optimization of the electrochemical genosensor.

In particular, a procedure to modify the screen-printed carbon electrode surface by gold electrodeposition has been optimized. Gold-nanostructuration of the transducer surface allows oriented immobilization and spacing of DNA probes at the electrode surface whilst at the same time enhances transducer sensitivity.

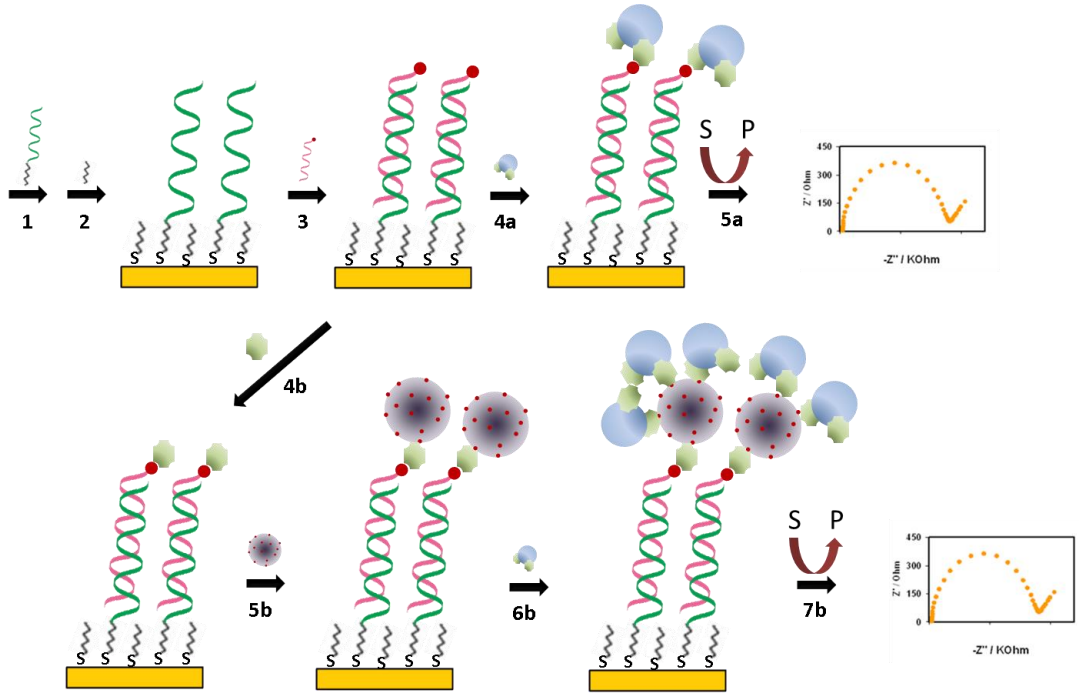

Figure 3.1 - Illustration of the different assay schemes. The biotinylated hybrid is formed on the gold electrode surface (1,2,3). Streptavidin-Alkaline Phosphatase is added (4a). After incubation of the proper substrate, enzymatic product is revealed by EIS (5a). Otherwise, streptavidin (4b) and biotinylated liposomes (5b) are added. The liposome-modified hybrid is then exposed to streptavidin-Alkaline Phosphatase (6b). After incubation of the substrate, the enzymatic product is revealed by EIS (7b).

Enzyme decorated liposomes are herein investigated for signal amplification in the electrochemical detection of miRNAs. The proposed method is based on thiolated DNA capture probes immobilized onto gold nanostructured carbon surfaces. The capture-probe-modified electrode is, then, allowed to react with the analyte (the target miRNA). Enzyme and Enzyme-decorated liposomes are used as labels to amplify the miRNA-sensing, by their association to the probe-miRNA hybrid generated onto the transducer (figure 3.1). Faradaic impedance spectroscopy was employed to characterize this amplification route.

Immobilization of the thiol-tethered DNA probe was qualitatively and quantitatively investigated by means of faradic impedance spectroscopy. Electrochemical transduction of the hybridization process was also performed by means of faradic impedance spectroscopy with an enzyme-amplified detection scheme, based on the coupling of a streptavidin-alkaline phosphatase conjugate and biotinylated target sequences (figure 3.1). Streptavidin-alkaline phosphatase conjugate catalyzes precipitation of an insoluble and insulating product onto the sensing interface increasing the resistance to the electron transfer, used as analytical signal. In a first approach a direct streptavidin conjugated enzyme binding to the hybrid formed with the interaction of biotinylated target sequence with DNA probe immobilized on the surface was used. In a second approach, biotin-tagged liposomes were used as functional tethers for streptavidin enzyme conjugates. Owing to their dimension in the nanoscale and thus to their large surface area they are capable of carrying a large number of enzyme molecules.

The two strategies have been characterized in term of analytical parameters and results, here, reported.

3.1 Material and methods

3.1.1 Reagents

Dithiothreitol (DTT), 6-mercapto-1-hexanol (MCH), streptavidin–alkaline phosphatase (S2890, Strept-AP, 2:1 conjugation stoichiometry), streptavidin (S4762, Strept), diethyl pyrocarbonate (DEPC), 1-naphthyl phosphate, 5-bromo-4-chloro-3-indolyl phosphate (BCIP), BCIP/nitro blue tetrazolium mixture [BCIP/NBT (cat. no. B-1911)], bovine serum albumin (BSA), Tris–HCl, diethanolamine (DEA), dimyristoylphosphatidylethanolamine (DMPE), distearoylphosphatidyl choline (DSPC) and cholesterol were obtained from Sigma–Aldrich (Milan, Italy). Biotin-XDHPE was obtained from Invitrogen Molecular Probes (Eugene, OR). Disodium

hydrogenphosphate, potassium hexacyanoferrate (III and II), sulphuric acid, magnesium and potassium chloride were purchased from Merck (Milan, Italy). NAP-10 columns of Sephadex G-25 were obtained from Amersham Pharmacia Biotech (Uppsala, Sweden). MilliQ water (DEPC treated for RNA analysis) was used throughout this work. Synthetic oligonucleotides were obtained from MWG Biotech AG (Germany):

Probe (DNA-SH): 5' GAG-ACC-CAG-TAG-CCA-GAT-GTA-GCT – SH 3'
Target: 5' AGC-UAC-AUC-UGG-CUA-CUG-GGU-CUC –biotin 3'
Non-complementary: 5′ UAG-CAG-CAC-GUA-AAU-A-biotin-3′

Prior to use, the thiol-modified oligonucleotides were treated with DTT. This reagent allowed reduction and cleavage of oligo dimers eventually obtained by oxidative coupling of two DNA-SH molecules (i.e. DNA-S-S-DNA). The lyophilized oligonucleotides were dissolved in a 10 mM Tris-HCl buffer solution (pH 8.3) containing 20 mM of DTT. The reaction was allowed to proceed for 2 h at room temperature. The thiolated DNA was then purified by elution through a NAP-10 column of Sephadex G-25 using 0.5 M phosphate buffer (pH 7.4). DNA-SH stock were prepared in the same buffer and stored frozen.

3.1.2 Liposome Preparation

Liposomes were prepared as described in paragraph 2.1.2.

3.1.3 Electrochemical measurement

All electrochemical measurements were performed with an AUTOLAB PGSTAT 10 digital potentiostat/galvanostat. The GPES 4.9004 software (Eco Chemie BV, Utrecht, The Netherlands) was used for cyclic voltammetry; the FRA2 module was used for faradaic impedance experiments. All potentials were referred to the screen-printed silver pseudo-reference electrode; the experiments were carried out at room temperature. Faradaic impedance measurements were carried out in the presence of 5 mM $[Fe(CN)_6]^{3/4-}$ redox probe (equimolecular mixture in 0.1 M KCl). An alternative

voltage of 10 mV in amplitude (peak to peak), within the frequency range 100 kHz–10 mHz, was superimposed to the applied bias potential. The dc potential was set up at +0.13 V, the formal potential of the $[Fe(CN)_6]^{3/4-}$ redox probe. Experimental spectra, presented in the form of complex plane diagrams (i.e., Nyquist plots), were fitted with proper equivalent circuits using the facilities of the FRA2 software 4.9004 (EcoChemie). Both charge transfer resistance and Δ charge transfer resistance values were taken as analytical signals. The modified Randles circuit was successfully applied to fit data acquired.

3.1.4 Electrode modification by gold electrodeposition

The screen-printed electrochemical cell consisted of a planar, three electrodes strip, based on a carbon (or gold) working electrode, a carbon counter electrode and a silver pseudoreference electrode. Materials and procedures to screen-print the electrode transducers are described previously published papers [81]. Prior to immobilization of the thiol-tethered DNA probe, carbon working electrodes were modified with gold by potential-sweeping electrodeposition, through Cyclic Voltammetry (CV) with the following fixed parameters [16]: a scan rate of 50 mV/s, a cathodic switching potential of -0.6 V and an anodic switching potential of +1.5 V. Cycle number of potential scan and the Au(III) concentration in solution were optimized in order to obtain the better surface and morphology for the genosensor. The voltammetric behavior of Au(III) has been studied at a screen printed carbon electrodes (SPCEs) in a 0.01 M Na_2SO_4, 0.01 M H_2SO_4, and 1 mM $HAuCl_4 \cdot 3H_2O$ solution.

3.1.5 Probe immobilization

The gold modified working electrode surface of these planar sensors was exposed to the thiolated oligonucleotide solution (10 μL, 2 μM in 0.5 M phosphate buffer, pH 7). Chemisorption was allowed to proceed overnight (≈16 h) with electrodes stored in Petri dishes to protect the solutions from evaporation. The immobilization step was followed by treatment with a spacer thiol. A 10 μL drop of 1 mM aqueous solution of MCH was placed onto the probe-modified surfaces for 1h. Prior to the hybridization reaction, the modified electrodes were washed twice with 30 μL of phosphate buffer.

3.1.6 Hybridization procedure

Hybridization experiments were carried out using biotinylated target sequences in a direct format. Probe-modified gold electrodes were exposed to a 10 µL drop of the biotinylated target sequence solution (in 0.5 M phosphate buffer) for 20 min. A biotinylated non-complementary sequence was used as the negative control. After hybridization, the sensors were washed twice with 30 µL of diethanolamine 0.1 M, $MgCl_2$ 1 mM, KCl 100 mM; pH 9.6 (DEA buffer) in the case of strept-AP assay or with 0.1 M phosphate buffer, pH 7.4 (PB) in the biotin-tagged liposome assay scheme.

3.1.7 Labeling and EIS detection

Strept-AP-based assay: the biotinylated hybrid was reacted with 10 µL of a solution containing 0.8 U/mL of strept-AP conjugate and 10 mg/mL of BSA (as the blocking agent) in DEA buffer. After 20 min, the sensors were washed twice with 30 µL of DEA buffer. The enzyme-modified surfaces were then incubated with 30 µL of the BCIP/NBT mixture for 20 min. After precipitation of the insoluble and insulating product and prior to impedimetric measurements, the sensors were washed with 0.1 M KCl for 10 s.

Enzyme-decorated Liposome assay: The biotinylated hybrid obtained at the electrode surface was reacted with a 10 µL drop solution containing 0.05 mg/L of streptavidin in PB. After 20 min, the genosensors were washed twice with 30 µL of HEPES buffer and were then reacted with liposome solution (20 min, room temperature). The final configuration was reacted with a 10 µL drop solution containing 0.8 U/mL of the streptavidin–alkaline phosphatase conjugate and 10 mg/mL of BSA in DEA buffer. After 20 min, genosensors were washed twice with 30 µL of DEA buffer. The enzyme-liposome-modified surfaces were then incubated with 30 µL of the BCIP/NBT mixture for 20 min. After precipitation of the insoluble and insulating product and prior to impedimetric measurements, the sensors were washed with 0.1 M KCl for 10 s. Each result is the mean and standard deviation of at least three measurements.

3.1.8 SEM-EDX Characterization of sensor surface

Scanning electron microscopy (SEM) was performed on uncoated samples using a field emission scanning microscope ΣIGMA (Carl Zeiss Microscopy GmbH, Germany). The images were acquired using the in-lens secondary electron detector with an acceleration potential of 8 kV at a working distance of 8.4 or 8.5 mm and using the BSD detector with an acceleration potential of 9 kV at a working distance of 8.4 or 8.5 mm. The elements contained into the matrix were determined using energy-dispersive X-ray spectroscopy (EDX) that was performed by using a 10 mm^2 silicon drift detector (X-Act) coupled with the SEM microscope operated by the INCA software (Oxford Instruments). In this second case, the operative voltage of the electron source was about 9 kV and the working distance was 8.5 mm to maximize the X-ray photon counts. Prior to SEM imaging, samples were thoroughly rinsed with Milli-Q water and dried underpressure in a vacuum desiccator with a standard membrane pump for few hours.

3.2 Results

3.2.1 Gold electrodeposition on screen printed carbon electrodes

Cyclic voltammograms (CVs) for the electroreduction of a solution of 1 mM $HAuCl_4 \cdot 3H_2O$, in 0.01 M Na_2SO_4 and 0.01 M H_2SO_4 at a SPCE are shown in figure 3.2. On the negative sweep of the first scan (from +1.5 V to –0.6 V vs. silver pseudo reference) a broad reduction peak is observed at +0.16 V, indicating the reduction of Au(III) to Au(0) inducing the deposition of nanoparticles onto the electrode surface.

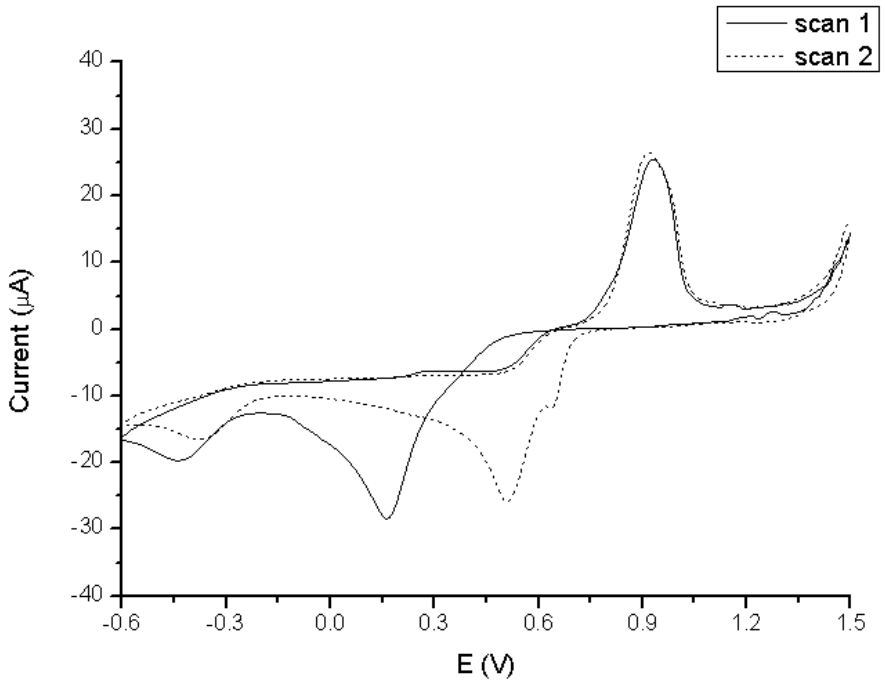

Figure 3.2 – Cyclic voltammetry in 1 mM $HAuCl_4 \cdot 3H_2O$, 0.01 M Na_2SO_4 and 0.01 M H_2SO_4 solution at a SPCE. Potential scan: from +1.5 to -0.6 V; step potential = 2.44 mV; scan rate = 50 mV/s.

On the reverse sweep, a current crossover is observed at +0.63 V which is indicative of nucleation growth kinetics. This is followed by a large anodic process (near +0.9 V) due to both electrodissolution of Au(0) and the formation of an oxide layer on the electrodeposited gold (solid line in figure 3.2).

On the second scan, it can be seen that there is a large positive shift (from +0.16 to +0.51 V) in the onset for Au(III) reduction due to nucleation sites created on the first scan. There is also a cathodic peak at +0.64 V characteristic of the reduction of gold oxide formed in the first scan when the potential was scanned to 1.5 V. In addition, no current crossover was observed after the first scan (dashed line in figure 3.2).

The concentration of $HAuCl_4$ and the number of cycles for the electrodeposition of gold on the electrode surface play an important role for the morphology, size and uniformity of particles [241]. Figure 3.3 shows the influence of these variables by analyzing the electron transfer resistance values (R_{et}) of a redox probe by EIS measurement.

The number of cyclic potential scans of the electrodeposition step were varied from 1 to 15 and optimal number of scans was assessed by EIS measurement of the electron transfer resistance of a redox probe. Thus, after each electrodeposition scan, the sensor

is rinsed with deionized water and then exposed to a 5 mM $[Fe(CN)_6]^{3/4-}$ redox probe (1:1 mixture in 0.1M KCl) solution and the impedance spectra recorded.

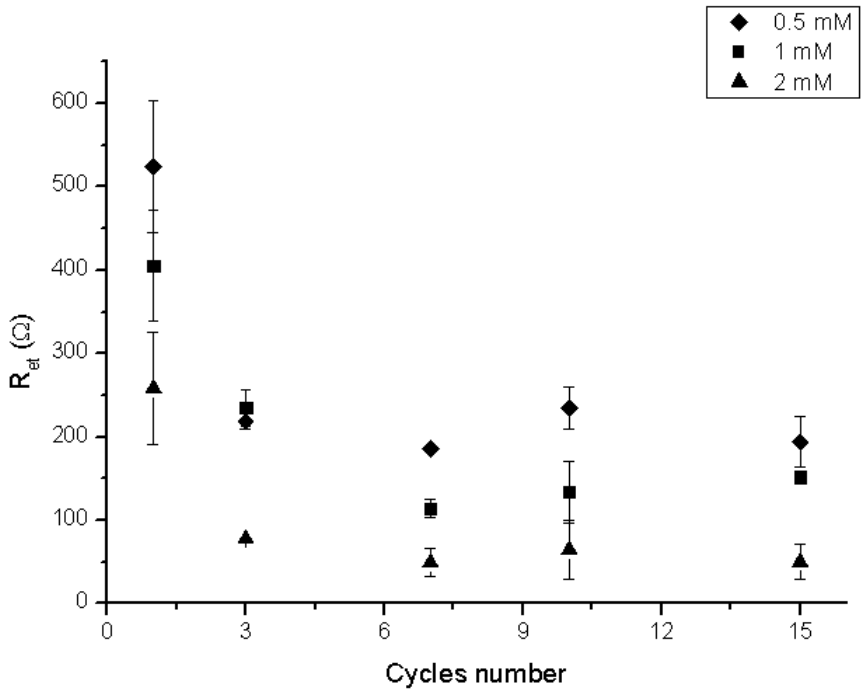

Figure 3.3 – Electron transfer resistance recorded on screen printed carbon electrodes modified varying cycles number (1, 3, 7, 10, 15) and Au(III) concentration (0.5, 1 and 2 mM 0.01 M Na_2SO_4 and 0.01 M H_2SO_4). All other experimental condition are the same reported in figure 3.2. Each point represents the mean of at least three measurements and the error bars the corresponding standard deviation.

The electron transfer resistance decreases with increasing the cycle number of potential scan (figure 3.3), reaching a constant value after 7 cycles (an R_{et} value of 54.8±8.6 Ω, 133.4±19.0 Ω and 205.0±26.0 Ω for 2 mM, 1 mM and 0.5 mM Au(III) concentration respectively). Based on shortening the time necessary for electrodeposition, the number of potential scans for electrodeposition was determined to be 7 in the following experiments. The $AuCl_4^-$ concentration was varied in the range 0.5 - 2.0 mM, obtaining a decrease of R_{et} increasing the Au(III) concentration. However, as reported in literature [241], the most homogenous deposits have been obtained using low Au(III) concentrations. This data was also confirmed by SEM morphological studies. For this reason, an $AuCl_4^-$ concentration of 1 mM was chosen as compromise among R_{et} value and morphology of the surface.

3.2.2 Electrochemical characterization of the sensor surface

The resulting modified electrodes (AuSPCEs) were then characterized using CV in 0.5 M H_2SO_4. Figure 3.4a (dashed line) shows the electrochemical response of the AuSPCE electrode scanning between +0.2 and +1.4 V. The presence of a broad oxidation peak is indicative of the formation of several kinds of Au ‘‘oxides’’ resulting from a very complicated sorption mechanism of OH^- ions onto different crystallographic faces [156, 242].

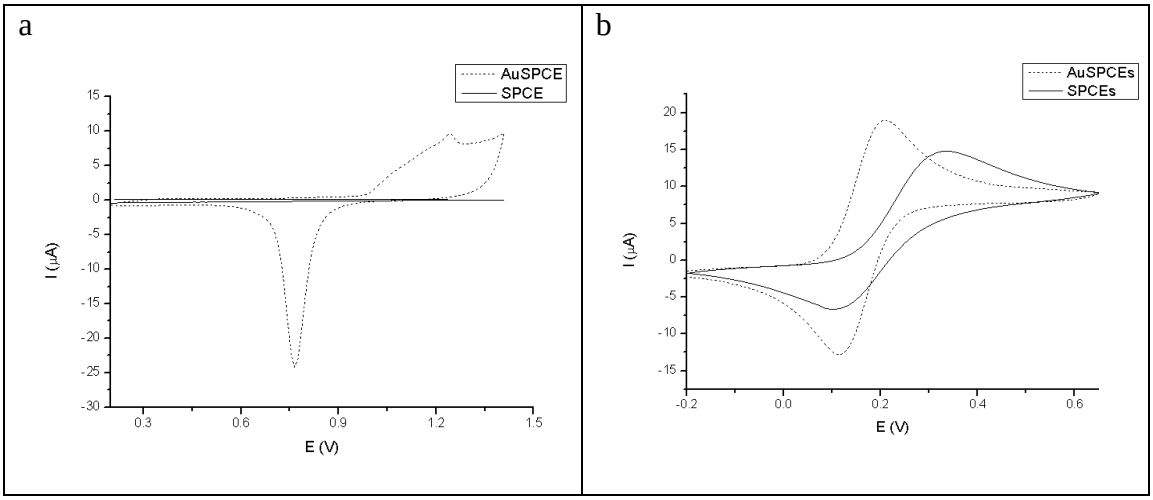

Figure 3.4 – a) Cyclic voltammetric signal of SPCE (solid line) and AuSPCE (dashed line) in 0.5 M H_2SO_4. Potential scan: from 0.2 to +1.4 V; step potential = 2.44 mV; scan rate = 100 mV/s. b) Cyclic voltammetric signal of SPCE (solid line) and AuSPCE (dashed line) in 5 M $Fe(CN)_6^{4-}$ (0.1 M KCl supporting electrolyte). Potential scan: from –0.2 to +0.65 V; step potential = 2.44 mV; scan rate = 10 mV/s.

On the reverse sweep, the peak at +0.76 V corresponded to the subsequent reduction of the oxides previously formed. In order to confirm the presence of gold on the carbon surface, a CV in 0.5 M H_2SO_4 was performed using unmodified screen printed carbon electrode (solid line in figure 3.4a).

The recorded charge under the reduction peak was used for the characterisation of the electroactive electrode area [176]. Assuming 482 μC/cm^2 to be the charge required for the reduction of a monolayer of oxides on polycrystalline gold electrodes [235] and calculating the area of the peak 23.64 ± 1.16 μC at +0.76 V, an electrochemically active area of 4.90 ± 0.24 mm^2 was calculated (RSD 4.9% n= 5). Furthermore, the electrochemically active surface of the Au-SPCEs was also evaluated by CV in presence of the 5 mM ferrocyanide in 0.1 M KCl (dashed line in figure 3.4b) with the

same procedure reported in chapter 2 using the Randles-Sevcik equation. An electrochemically active surface of 4.87 ± 0.16 mm^2 for SPCEs modified with 7 cycles in 1 mM of Au(III) was calculated from the results (geometrical area = 7.07 mm^2). This value was in good agreement with that previously evaluated. Additionally, the small relative standard deviation (RSD) found for these measurements (3.27 % [n= 5]) indicated the good reproducibility of the gold electrodeposition.

3.2.3 Surface Characterization of Electrodeposited Gold using SEM and EDX

Information on the shape and size of gold deposits was obtained by SEM observations. The SEM micrographs were analyzed with Image J Software (http://imagej.nih.gov/ij/) to obtain the information about particle size distribution. Figure 3.5 shows typical SEM micrographs of the bare SPCE (A) and AuSPCE (electrodeposited from 1 mM Au(III) solution) (B). Au was electrodeposited following the CV optimized conditions reported above. The SEM images confirm the formation of nanosized gold cluster with an average size of 65.1 ± 38.4 nm (figure 3.6) on the carbon surface. The electrodeposited gold can be separated into two distinct populations: the first one is related to small and spherical-shaped NPs and the second one to larger, aggregate-like NPs. Au-deposits were absent in the negative control (the unmodified carbon surface). In order to further characterize the Au-deposits, SEM analyses were carried out for two different concentration of Au(III). An increase in the particle density and in average size as a function of the Au(III) concentration was observed (figure 3.5C and D) illustrating a gradual coalescence phenomenon [241]. Electrode surface element analysis by EDX of the Au-SPCE was also performed.

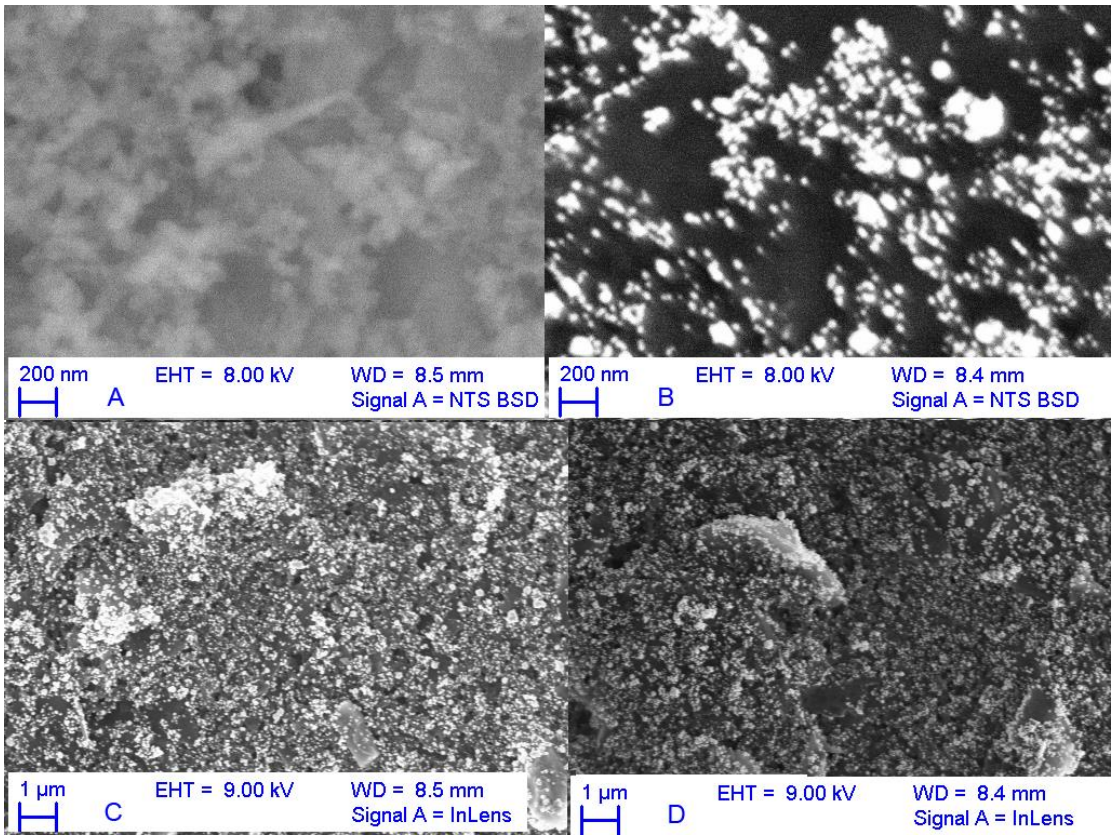

Figure 3.5 - SEM image of bare (A) and 1 mM gold modified (B) screen-printed carbon electrode prepared in experimental conditions as reported in the text using BSD detector; SEM image of 2 mM (C) and 1 mM gold modified (D) screen-printed carbon electrode prepared in experimental conditions as reported in the text using InLens detector.

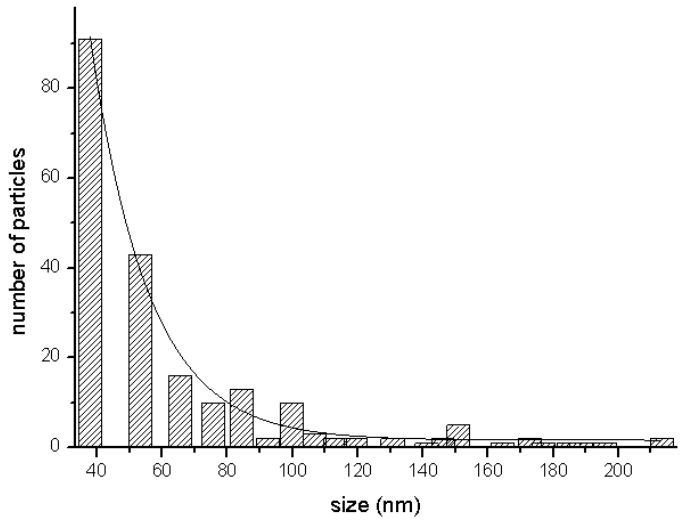

Figure 3.6 – Size distribution (radius) of clusters analyzed through the SEM image obtained on a SPCE modified with 1 mM Au(III) electrodeposition solution.

In tables 3.1 are reported the results. Analyses were carried out on two sets of electrodes in an attempt to determine the presence of gold.

	SPCE	1mM Au-SPCE	2mM Au-SPCE
C	92.91	85.16	77.87
O	3.17	2.44	2.03
Cl	3.91	2.69	3.81
Au	-	9.71	16.29

Table 3.1A – Weight% EDX analysis of elements of a big area of the electrode

	SPCE	1mM Au-SPCE	2mM Au-SPCE
C	96.16	96.23	95.34
O	2.47	2.07	1.86
Cl	1.37	1.03	1.58
Au	-	0.67	1.22

Table3.1B – Atomic% EDX analysis of elements of a big area of the electrode

	SPCE	1mM Au-SPCE	2mM Au-SPCE
C	96.83	86.71	91.25
O	1.85	-	-
Si	0.32	-	-
Cl	0.99	-	-
Au	-	13.29	8.75

Table 3.1C - Weight% EDX analysis of elements of a point of the electrode

	SPCE	1mM Au-SPCE	2mM Au-SPCE
C	98.11	99.07	99.42
O	1.40	-	-
Si	0.14	-	-
Cl	0.34	-	-
Au	-	0.93	0.58

Table 3.1D - Atomic% EDX analysis of elements of a point of the electrode

One set of electrodes was used as a negative sample and was not expected to contain

gold because it underwent CV in 10 mM H_2SO_4. The other electrode underwent gold electrodeposition and might exhibit a gold peak. Results confirm that the main components of the AuSPCE electrode surface are C and Au, with traces of chloride, silicon and oxygen.

The presence of Si, O and Cl elements is due to the screen-printing ink composition, according to the information provided with the ink by the manufacturer. In particular, quartz (SiO_2) is present in the ink as mineral filler whereas the chlorine peak is due to the presence of vinyl chloride and acrylate copolymer, the binder used in the printing process. EDX analysis also confirms that gold deposits are dependent from the Au(III) concentration of the electrodeposition solution: both weight and atomic analysis confirm an increasing of gold with a 2 mM Au(III) solution.

3.2.4 Optimization of the impedimetric genosensor

Electrode surfaces with lower probe densities show a limited number of biorecognition sites, whereas higher surface densities can cause steric and electrostatic interference between packed probes and the incoming target and liposomes.

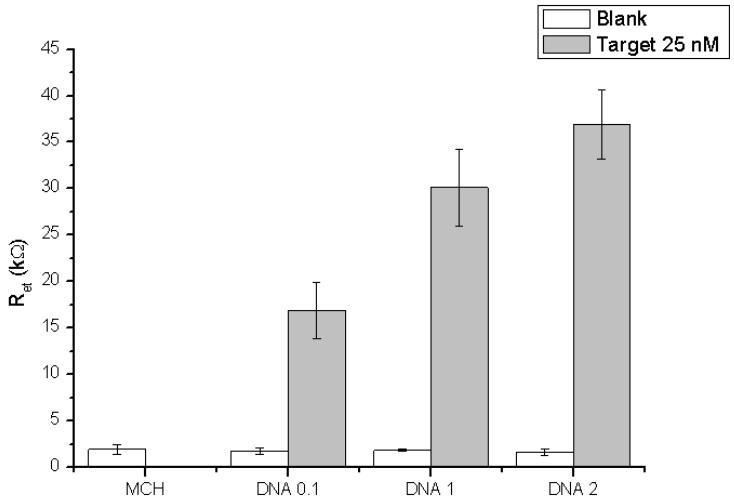

Figure 3.7 - Influence of probe concentration on hybridisation reaction. 0.1, 1 and 2 µM in 0.5 M phosphate buffer of DNA-SH were tested with exposure of the modified surface to a blank solution or 25 nM target concentration. Other conditions as described in the materials and methods section. The bars are the average of at least three measurements and the error bars the corresponding standard deviation.

The optimal surface coverage was then experimentally assessed by varying the capture probe concentration in a range between 0.1 and 2 μM. The higher hybridization yields were obtained with electrodes modified with 2 μM of the thiolated probe solution (figure 3.7) and thus this concentration was used for further measurements. Electrochemical measurements were also performed in order to evaluate the effect of hybridization time (figure 3.8).

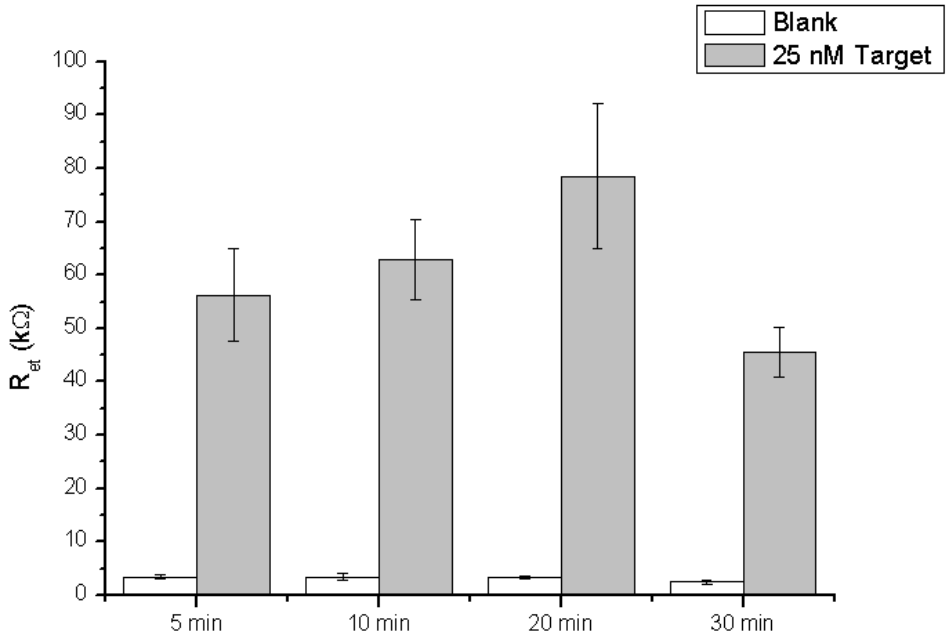

Figure 3.8 - Influence of hybridization time reaction. 2 μM in 0.5 M phosphate buffer of DNA-SH was tested with exposure of the modified surface to a blank solution or 25 nM target concentration fr 5, 10, 20 and 30 min. Other conditions as described in the materials and methods section. The bars are the average of at least three measurements and the error bars the corresponding standard deviation.

The higher hybridization yields were obtained with electrodes modified with 2 μM of the thiolated probe solution exposed for 20 min to complementary sequence and thus this time was used for further measurements.

3.2.5 Liposome assay optimization

In order to further optimize the analytical assay, the influence of the liposome concentration on electrochemical signals were investigated.

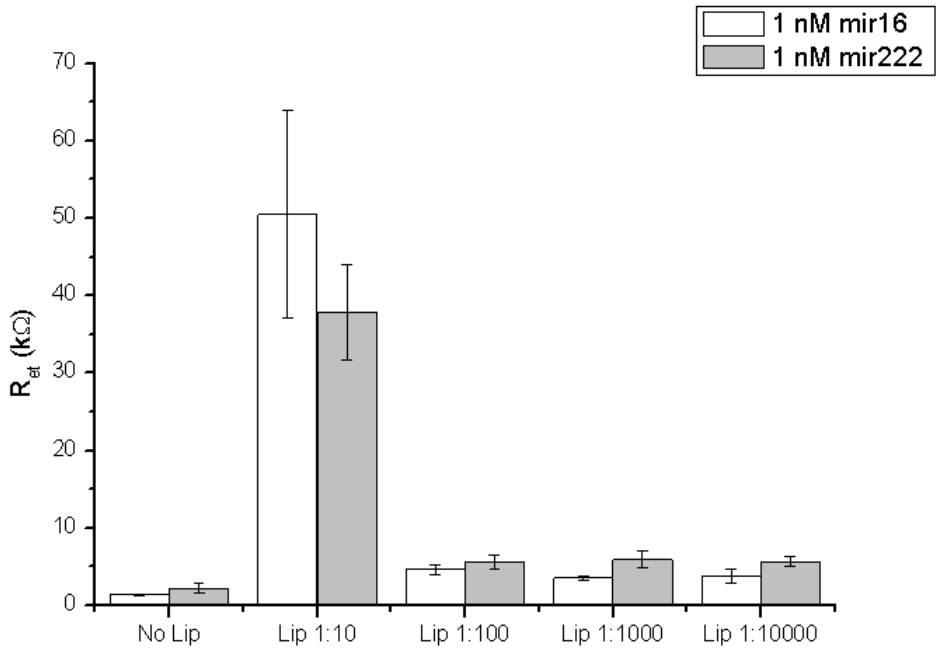

Figure 3.9 - Influence of liposome dilution on the analytical signals registered in liposome enzymatic assay. A comparison with enzymatic assay is also showed. Probe-modified sensors were exposed to a 10 µL drop of non-complementary sequence solutions (blank) and biotinylated complementary target sequence solutions (target 1 nM in phosphate buffer) for 20 min. Biotinylated hybrid was then exposed to a 0.5 mg/L streptavidin solution in phosphate buffer for 20 min. Different liposome dilutions (1:10, 1:100, 1:1000 and 1:10000 in HEPES buffer) were incubated for 20 min. After labelling with the streptavidin-alkaline phosphatase conjugate (0.8 U/mL), the sensors were exposed to 30 µL of BCIP/NBT mixture for 20 min. Further details are available in the Materials and Methods section. The bars are the average of at least three measurements and the error bars the corresponding standard deviation.

A series of sensors was exposed to increasingly liposome dilutions (1:10, 1:100, 1:1000 and 1:10000 in HEPES buffer) while keeping constant streptavidin and enzyme concentration. Experimental data, summarized in figure 3.9, show how both the signal due to the nonspecific adsorption of the liposome and that due to its specific coupling with the biotinylated hybrid changed with the dilution. These results suggested that optimal analytical signal (compatibly with minimal aspecific signal) could be achieved using 1:1000 dilution. This value was used for all subsequent experiments.

3.2.6 Calibration Curves

A non-complementary target (miRNA-16) at concentrations of 50, and 100 pM was analyzed on a thiolated capture probe layer formed after gold electrodeposition deposition. The non-complementary control target sequence was biotynilated but was otherwise non-complementary to the immobilized capture probe. All the concentrations tested gave a similar impedrimetic signal (ΔR_{et} 0.10 ± 0.01 kΩ), comparable to the phosphate buffer measurement, demonstrating that the non-complementary amplicon has no cross reactivity with the electronucleated immobilized capture probes and did not interact non specifically with the unprotected SPCE. To demonstrate the analytical performances of the label based impedimetric assay a calibration experiment was designed for both assays (figure 3.10 and 3.11). When analyzing synthetic target solutions whose concentration was increased by orders of magnitude, a linear response were observed until a plateau was achieved.

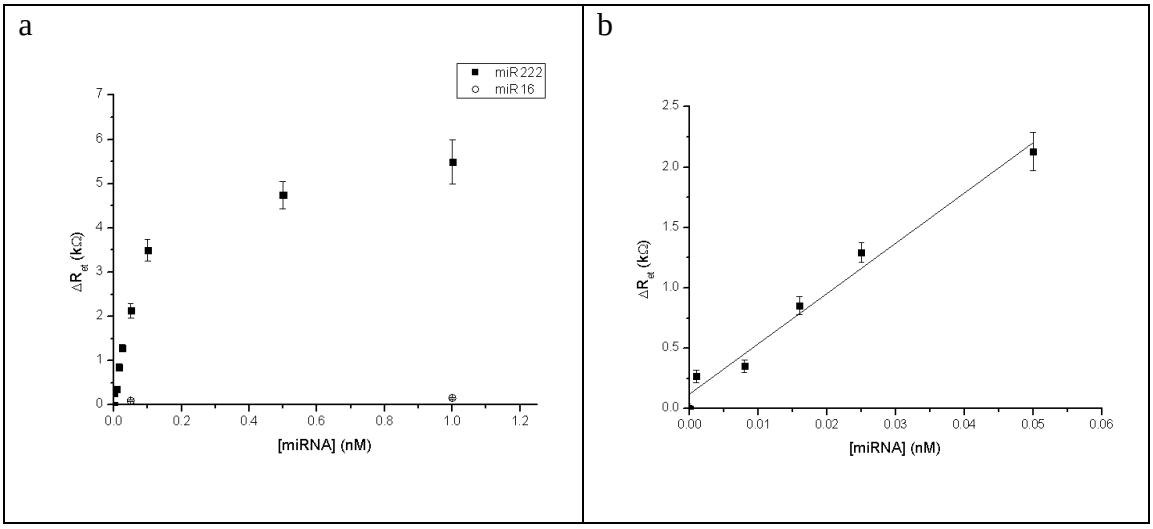

Figure 3.10 – a) Calibration plot for synthetic oligonucleotides from 0 to 1 nM miRNA-222 concentration.0.05 and 1 nM miRNA-16 was exposed to probe modified electrode as negative control; b) Calibration plot in the low concentration range (0, 0.001, 0,008, 0.016, 0.025 and 0.05 nM of miRNA-222).Further details are available in the materials and methods section. Each point represents the mean of at least three measurements and the error bars the corresponding standard deviation.

In the streptavin alkaline phosphatase conjugated assay, the analytical signals varied linearly (R^2 = 0.975) with the target concentration from 0 to 0.05 nM (figure 3.11b). Signals leveled off for higher concentrations, indicating that saturation of all available

probes was achieved; moreover, the non-specific signal of biotinylated non-complementary oligomers was negligible up to 1 nM. Within the linear analytical range, the sensitivity was 41.6 kΩ/nM, with an estimated detection limit of 1 pM and an average RSD of 15%.

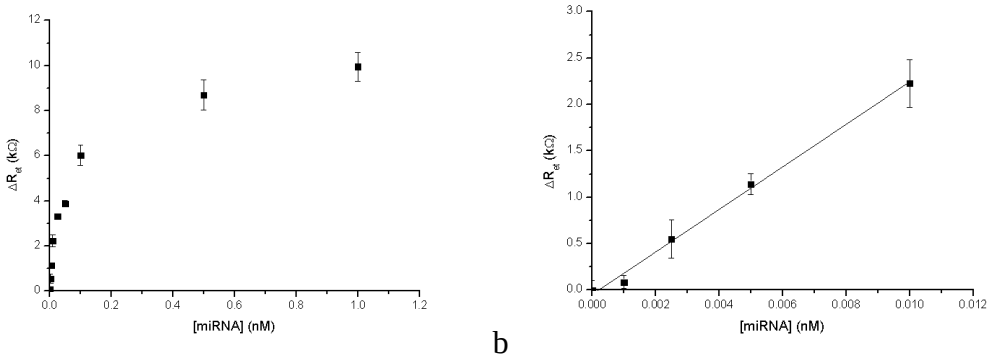

a b

Figure 3.11 – a) Calibration plot for synthetic oligonucleotides from 0 to 1 nM miRNA-222 concentration; b) Calibration plot in the low concentration range (0, 0.001, 0,0025, 0.005 and 0.01 nM of miRNA-222).Further details are available in the materials and methods section. Each point represents the mean of at least three measurements and the error bars the corresponding standard deviation.

In the liposome assay, the genosensor response varied linearly ($R^2 = 0.994$) with the target concentration between 0 pM to 10 pM (figure 3.11b). Signals leveled off for higher concentrations, indicating that saturation of all available probes was achieved; moreover, the non-specific signal of biotinylated non-complementary oligomers was negligible up to 1 nM (data not shown). Within the linear analytical range, the sensitivity was 229.1 kΩ/nM, with an estimated detection limit of 0.6 pM and an average RSD of 18%.

3.3 Discussion

In the present chapter the use of Alkaline Phosphatase-decorated liposome as label for the impedimetric detection of miRNA was proposed using screen printed carbon electrodes modified with gold nanoclusters by electrodeposition. Liposomes prepared and optimized as described in chapter 2 has been used in the present work. These biotin tagged liposomes were exposed to the biotinylated hybrid formed on the electrode

surfaces and then to streptavidin-alkaline phosphatase. Furthermore, since transducer surface gold nano-structuring presents an excellent potential for the optimal oriented immobilization and spacing of DNA probes at the electrode surface whilst at the same time enhancing transducer sensitivity, it has been optimized a procedure to nanostructure the screen-printed carbon electrode surface by gold electrodeposition. The capture probe is immobilized on the nanostructured surface with the well-known chemistry of thiols. The capture-probe-modified electrode is, then, allowed to react with the analyte (the target biotinylated miRNA). Then, the biotinylated hybrid is exposed to the enzyme-decorated liposomes. The product of the enzymatic reaction was then electrochemically monitored using impedance spectroscopy.

The number of cyclic potential scans of the electrodeposition step were varied from 1 to 15 with Au(III) concentration and optimal parameters were assessed by EIS measurement of the charge transfer resistance of a redox probe. Modified sensors with optimized procedure for nanostructuration with gold, where then characterized by electrochemical, SEM and EDX experiments. CV in H_2SO_4 and EDX confirm the presence of gold in treated electrodes. For all these experiments unmodified screen printed electrodes were used as negative control. Microscopy allows to determinate the size distribution, showing the presence of some aggregate, but with an high concentration of small particles with radius minor than 100 nm.

In figure 3.12 are reported the electron transfer resistances for the different steps of the assay.

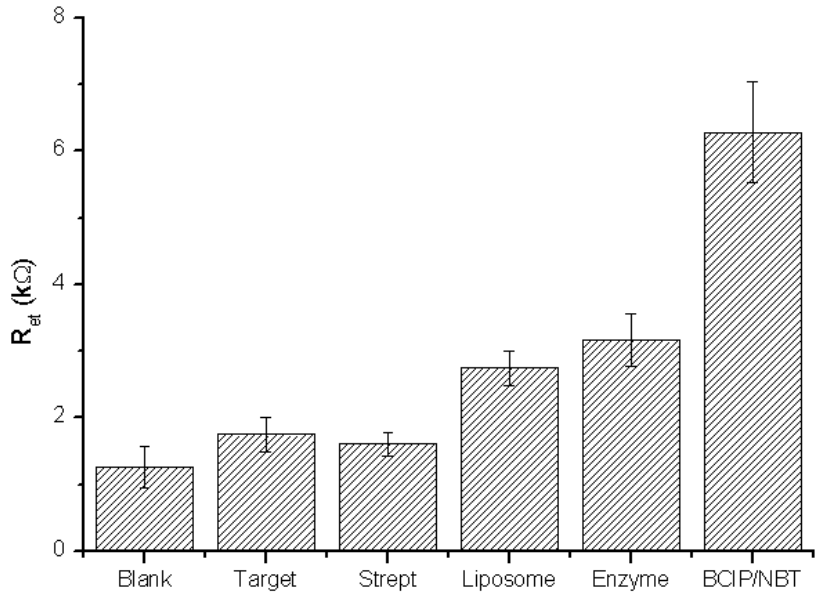

Figure 3.12 – Electron transfer resistances for the measurements corresponding to 1) probe functionalized electrode; 2) after interaction with 1 nM miRNA target; 3) after treatment with streptavidin; 4) after interaction with liposome; 5) after interaction with strept-AP; 6) after interaction with the substrate. Data are recorded in 0.1 M KCl in the presence of $Fe(CN)_6^{3-/4-}$*, 5 mM (molar ratio 1:1).*

The hybridization event is accompanied by a relatively small increase of the electron-transfer resistance at the electrode. These results are consistent with the fact that the formation of the duplex on the surface electrostatically repels the redox probe, $[Fe(CN)_6]^{3/4-}$, and thus the interfacial electron transfer resistance gradually increases upon the buildup of the assembly. The association of the streptavidin, slightly decreases the interfacial electron-transfer resistance. On the contrary, the association of the biotin-tagged liposome and enzyme alter the electrode transfer resistance, probably due to the beared negative charge. Furthermore, the biocatalyzed precipitation of the insulating product determines an important increase of the electron-transfer resistance.

3.4 Conclusions

Both the assays studied demonstrate the possibility to increase the sensitivity of the assay in comparison with the label free scheme. In the first strategy, streptavidin conjugated alkaline phosphatase is bound to the biotinylated hybrid causing the formation of an enzyme rich network. This signal amplification produces a sensitivity of

41.6 kΩ/nM, with an estimated detection limit of 1 pM and an average RSD of 15%. This higher sensitivity was attributed to the biocatalytic product used as biorecognition element for the hybridization event. Another hypothesis is the increased probe density immobilized on the surface. In order to confirm two different experiment were performed: a chronocoulometric detection and EDX measurements. Both measure failed. Chronocoulometric detection gives high aspecific signals, probably due to the adsorbion on ruthenium complex on graphite. The EDX measurement was performed in order to quantify probes through the sulfur atom of the thiolated capture probe. Unfortunately, sulfur was also present on the negative control, probably due to the electrodeposition process made in presence of sulfuric acid.

In the second strategy biotin-tagged liposomes have been tested. Liposomes, owing to their large surface area, are capable of carrying a large number of streptavidin conjugated alkaline phosphatase. The biotin tags provides an anchoring site that links the liposome probe to the biorecognition assembly and to enzyme molecules. Compared to enzyme assay, liposome assay allows a 5-fold enhancement of the electroanalytical signal using impedance spectroscopy.

In summary both the strategies seems interesting for signal amplification. Moreover, it is important to note that this method is not limited to only the hybridization assay systems, but can also be extended other applications and other enzyme linked affinity assay.

Chapter 4 – Label-Free impedimetric detection of miRNA using biotinylated conducting polymer modified electrodes

This chapter describes the development of a label-free genosensor using screen printed electrodes. Conducting polymer of biotinylated bis(2,2′-bithien-5-yl)methane is herein investigated as recognition unit of a biosensor for selective electrochemical detection of miRNAs sequences. This monomer was potentiodynamically polymerized to form films on the surface of screen printed electrodes for the EIS transduction. On top of these films, streptavidin was immobilized by complexing the biotin moieties of the polymer. Finilly, recognizing biotinylated oligonucleotide capture probe was immobilized by complexing the surface-immobilized streptavidin. This structure served as recognition element of the complementary miRNA sequence via hybridization event. Faradaic impedance spectroscopy was applied to characterize these amplification routes.

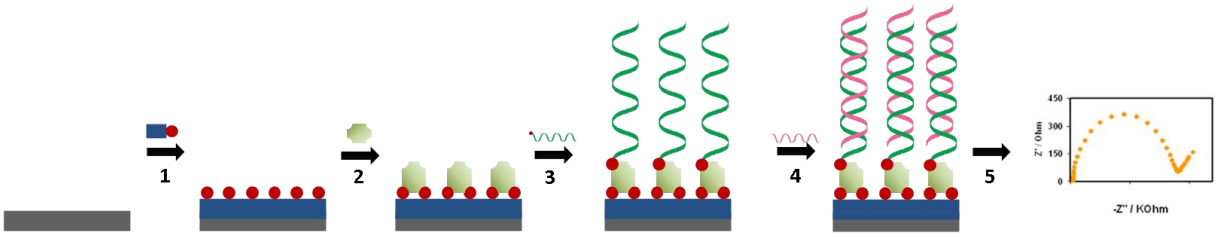

Figure 4.1 - Illustration of the assay scheme. Electrode surface is exposed to a biotinylated monomer water solution and electropolymerization is started (1). The biotinylated film is then exposed to a streptavidin solution (2). Biotinylated DNA capture probe is immobilized on the surface (3). After incubation of target oligonucleotide solution (4) the hybrid is formed on the electrode surface and revealed by EIS (5).

4.1 Materials and methods

4.1.1 Reagents

Streptavidin from Streptomyces avidinii and ethanol (96%) were from Sigma-Aldrich. Disodium hydrogen phosphate, sodium dihydrogen phosphate, potassium

hexacyanoferrate (III and II), sodium chloride, tetra-n-butylammonium bromide [(TBA)Br] and acetonitrile were from Merck. Bis(2,2′-bithien-5-yl)-(4-hydroxyphenyl)methane biotin ester was synthesized according to the literature procedure [173] by Kutner's group. MilliQ water (DEPC treated for RNA analysis) was used for preparation of solutions. Synthetic oligonucleotides were from MWG Biotech AG.

Probe (DNA-biot): 5' GAA-ACC-CAG-CAG-ACA-ATG-TAG-CT – biotin 3'.

Target: 5' AGC-UAC-AUU-GUC-UGC-UGG-GUU-UC – 3'.

Non-complementary: 5′ UAG-CAG-CAC-GUA-AAU-A-3′

4.1.2 Electrochemical measurements

Electrochemical measurements were performed with a three-electrode cell using the Autolab PGSTAT10 electrochemistry system equipped with the FRA2 module (EcoChemie). The SPE devices were composed of planar electrodes, i.e., a carbon auxiliary electrode, an Ag pseudo-reference electrode, and a gold working electrode. CV measurements were performed in the range between +0.5 and +1.3 V with a scan rate of 50 mV/s. The EIS measurements were performed with an alternating voltage of the 10 mV amplitude at open circuit potential (OCP) of +0.20V used as the bias potential in the frequency range of 10 mHz to 50 kHz. The EIS spectra were plotted as the complex plane diagrams (Nyquist plots). All potentials are referred to pseudo-reference electrode for measurements at the SPE.

4.1.3 Electropolymerization

Prior to the polymerization process, a multiple-pulse amperometric pretreatment of the gold surface was carried out in a stirred 0.5 M H_2SO_4, 10 mM KCl solution. The following triple-potential pulse sequence: -0.3 V for 0.30 s; 0.0 V for 0.30 s and +1.0 V for 0.15 s (150 cycles) was applied. Potentiodynamic deposition of this polymer on the electrode surface was performed by linear cycling the potential in the range of +0.5 to 1.5 V as reported in figure 4.2. An anodic peak current is observed at +1.1 V resulted from oxidation of the bisthiophene moiety of the functional monomer leading to formation of the polymer film. In the first scan, two crossover occur at +0.9 and

+1.0 V, confirming that a nucleation process is occurring on the surface of the gold electrode [243].

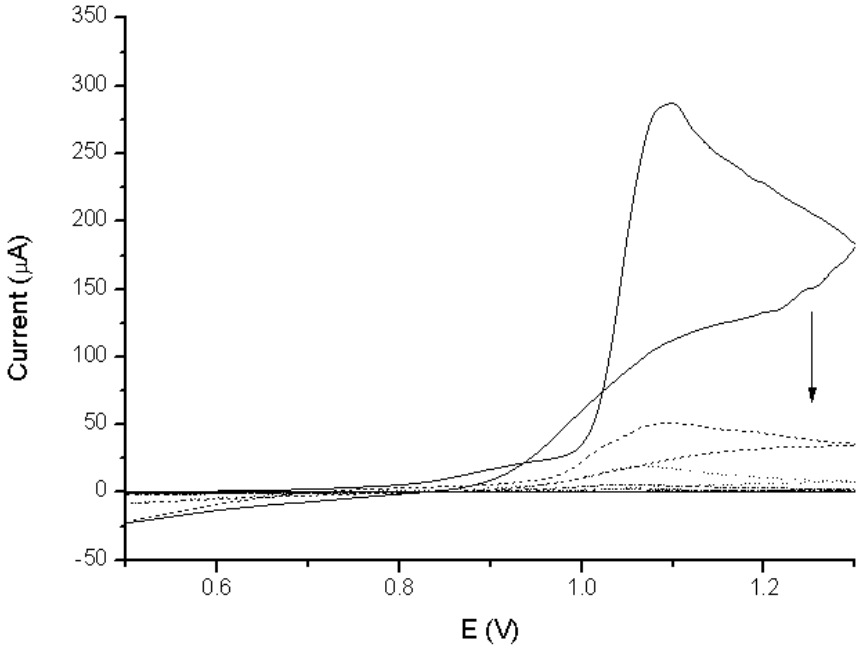

Figure 4.2 – Cyclic voltammetry at SPGE performed from +0.5 to 1.3 V at a scan rate of 50 mV/s in a 0.1 mM monomer solution in 10 mM [(TBA)Br] Ethanol:Acetonitrile:Water 1:1:10 (v/v/v) mixture. Voltammograms showed are referred to scans from 1 to 8.

Starting from the second scan, no crossover is present. This result confirm the deposition of a polymer film. A decreasing of the peak current is also observed increasing the number of scans, suggesting a conductivity decreasing. In paragraph 3.1.5 EIS characterization confirm this result through electron transfer resistance analysis.

In order to optimize the electropolymerization process for DNA probe immobilization, a set of electrodes was modified by using a different number of CV scan, exposed to 4 μM of DNA probe phosphate buffer solution and then tested with EIS. Another set of electrodes was modified by using the same number of scan and then tested with EIS (negative control). Another set of electrodes was modified with different number of scan, exposed to. Impedimetric measurements were performed in a 10 mM $Fe(CN)_6^{3-/4-}$ solution in 0.1 M phosphate buffer pH 7.4 (PB) The R_{et} values obtained are showed in figure 4.3.

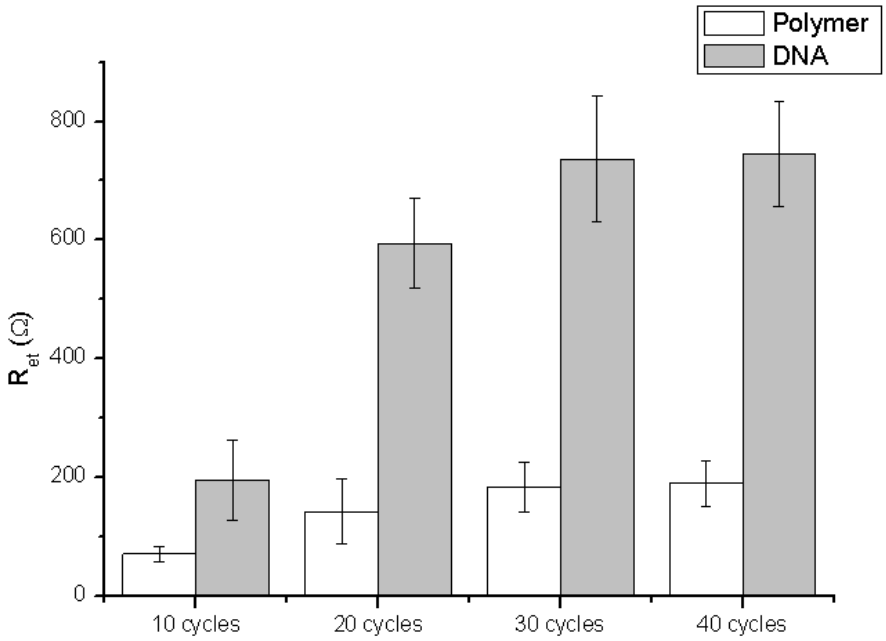

Figure 4.3 – Influence of number of cycles on the immobilization of DNA capture probe. 10, 20, 30 and 40 cycles were performed on two set of SPGEs, the first was analyzed by EIS in 10 mM $Fe(CN)_6^{3-/4-}$ solution in 0.1 M PBS as supporting electrolyte, the second was exposed to a 0.2 mg/L streptavidin solution in 0.1 M PBS for 20 min and then to a 4 µM biotinylated DNA probe solution in 0.1 M PBS. The bars are the average of at least three measurements and the error bars the corresponding standard deviation.

Results show an increasing of electron transfer resistances with the number of cycles for electropolymerization, reaching a constant value after 30 cycles. Based on shortening the time necessary for electropolymerization, the number of potential scans was determined to be 30 in the following experiments.

4.1.4 Redox probe optimization for EIS

In order to optimize the experimental conditions, the redox probe concentration was varied and R_{et} signals were monitored. SPGEs were modified with polymer using optimized conditions and then rinsed with deionized water. SPGEs were then exposed to 100, 10 and 1 mM $Fe(CN)_6^{3-/4-}$ solution in 0.1 M PB as supporting electrolyte. Figure 4.4 show the results obtained by EIS.

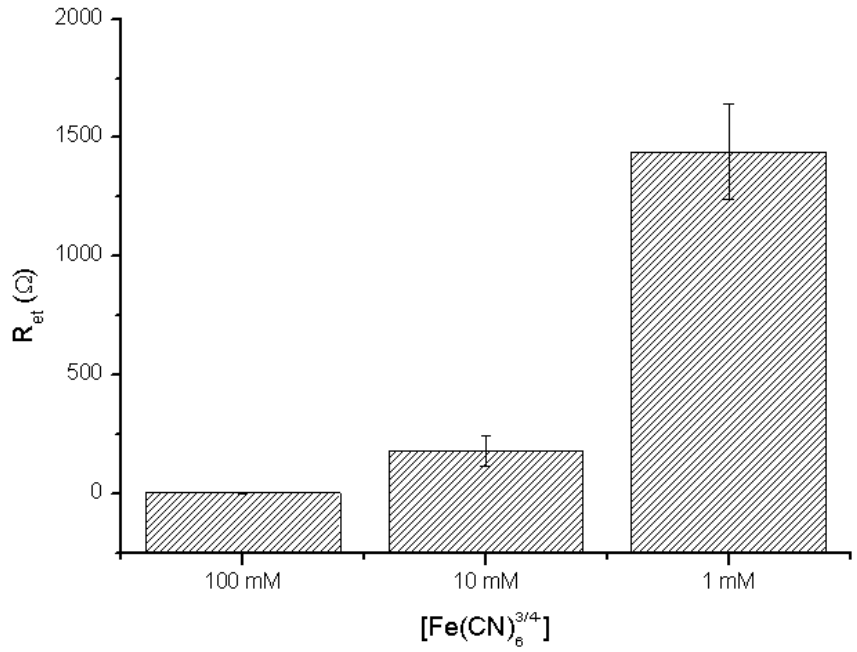

Figure 4.4 – Influence of redox probe concentration on EIS measurements of polymer modified sensors. The bars are the average of at least three measurements and the error bars the corresponding standard deviation.

The highest value of R_{et} was obtained with 1 mM $Fe(CN)_6^{3-/4-}$ that was used as optimized concentration in the following experiments.

4.1.5 EIS characterization and calibration curve

An impedimetric characterization was performed in order to evaluate the surface change after each step of incubation. In figure 4.5 impedance spectra (as Nyquist plot form) of different step of the assay (i.e. polymerization, streptavidin incubation, capture probe incubation and hybridization with different concentrations of target) are reported. Impedance increases after each step of incubation, and, moreover, the sensor is sensitive even when exposed to 1 pM concentration of miRNA.

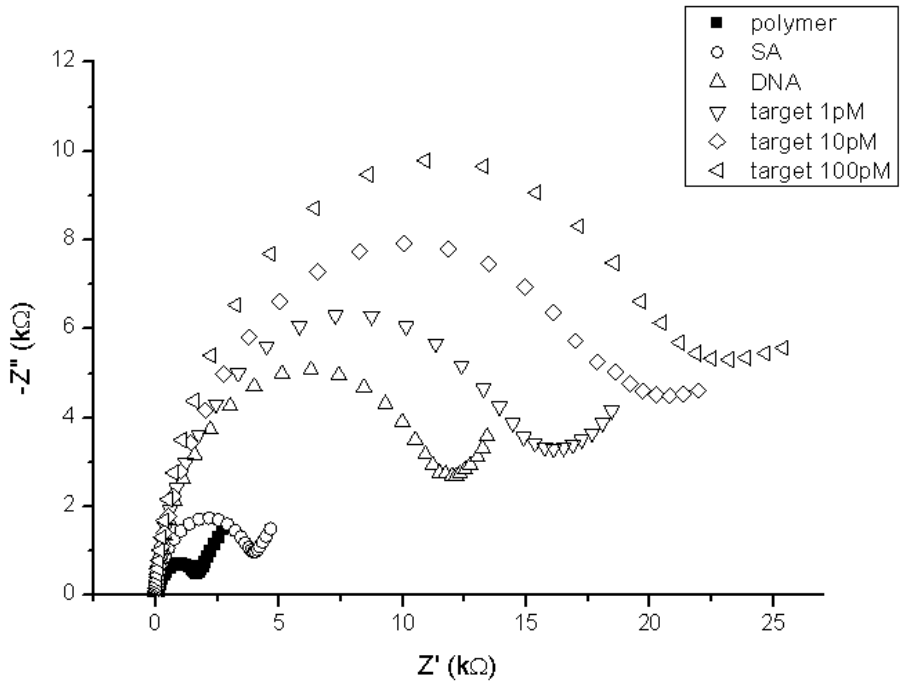

Figure 4.5 – Influence of the surface modification on impedimetric signals. Impedance spectra (Nyquist plots) are shown after polymerization, streptavidin incubation, capture probe incubation and 1,10 and 100 pM miRNA conctenctration. Further details are available in the materials and methods section.

To demonstrate the analytical performances of the impedimetric assay a calibration experiment was designed (figure 4.6). When analyzing target solutions whose concentration was increased by orders of magnitude, a linear response was observed. In the concentration range tested (0 to 100 pM), the genosensor response exhibited linear (R^2 = 0.98) dependence on target concentration with 0.14 kΩ/pM sensitivity and a relative standard deviation of 15% (expressed as mean of all concentration tested). Signals levelled off for higher concentrations, indicating that saturation of all available probes was achieved (data not showed); moreover, the non-specific signal of non-complementary oligomers was negligible up to 100 pM.

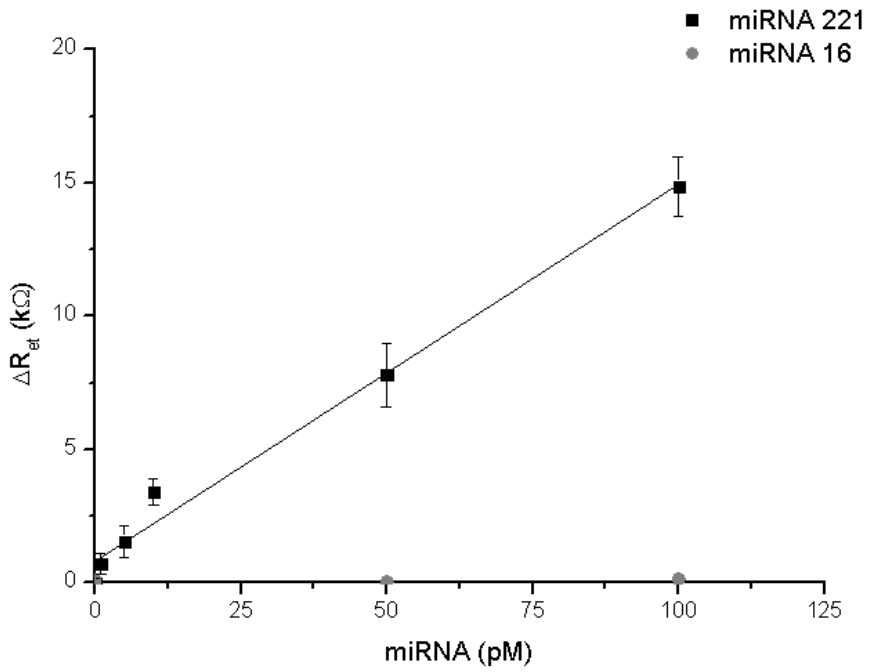

Figure 4.6 - Calibration plot for synthetic oligonucleotides. Probe-modified sensors were exposed to a 10 µL drop of the target sequence solution (0, 1, 5, 10, 50 and 100 pM) for 20 min. Further details are available in the materials and methods section. Each point represents the mean of at least three measurements and the error bars the corresponding standard deviation.

4.2 Discussion

This chapter describes the development of a label-free electrochemical genosensor based on the use of screen printed gold electrode transducers. The use of inexpensive sensors and the label-free detection scheme made such a biosensing approach particularly attractive. The short analysis time and the simplicity of the procedure were two additional advantages of the proposed assay. This indicator-free scheme relied on the increasing of electron transfer resistance as hybridization recognize event. It is usually accepted that the immobilization of the DNA probe onto the sensor surface plays a crucial role in genosensor preparation, deeply determining its bio-recognition capabilities. Immobilization of densely packed DNA probe layers was required during the analysis of synthetic oligonucleotides for efficiently suppressing the non-specific adsorption of such short sequences. Conductive polymer film was used as immobilization strategy for DNA capture probe.

A biotinylated monomer was potentiodynamically polymerized on the electrode surface

via CV. An anodic peak current is observed at +1.1 V (vs. silver pseudo reference electrode) resulted from oxidation of the bisthiophene moiety of the functional monomer leading to formation of the polymer film [173]. In the first scan, two crossover occur at +0.9 and +1.0 V, confirming that a nucleation process is occurring on the surface of the gold electrode [243]. Even if a conductive polymer film was deposited during the first scan, an increasing of peak current is expected during the following scans. Voltammograms instead show a decreasing of the peak current. This result could be explained with the negative charge beard by biotin, that increases the resistance of the surface, with consequent loss of conductivity. This result is also confirmed by EIS characterization, that show an increasing of R_{et} from 70.1 ± 1.2 Ω (bare electrode) to 183.4 ± 41.5 Ω (polymerized electrode with 30 cycles) registered in 10 mM $Fe(CN)_6^{3-/4-}$ in PBS.

Impedimetric characterization of figure 4.5 show how R_{et} increases with all step of incubation. This is due to intrinsic negative charged possessed by streptavidin, DNA capture probe and miRNA target, that naturally increase the resistance of the electron transfer.

In order to obtain the higher sensitivity of the genosensor, a characterization of electropolymerization process was performed. In particular, number of cylces tested show an increasing of the R_{et} value from 10 to 40 cycles. This is probably due to the increasing of thickness of the film and biotin coverage of the surface. R_{et} values in presence of capture probe also increase with the number of cycles, indicating an higher immobilization of the probe on the surface, reaching a highest and stable value at 30 cycles.

Calibration plot made with synthetic miRNA sequences show a linear range with 0.14 kΩ/pM (or 140 kΩ/nM) with a calculated LOD of 1.1 pM.

4.3 Conclusions

This chapter has described a disposable, indicator-free, electrochemical genosensor, based on polymer modified screen-printed gold electrodes. Biotinylated bis(2,2′-bithien-5-yl)methane monomer efficiently electropolymerized under potentiodynamic conditions. The biotin-containing resulting polymer film irreversibly bound streptavidin. This binding enabled preparation of a label-free biosensor for sequence-specific oligonucleotide determination. Noteworthy, the electropolymerization used for polymer deposition is a straightforward, low

cost, and repeatable way of the transducer surface modification, thus making biotin immobilization very attractive. The indicator-free genosensor was characterized by EIS measurements using mir221 synthetic oligonucleotide as a model. Specific detection of non complementary sequence (miR16) was achieved in conjunction with a 20 minute hybridization assay; a detection limit of 1.1 pM of miR-221 target sequence was obtained with a 140 kΩ/nM sensitivity. The use of conductive polymer film seems interesting for signal amplification. Moreover, it is important to note that this method is not limited to only the hybridization assay systems, but can also be extended to other affinity biosensors based on biotin-streptavidin chemistry.

Chapter 5 – Electrochemical and Photoelectrochemical Characterization of ITO-TiO_2-AuNRs Electrodes for Enzymatic miRNA Photoelectrochemical Detection

This chapter describes the electrochemical and photoelectrochemical characterization of ITO-TiO_2-AuNRs electrodes for the development of a photoelectrochemical genosensor. The use of AuNRs has two proprieties: reduce the bandgap of semiconductive TiO_2, that normally require UV source, permitting the use of visible light as source for photocurrent development; moreover, the layer of gold on the sensor surface, allow thiolated DNA probe to be immobilized.

Preliminary characterization and optimization of the photoelectrochemical route is herein described with preliminary results of enzymatic assay showed in figure 5.1, where ascorbic acid was used as enhancer of the photocurrent as product of the biocatalytic reaction with streptavidin conjugated alkaline phosphatase.

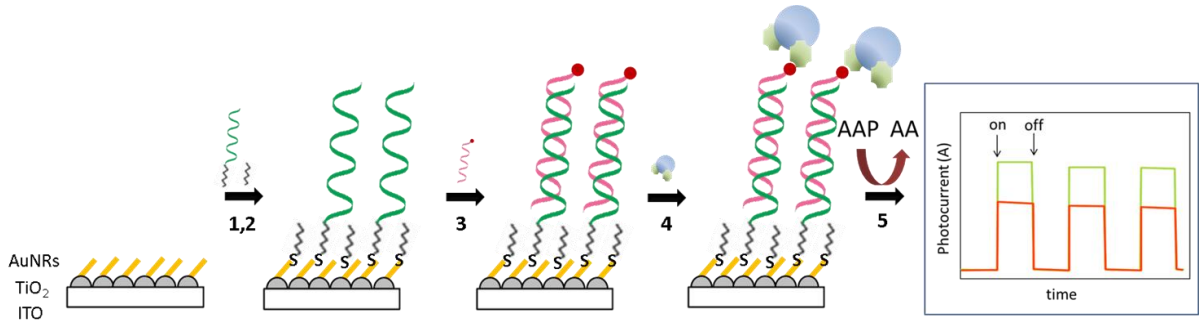

Figure 5.1 - Illustration of the assay scheme. The biotinylated hybrid is formed on the gold modified electrode surface (1,2,3). Streptavidin-Alkaline Phosphatase is added (4). After incubation of the proper substrate, enzymatic product is revealed by Chronoamperometry (5).

5.1 Materials and methods

5.1.1 Reagents

Dithiothreitol (DTT), 6-mercapto-1-hexanol (MCH), streptavidin–alkaline phosphatase (S2890, Strept-AP, 2:1 conjugation stoichiometry), diethyl pyrocarbonate (DEPC), ascorbic acid, L-ascorbic acid 2-phosphate trisodium salt, mercaptosuccinic acid (MSA), bovine serum albumin (BSA), Tris–HCl, were obtained from Sigma–Aldrich (Milan, Italy). Magnesium and potassium chloride were purchased from Merck (Milan, Italy). NAP-10 columns of Sephadex G-25 were obtained from Amersham Pharmacia Biotech (Uppsala, Sweden). ITO-TiO_2 electrode were purchased from Solaronix (Aubonne, Switzerland). AuNRs were synthetized and characterized by Dr. Ingrosso, CNR-IPCF. MilliQ water (DEPC treated for RNA analysis) was used throughout this work. Synthetic oligonucleotides were obtained from MWG Biotech AG (Germany):

Probe (DNA-SH): 5' GAA-ACC-CAG-CAG-ACA-ATG-TAG-CT – SH 3'
Target: 5' AGC-UAC-AUU-GUC-UGC-UGG-GUU-UC –biotin 3'

Prior to use, the thiol-modified oligonucleotides were treated with DTT. This reagent allowed reduction and cleavage of oligo dimers eventually obtained by oxidative coupling of two DNA-SH molecules (i.e. DNA-S-S-DNA). The lyophilized oligonucleotides were dissolved in a 10 mM Tris-HCl buffer solution (pH 8.3) containing 20 mM of DTT. The reaction was allowed to proceed for 2 h at room temperature. The thiolated DNA was then purified by elution through a NAP-10 column of Sephadex G-25 using 0.5 M phosphate buffer (pH 7.4). DNA-SH stock were prepared in the same buffer and stored frozen.

5.1.2 Electrochemical measurements

Electrochemical measurements were performed with a three-electrode cell using the Autolab PGSTAT10 electrochemistry system equipped with the FRA2 module (EcoChemie). A Pt wire, Ag/AgCl, and ITO-TiO_2-AuNRs disk served as the auxiliary, reference, and working electrode respectively using a 1 mL Plexiglas cell. Cyclic Voltammetry (CV) measurements were performed with a scan rate of 50 mV/s in different potential ranges. EIS measurements were performed with E_{dc} from -0.2 to

+0.8 V, in the range between -0.2 and +0.8 V, every 0.1 V with all the parameters showed in table 5.1.

Subscan number	Points	Frequency [Hz]	E_{ac} [V]
1	10	50000-5000	$8 \cdot 10^{-4}$
2	25	4900-50	$1 \cdot 10^{-3}$
3	15	49-4	$2 \cdot 10^{-3}$
4	15	3-0.1	$1 \cdot 10^{-2}$
5	9	0.09-0.02	$1.5 \cdot 10^{-2}$

Table 5.1 – EIS parameters for impedimetric characterization of the sensor

Photocurrents were measured with amperometry at a defined potential where the electrode show no capacitive current.

5.1.3 Light sources

Three different light sources were used. An UV lamp (Jelosil HG500, effective intensity: 30 mW cm^{-2}) emitting in the UV-A (315–400 nm) in air. An UV lamp emitting at 366 nm (CAMAG, Switzerland) and a commercial white LED (Nichia 3 mm White LED, 25 ° Through Hole from RS, Northants, UK) emitting in the visible range 400-700 nm with two maximum at 456 and 549 nm. .

5.1.4 Sensor modification

20 µL of the thiolated oligonucleotide solution (10 µM in 0.5 M in phosphate buffer) were placed on the electrode surface. Chemisorption was allowed to proceed overnight (≈ 16 h). During this period, the electrode cell was covered with parafilm in order to prevent the evaporation of the oligonucleotide solution. The immobilization step was followed by a post-treatment with 20 µL of 1 mM MCH water solution for 1 hour. Prior to hybridization reaction, the modified electrode were washed twice with 0.5 M phosphate buffer pH 7.2 (PB). The probe-modified electrodes were exposed to a 20 µL of the biotinylated target sequence in PB solution for 20 min. After hybridization, the sensor was washed twice with 0.1 M Tris-HCl, pH 9.8 (Tris). The biotinylated hybrid

obtained at the electrode surface was reacted with a 20 µL solution containing 4 U/mL of the streptavidin-alkaline phosphatase conjugate and 10 mg/mL of BSA in Tris buffer. After 20 minutes, the sensors were washed twice with Tris buffer. The photoelectrochemical cell was then covered with 750 µL of an L-ascorbic acid 2-phosphate trisodium salt solution (10 mg/mL in Tris buffer). After 20 minutes of incubation, photocurrent was measured with an amperometric detection under illumination of opportune light source. The ascorbic acid enhanced photocurrent was taken as the analytical signal. All photoelectrochemical measurements were referred to the Ag/AgCl wire reference electrode. The experiments were carried out at room temperature (25°C).

5.2 Results

5.2.1 Characterization of ITO-TiO_2 electrode with CV

Different potential ranges were tested in CV in order to determinate the potential window of capacitive current. In figure 5.2a are reported all the voltammograms registered at 50 mV/s in 0.1 M KCl.

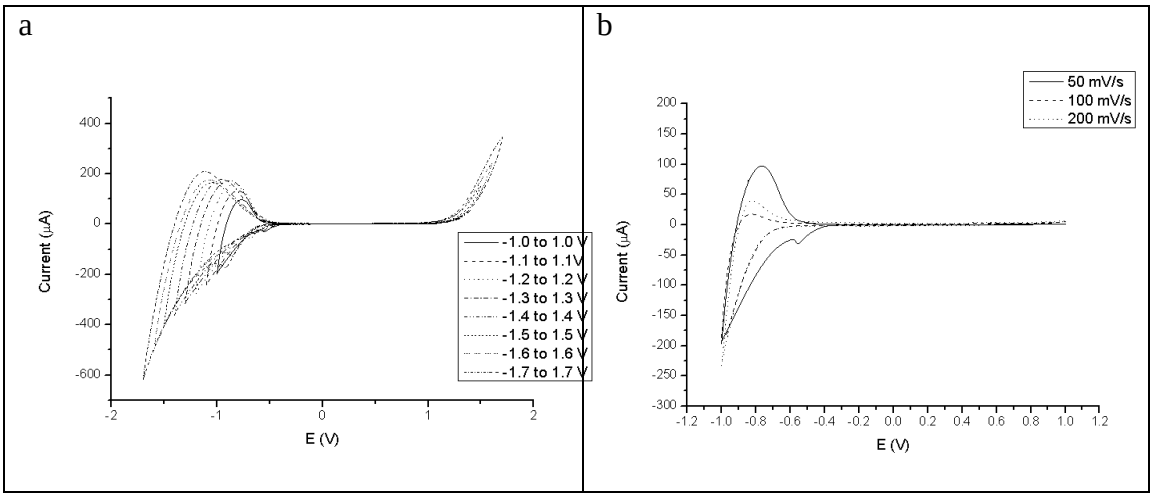

Figure 5.2 – a) Cyclic voltammograms registered in 0.1 M KCl at 50 mV/s on TiO_2/ITO electrode from negative to positive potential direction; b) Cyclic voltammograms registered in 0.1 M KCl at 50, 100 and 200 mV/s from -1 to 1 V.

All voltammograms show a large potential range where the current is only capacitive. In this range the absence of faradaic phenomenon on the electrode surface preserves the electrode to be modified with degradative processes. The window of interest

resulted between -0.2 to +0.8 V. In order to determinate the scan rate influence on the sensor, in figure 5.3b are reported voltammograms registered at different scan rate. The voltammograms show that at high scan rate no big difference occurs on the faradaic current at potential lower than -0.5 V. The anodic peak registered around -0.75 V is probably related to the H^+ reduction to H_2, but it is not possible to exclude a tribute to this peak current from TiO_2 film.

5.2.2 Characterization of ITO-TiO2 electrode with EIS

Impedance spectroscopy was used in order to estimate some TiO_2 properties as semiconductor electrode. In particular, the flat band potential E_{fb}, donor density N_D and the spacial charge thickness L_{dl}. E_{fb} and N_D were obtained from Mott – Schottky equation [244]:

$$\frac{1}{C^2} = \frac{2}{e\varepsilon\varepsilon_0 A^2 N_D}\left(E - E_{fb} - \frac{k_B T}{e}\right)$$

Here C and A are the interfacial capacitance and area, respectively, E the applied voltage, k_B is Boltzmann's constant, T the absolute temperature, and e is the electronic charge. Therefore, a plot of $1/C^2$ against E should yield a straight line from which E_{fb} can be determined from the intercept on the E axis. The value of N_D can also be conveniently found from the slope knowing ε and A of the electrode.

L_{dl} was instead calculated from the equation:

$$L_{dl} = \left(\frac{2\varepsilon\varepsilon_0}{eN_D}\right)^{1/2}\left(E - E_{fb} - \frac{k_B T}{e}\right)^{1/2}$$

Figure 5.3a show the Nyquist plot registered at +0.8 V, and figure 5.3b all plots registered for each E_{dc} (from -0.2 to +0.8 V). For this and for all the other spectra registered a fitting with the following circuit was made in order to evaluate the capacitance for Mott – Schottky method: $R_s(R_1C_1)(R_2C_2)(R_3C_3)(R_4C_4)$ (figure 5.4).

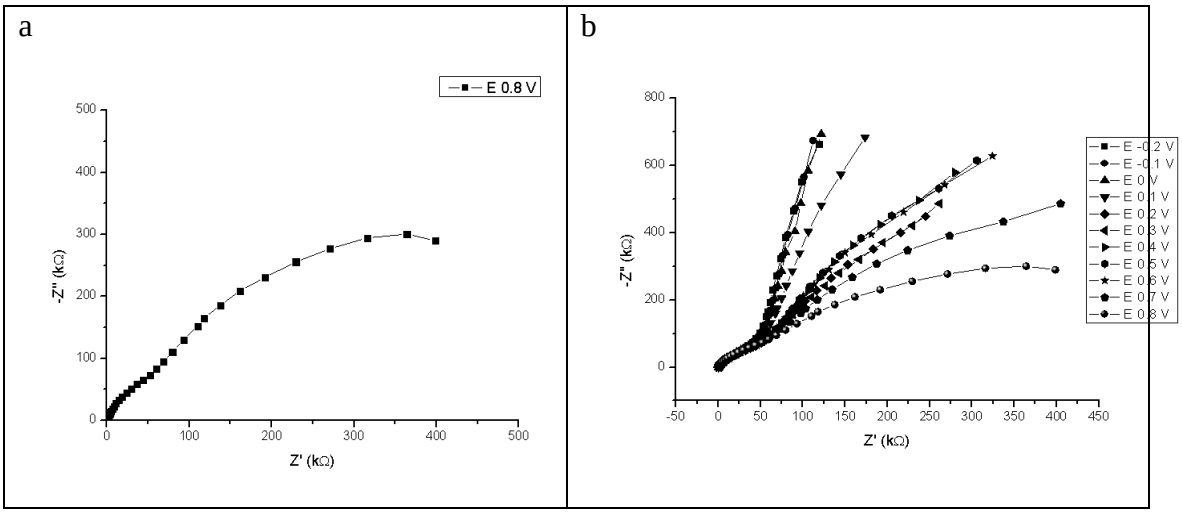

Figure 5.3 – a) Nyquist plot registered in 0.1 M KCl at ITO-TiO_2 electrode; b) Nyquist plots registered in 0.1 M KCl at ITO-TiO_2 electrode from -0.2 to +0.8 mV.

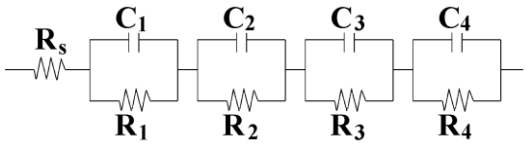

Figure 5.4 – Equivalent circuit used for fitting.

All the data calculated with the fitting are here reported in table 5.2. R_s is the resistance of the solution, and is usually independent to the applied E_{dc}.

E_{dc}	R_s (Ω)	R_1 (Ω)	R_2 (Ω)	R_3 (Ω)	R_4 (Ω)	C_1 (F)	C_2 (F)	C_3 (F)	C_4 (F)
-200	407	5,91E+06	4,80E+04	4,28E+03	6,20E+02	1,16E-05	7,10E-06	7,97E-06	2,22E-06
-100	403	6,72E+06	5,12E+04	5,15E+03	6,70E+02	1,14E-05	7,06E-06	7,55E-06	2,12E-06
0	399	6,34E+06	5,28E+04	5,32E+03	6,65E+02	1,10E-05	6,75E-06	7,18E-06	2,04E-06
100	396	3,79E+06	5,51E+04	5,82E+03	6,92E+02	1,10E-05	6,45E-06	6,74E-06	1,96E-06
200	391	1,19E+06	5,92E+04	7,95E+03	7,02E+02	1,37E-05	6,20E-06	5,90E-06	1,88E-06
300	387	1,25E+06	6,38E+04	7,59E+03	6,80E+02	1,29E-05	5,94E-06	5,73E-06	1,85E-06
400	382	1,61E+06	6,32E+04	6,63E+03	6,94E+02	1,16E-05	5,63E-06	5,86E-06	1,80E-06
500	378	1,63E+06	6,27E+04	6,09E+03	6,66E+02	1,09E-05	5,43E-06	5,88E-06	1,73E-06
600	374	1,60E+06	6,36E+04	5,74E+03	6,69E+02	1,05E-05	5,27E-06	5,88E-06	1,69E-06
700	370	9,48E+05	6,52E+04	5,82E+03	6,50E+02	1,07E-05	5,07E-06	5,59E-06	1,67E-06
800	366	5,67E+05	6,23E+04	5,32E+03	6,79E+02	1,06E-05	4,77E-06	5,82E-06	1,63E-06

Table 5.2 – Resitances and Capacitance calculated from the fitting with the circuit $R_s(R_1C_1)(R_2C_2)(R_3C_3)(R_4C_4)$.

In this particular case, instead, a slow linear dependence to E_{dc} is observed, even if the average value is 387±14 Ω. Starting from the value of R_s evaluated at 0 V, with a conductivity for 0.1 M KCl assumed 12.9 $mS \cdot cm^{-1}$ [245] a cell constant of 5.11 cm^{-1} was calculated. Mott – Schottky diagram as C_1^{-2} vs E is reported in figure 5.5, with the linear range from +0.2 to +0.6 V. Intercept and slope were calculated (intercept = $3.36 \cdot 10^9$ F^{-2} slope = $9.75 \cdot 10^6$ F^{-2}/mV), assuming ε for TiO_2 equal to 173 [246], ε_0 = $8.85 \cdot 10^{-12}$ F/m [247], A = $7.07 \cdot 10^{-6}$ m^2 (3 mm diameter) and e = $1.6 \cdot 10^{-19}$ C [247], give a -344 mV and $1.68 \cdot 10^{22}$ cm^{-3} as E_{fb} and N_D respectively.

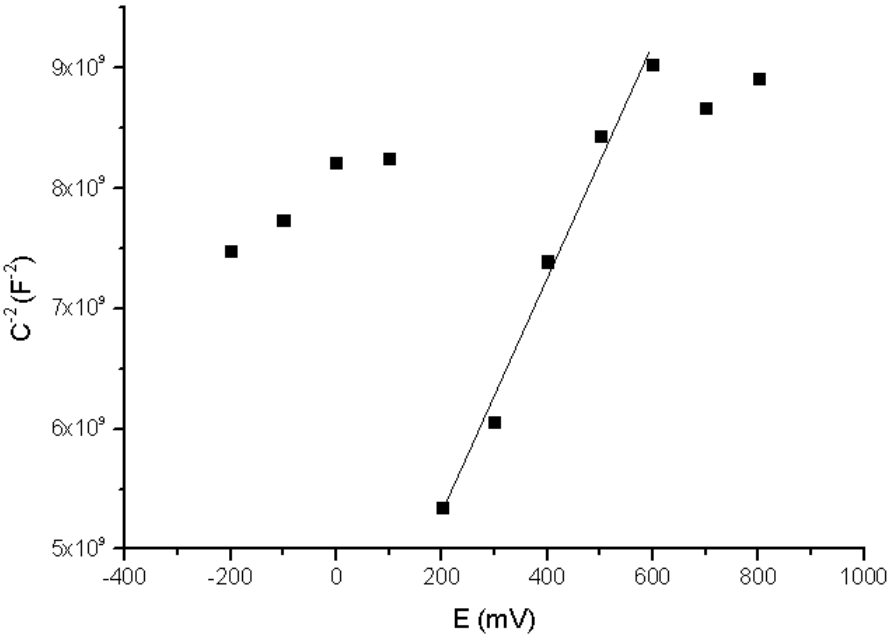

Figure 5.5 - Mott–Schottky plot for ITO/TiO2 in 0.1 M KCl solution.

Finally, knowing E_{fb} and N_D, it is possible to estimate the dimension of the charge space L_{dl} versus E_{dc} (figure 5.6). In the range potential evaluated L_{dl} profile is linear (R^2 0.98) with a slope of 0.71 nm/V and intercept of 0.61 nm.

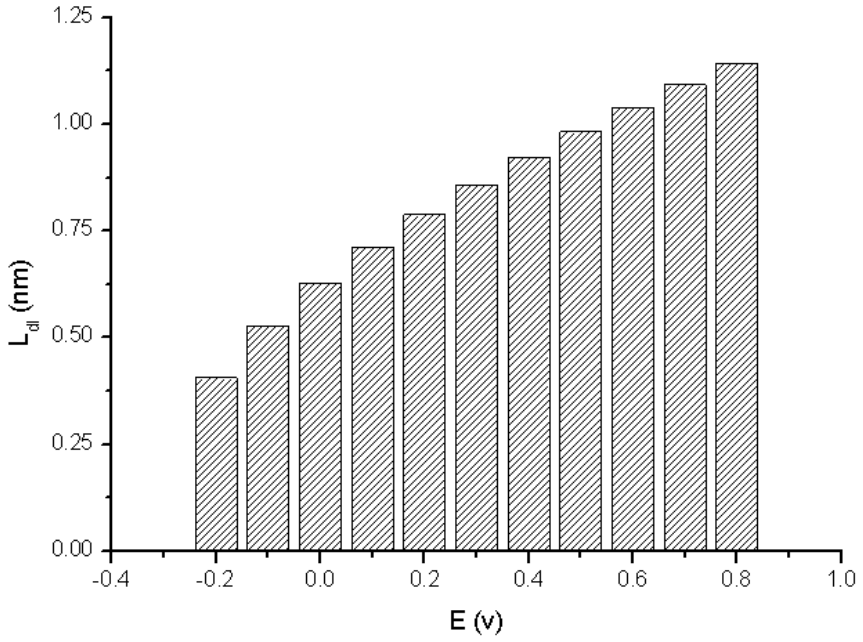

Figure 5.6 – Influence of the applied potential on the spacial charge thickness (Ldl) for ITO-TiO2 electrode assuming a flat band potential E_{fb} and a donor density N_D of -344 mV and $1.68 \cdot 10^{22}$ cm^{-3} respectively.

5.2.3 Photoelectrochemical characterization of ITO-TiO_2 electrode

A photoelectrochemical characterization of the bare ITO-TiO_2 electrode, MSA modified electrode (ITO-TiO_2-MSA) and AuNRs modified electrode (ITO-TiO_2-AuNRs) were performed. MSA was used in order to bind AuNRs to TiO_2 through its –COOH moieties. Finally, a DNA-SH modified ITO-TiO_2-AuNRs was also tested. The lamp used for all of these investigations is a UV lamp from Jelosil.

ITO-TiO_2

This electrode was used for an intensive electrochemical characterization (showed in the previous paragraph) and successively used for photoelectrochemical tests. CV tests were performed with this electrode in dark and under UV illumination from -0.2 to +0.8 V in 0.1 M KCl and in 10 mM Ascorbic Acid (AA) at 50 mV/s (figure 5.6a).

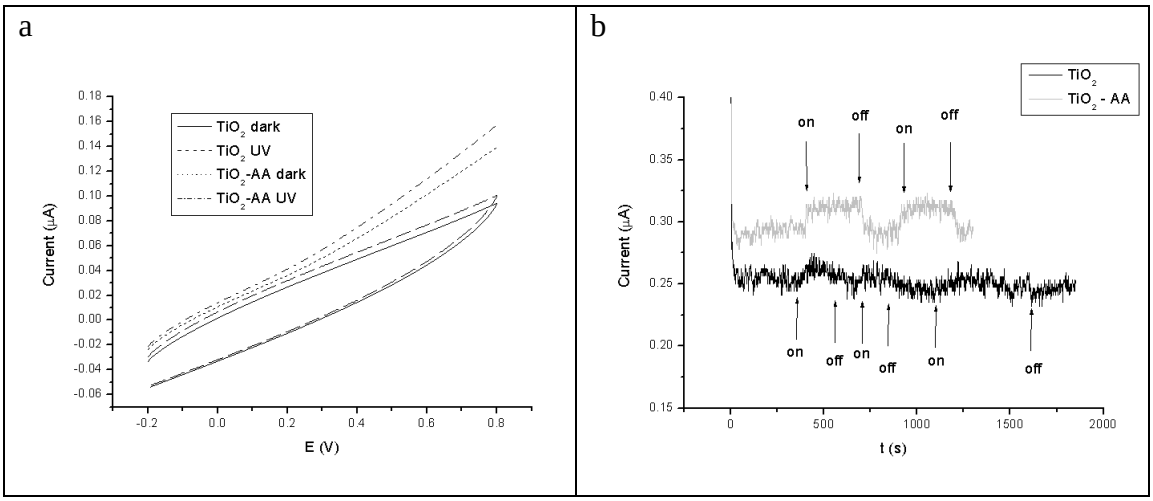

Figure 5.6 – a) Cyclic voltammograms from -0.2 to +0.8 V in dark and under UV illumination in 0.1 M KCl and 10 mM Ascorbic Acid in 0.1 M KCl; b) Voltage-dependent photocurrent at 0 V in 0.1 M KCl as a function of time upon turning the incident UV light on and off without (black line) and with (gray line) Ascorbic Acid of ITO-TiO_2 electrode.

Photocurrents were registered at 0 V. This potential was chosen in the range -0.2 and +0.8 V estimated in the previous paragraph as the range where current is only capacitive. Chronoamperograms show an increase of photocurrent with the enhancer AA and an increase of the current under illumination.

From the reported data is clear the light dependence of the current, especially in the presence of AA. The small increase of the current with ligh was attributed to change in the crystal structure due to the electrochemical characterization.

ITO-TiO_2-MSA

Electrode modified with MSA was first tested with CV from -0.2 to +0.8 V in 0.1 M KCl and from -0.2 to +1.4 V in 10 mM AA in 0.1 M KCl. Voltammograms in figure 5.7 show an evident light dependence.

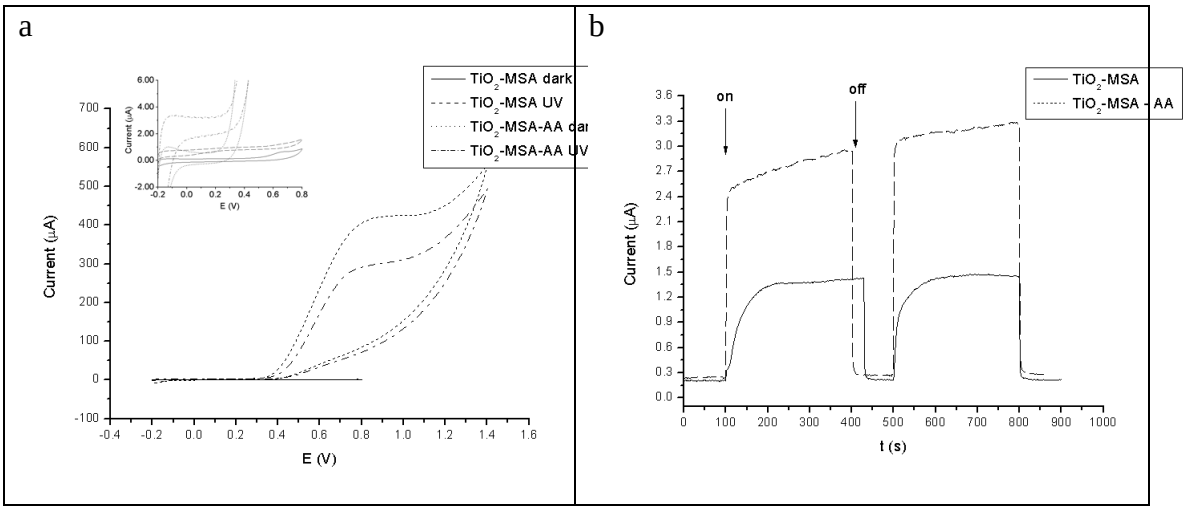

Figure 5.7 – a) Cyclic voltammograms from -0.2 to +0.8 V in dark and under UV illumination in 0.1 M KCl and from -0.2 to +1.4 V in 10 mM Ascorbic Acid in 0.1 M KCl; b) Voltage-dependent photocurrent at 0 V in 0.1 M KCl as a function of time upon turning the incident UV light on and off without (solid line) and with (dash line) Ascorbic Acid of ITO-TiO_2-MSA electrode.

Also in this experiment photocurrents were registered at 0 V. Chronoamperograms show a high increase of photocurrent under illumination.

ITO-TiO_2-AuNRs

Electrode modified with AuNRs was first tested with CV from -0.2 to +0.8 V in 0.1 M KCl and from -0.2 to +1.4 V in 10 mM AA in 0.1 M KCl. Voltammograms in figure 5.8 show an evident light dependence.

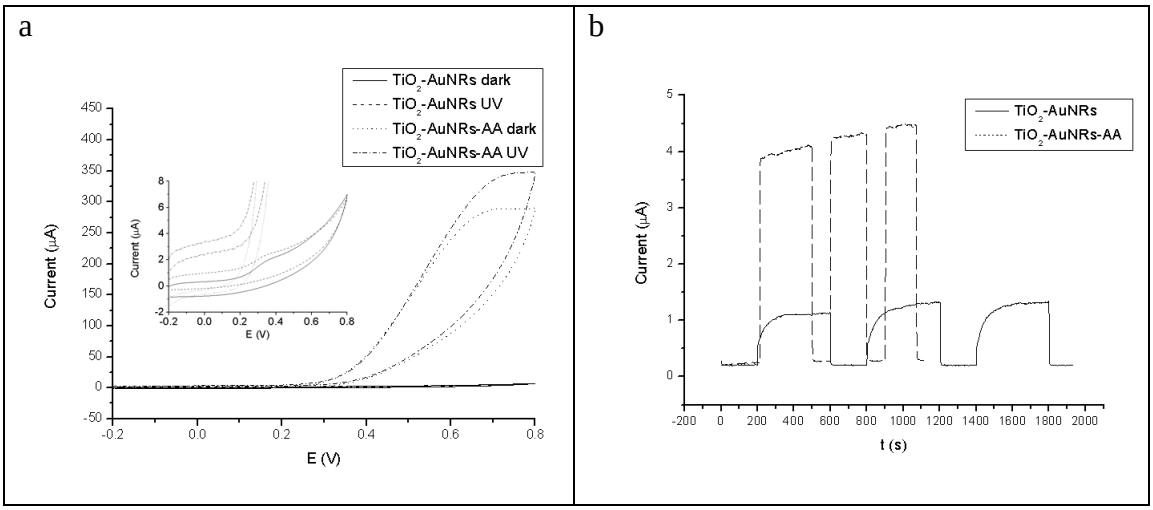

Figure 5.8 – a) Cyclic voltammograms from -0.2 to +0.8 V in dark and under UV illumination in 0.1 M KCl and 10 mM Ascorbic Acid in 0.1 M KCl; b) Voltage-dependent photocurrent at 0 V in 0.1 M KCl as a function of time upon turning the incident UV light on and off without (solid line) and with (dash line) Ascorbic Acid of ITO-TiO_2-MSA-AuNRs electrode.

Also in this experiment photocurrents were registered at 0 V. Chronoamperograms show a high increase of photocurrent under illumination.

ITO-TiO_2-AuNRs-DNA

DNA modified electrode was first tested with CV from -0.2 to +0.8 V in 0.1 M KCl and from -0.2 to +1.4 V in 10 mM AA in 0.1 M KCl.

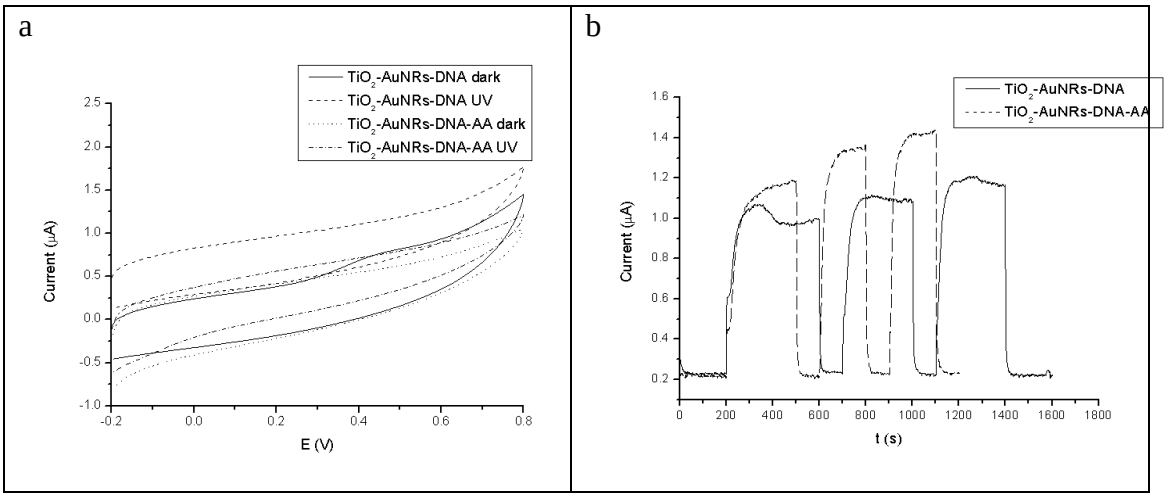

Figure 5.9 – a) Cyclic voltammograms from -0.2 to +0.8 V in dark and under UV illumination in 0.1 M KCl and 10 mM Ascorbic Acid in 0.1 M KCl; b) Voltage-dependent photocurrent at 0 V in 0.1 M KCl as a function of time upon turning the incident UV light on and off without (solid line) and with (dash line) Ascorbic Acid of ITO-TiO_2-MSA-AuNRs-DNA electrode.

Voltammograms in figure 5.9 show an evident light dependence. Also in this experiment photocurrents were registered at 0 V. Chronoamperograms show an increase of photocurrent under illumination.

5.2.4 Ascorbic acid calibration plot

In order to use a smaller and easy to use light source, photoelectrochemical characterization in presence of AA were performed with a CAMAG lamp (366 nm). Morover, due to the gold propriety to reduce the band gap energy of titanium dioxide, a visible light source was tested using a white LED (RS).

The LED used in these experiment was characterized and the spectra registered reported in figure 5.10.

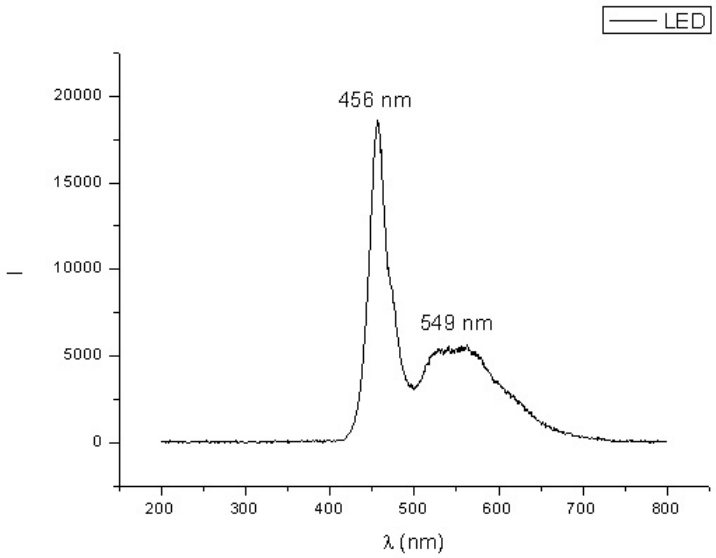

Figure 5.10 - Spectrum of the white LED showing blue light (peak at about 456 nm) and the more broadband Stokes-shifted light emitted at roughly 500–700 nm.

Photocurrents were registered using an unmodified ITO-TiO_2 electrode in PB (figure 5.11). In table 5.3 are reported results using both light source at different concentration of Ascorbic Acid (AA). Currents reported are extrapolated from the third photocurrent registered. Photocurrents registered with UV source presented an irregular form, probably due to the light power of the lamp, not designed for this kind of experiments (data not shown).

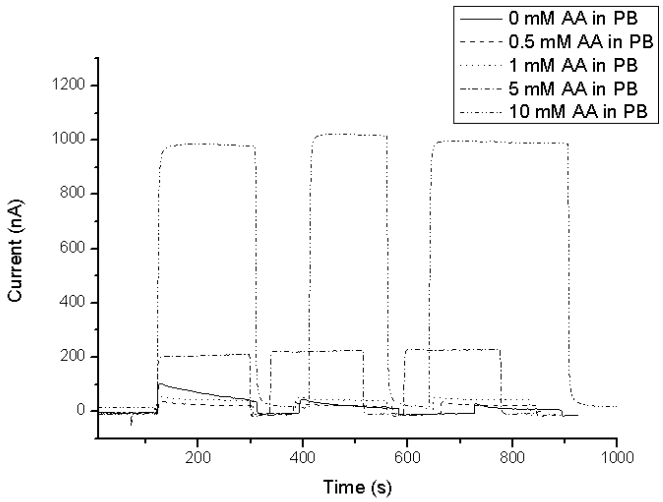

Figure 5.11 - Voltage-dependent photocurrent at 0 V as a function of time upon turning the incident LED light on and off at 0, 0.5, 1, 5 and 10 mM Ascorbic Acid in 10 mM phosphate buffer pH 7.4 of ITO-TiO_2 electrode.

AA in PB (mM)	LED (nA)	UV 366 nm (nA)
0	14	215
0.25	-	294
0.5	32	542
1	53.7	582
5	237	935
10	999	932

Table 5.3 – Influence of AA concentration in phosphate buffer 10 mM on the photocurrents registered at 0 V applied potential on a ITO-TiO_2 electrode with LED and UV source light.

The same experiment was then performed with a gold modified ITO-TiO_2 electrode. Photocurrents registered with LED source are reported in figure 5.12 and results summarized in table 5.4

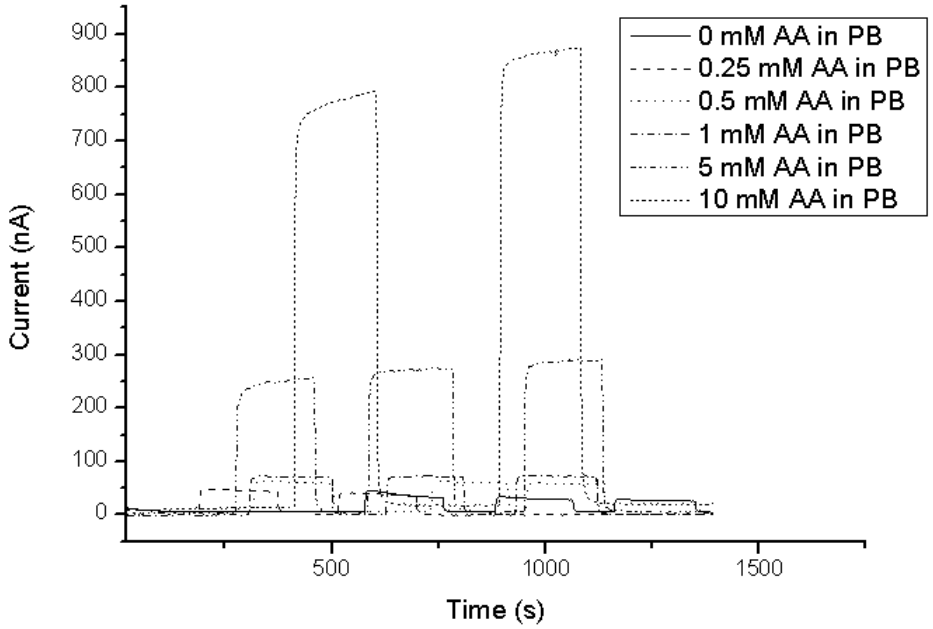

Figure 5.12 - Voltage-dependent photocurrent at 0 V as a function of time upon turning the incident LED light on and off at 0, 0.25, 0.5, 1, 5 and 10 mM Ascorbic Acid in 10 mM phosphate buffer pH 7.4 of gold modified ITO-TiO_2 electrode.

AA in PB (mM)	LED (nA)	UV 366 nm (nA)
0	25.6	856
0.25	37.9	901
0.5	57.3	897
1	71.4	880
5	288.2	812
10	940	690

Table 5.4 – Influence of AA concentration in phosphate buffer 10 mM on the photocurrents registered at 0 V applied potential on a ITO-TiO_2-AuNRs electrode with LED and UV source light.

Currents reported are extrapolated from the third photocurrent registered. Also in this experiment, photocurrents registered with UV source presented an irregular form, probably due to the light power of the lamp, not designed for this kind of experiments (data not shown).

An interesting route of these electrodes is the possibility to regenerate the surface after exposure to AA. During experiments was observed that an accurate wash with water was necessary in order to obtain the starting photocurrent. This was observed after a measure performed on the blank (0 mM AA in phosphate buffer) immediately after a 10 mM AA solution measurement.

In order to confirm the same photoelectrochemical behavior of AA on gold ITO-TiO_2 electrode with Tris buffer, another calibration was performed. Because of the irregular and not reproducible form of the photocurrents generated by the UV lamp, starting from this experiment, the only light source used was the white LED. In table 5.5 are summarized all the photocurrent registered: it is evident that the photoelectrochemical behavior of AA in Tris buffer pH 9.8 is lower than in phosphate buffer pH 7.4.

AA in TRIS (mM)	LED (nA)
0	9.3
0.25	10.9
0.5	13.9
1	23
5	125.5
10	252

Table 5.5 – Influence of AA concentration in Tris buffer 10 mM on the photocurrents registered at 0 V applied potential on a ITO-TiO_2-AuNRs electrode with LED source light.

5.2.5 Hybridization assay

In order to demonstrate the analytical performances of the label based photoelectrochemical assay a preliminary calibration experiment was designed starting from these conditions (figure 5.13).

The analytical signals increased with the target concentration from 0 to 50 nM (figure 5.13b). Within the linear analytical range, the sensitivity was 1.85 nA/nM, with an estimated detection limit of 2 nM and an average RSD of 5%. In order to exclude any phenomenon of non-specific adsorbtion of the enzyme on the surface or a spontaneous hydrolysis of the substrate AAP, the following experiments were performed using electrodes exposed to 50 nM target solution used for calibration experiment.

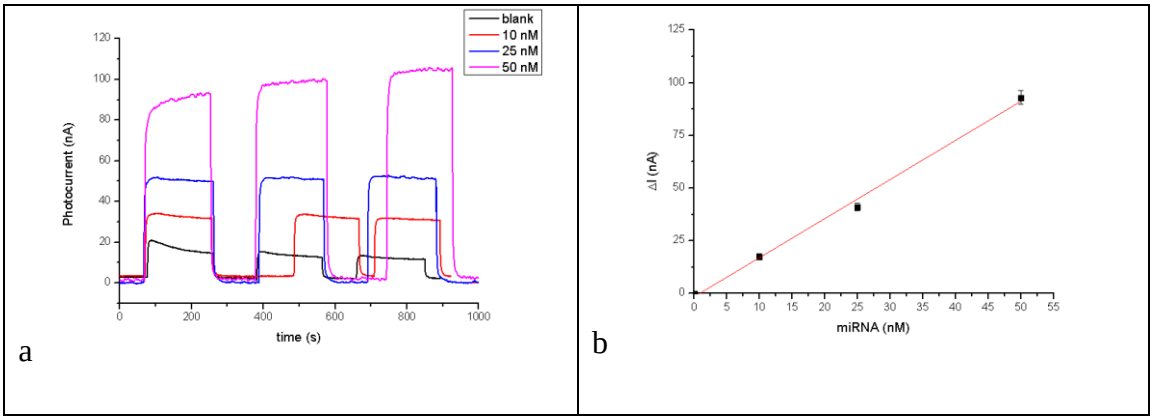

Figure 5.13 – a) Amerograms for the measurements corresponding to increased concentration of miRNA target (0, 10, 25, 50 nM in PB). Data are recorded at 0.0 V in Tris buffer in presence of 10 mg/mL AAP. Further details are reported in the material and methods section. b) Calibration plot for synthetic oligonucleotides in the enzymatic assay. Probe-modified sensors were exposed to a 20 µL drop of the biotinylated target sequence solution for 20 min. Each point represents the mean of at least three measurements and the error bars the corresponding standard deviation.

The hybrid modified gold electrodes were washed with Tris buffer and a measure in absence of AA or AAP was made in Tris buffer showing a photocurrent value comparable to the one registered with the blank (6.3 nA vs 10.5 nA respectively). The same sensor was then washed with 0.5 M PB and exposed for 30 min to a AAP solution in PB. Phosphate ions present in solution naturally inhibits the enzyme,

avoiding the AA product of the biocatalysis. The photocurrent registered was comparable to the one registered with the blank (12.6 nA vs 10.5 nA).

5.3 Discussion

In the present chapter the use of Alkaline Phosphatase as label for the photoelectrochemical detection of miRNA was proposed using gold modified titania electrodes. Gold nanorods, (prepared and charachterized by Dr. Ingrosso) were used in order to immobilize thiolated DNA probe. Streptavidin alkaline phosphatase was exposed to the biotinylated hybrid formed on the electrode surface. Prior to biosensor development, an electrochemical and photoelectrochemical characterization of the electrode surface was performed.

One of the fundamental properties of any semiconductor–electrolyte system is its flat-band potential. Of primary importance in the development of photoelectrochemical systems is understanding the relationship between semiconductor and electrolyte energy levels. As described in chapter 1, the valence and conduction-band edges (VB and CB, respectively), the band-gap energy (E_G), and the Fermi level (E_F), which is the energy at which the probability of an electronic state being occupied is 0.5, represent important parameter that characterized a semiconductor-electrolyte interface. Mott–Schottky equation was used to determine the flat-band potential of the TiO_2 electrode in order to demonstrate its n-type semiconductor behavior. Prior to obtain the Mott–Schottky plot, a series of CVs were performed in order to establish the non-faradaic potential range, that resulted from -0.2 to +0.8 V. Mott–Schottky plot was constructed showing an n-type semiconductor for TiO_2-ITO electrode. Mott–Schottky diagram as C_1^{-2} vs E reported in figure 5.5 gave an intercept and a slope of $3.36 \cdot 10^9$ F^{-2} and $9.75 \cdot 10^6$ F^{-2}/mV respectively. From Mott – Schottky equation is possible to calculate -344 mV and $1.68 \cdot 10^{22}$ cm^{-3} as E_{fb} and N_D respectively. Results are in good agreement with data of the literature [248].

A photoelectrochemical characterization with AA was performed in order to demonstrate the enhancement behavior of an electron donor molecule. Calibration plot obtained with AA in Tris buffer, indicate the effective increase of the photocurrent registered on the gold modified titania electrodes.

A LED lamp with maximum λ in the visible region was experimentally chosen for the assay. Starting from the scheme of the enzymatic assay developed in the previous chapters, a phosphorylated ascorbic acid was used as substrate of the biocatalytic reaction in order to recognize the hybridization event on the gold modified electrode surface. The capture probe was immobilized on the nanorods with the well-known chemistry of thiols. The capture-probe-modified electrode is, then, allowed to react with the analyte (the target biotinylated miRNA). Then, the biotinylated hybrid is exposed to the enzyme streptavidin conjugate and the product of the enzymatic reaction was then electrochemically monitored using chronoamperometry. With non-optimized parameter of the scheme, a preliminary calibration plot with synthetic miR-221 oligonucleotide was performed in the range of 0 to 50 nM in PB.

5.4 Conclusions

Commercial titania electrode modified with gold nanorods was used in order to develop a genosensor for miRNA detection. After an electrochemical and a photoelectrochemical characterization of the electrode surface, a preliminary calibration plot was evaluated. First results showed that photoelectrochemistry recognizes hybridization event of miRNA target with its capture probe. Moreover, the use of AuNRs allows the use of visible source light with titania nanocrystals based electrodes, and the possibility to immobilize thiolated capture probe. The investigated assay demonstrate the possibility to develop a simple detection scheme with commercial semiconductor electrode and commercial low cost light sources. This enzyme amplification produces a sensitivity of 1.85 nA/nM, with an estimated detection limit of 2 nM and an average RSD of 5%. LOD estimated is too high for the specific application, but the possibilities to develop new assay scheme with nanoarchitectures rich in enzyme (like liposome) could further increase the sensitivity of the method.

Chapter 6 – General discussion and conclusions

The present work was focused on the development of electrochemical geno-assay using different types of nanomaterials (liposomes, gold nanoparticles, polymer films and titania films) for miRNA detection. In particular, miRNA 221 and 222, considered as potential candidates for biomarkers of lung cancer, were chosen as analytical target. The final goal is to develop simple and low cost platforms for miRNAs subpicomolar detection.

6.1 Electrochemical genosensors

6.1.1 Enzyme and Enzyme decorated liposome based assays

The features of the DNA probe immobilization process and the formation of DNA-SH/MCH mixed monolayers with different pretreatment of screen printed gold electroes were qualitatively investigated by faradic impedance spectroscopy, using the $[Fe(CN)_6]^{3/4-}$ mixture as the redox probe and cyclic voltammetry using $[Fe(CN)_6]^{4-}$ and H_2SO_4. Results show how pretreatment is necessary in order to obtain impedimetric reproducible signals. The amount of thiol-tethered DNA probe immobilized at the sensor surface was quantified through chronocoulometric measurements, in the presence of $[Ru(NH_3)_6]^{3+}$. This complex exchanged with K^+, the cation natively compensating the polyanionic backbone of the oligonucleotides.

Electrochemical Impedence Spectroscopy (EIS) was chosen as electroanalytical technique due to its intrinsic property that allows a label-free detection scheme. In a first approach, a label-free detection scheme, based on the recognition of hybrid formed exposing target sequence on the capture probe modified gold electrode, was tested showing a low sensitivity. In order to increase the sensitivity of the assay, an enzyme amplification route was investigated. In this case, the hybrid formed on the electrode surface was labeled using the enzyme Alkaline-Phosphatase. The high bio-catalytic activity of the alkaline phosphatase label provided a huge number of insoluble molecules for each target strand recognized by the immobilized probe. Therefore, compared to the label-free detection scheme, the sensitivity of the assays

was dramatically enhanced. Interesting detection limits were obtained upon using the BCIP/NBT mixture as the enzymatic substrate and EIS as the electrochemical method (180 pM of synthetic oligonucleotides with a sensitivity of 1.89 kΩ/nM and an RSD of 14%). A total analysis time of about 1 h was employed for the analysis of synthetic sequences.

Enzyme-decorated liposomes were then tested as labels in order to amplify the miRNA-electrochemical sensing. Liposomes were used to tether multiple molecules of enzyme in order to increase sensitivity of enzyme label biosensor. Herein, a procedure to obtain biotin-tagged liposomes has been adapted starting from procedure reported in literature [131]. These biotinylated liposomes were characterized by DLS, showing a hydrodynamic diameter of ≈150 nm. Average diameters of prepared liposomes were determined at the day of preparation and compared with those after incubation for 30 days at 4°C (stability test). Aggregation of liposomes during the stability test was negligible. In order to confirm the presence of biotin on the vesicle surface, free streptavidin and streptavidin conjugated alkaline phosphatase were used to allow the aggregation of liposomes through biotin-streptavidin binding. Results show how hydrodynamic diameter increases in presence of both molecules.

Biotin tagged liposomes were anchored on biotinylated hybrid thorough a streptavidin molecule. The enzymatic conjugate was, then, anchored trough biotin tags present on the liposome. Therefore, compared to the enzyme based detection scheme, the sensitivity of the assays was enhanced. Interesting detection limits were obtained upon using the BCIP/NBT mixture as the enzymatic substrate and EIS as the electrochemical method (37 pM of synthetic oligonucleotides with a sensitivity of 10.3 kΩ/nM and an RSD of 15%). A total analysis time of about 2 h was employed for the analysis of synthetic sequences.

6.1.2 Nanostructuration of the electrode surface

In order to increase sensitivity, screen printed carbon electrodes were modified with gold nanoclusters by electrodeposition. Biotin tagged liposomes were exposed to the biotinylated hybrid formed on the electrode surfaces and then to streptavidin-alkaline phosphatase. The product of the enzymatic reaction was then electrochemically monitored using impedance spectroscopy.

Cyclic voltammetry conditions for gold electrodeposition were optimized in order to obtain the best analytical performance. Modified sensors with optimized procedure for nanostructuration with gold, where then characterized by electrochemical, SEM and EDX experiments. CV in H_2SO_4 and EDX confirm the presence of gold in treated electrodes. For all these experiments unmodified screen printed electrodes were used as negative control. Scanning Electron Microscopy allows to determinate the size distribution, showing the presence of some aggregate, but with an high concentration of small particles with radius minor than 100 nm.

Biotin-tagged liposome based assay has been tested and compared with an enzyme based assay. Both the schemes studied demonstrate the possibility to increase the sensitivity of the assay in comparison with the label free scheme. In a first strategy, streptavidin conjugated alkaline phosphatase is bound to the biotinylated hybrid causing the formation of an enzyme rich network. This signal amplification produces a sensitivity of 41.6 kΩ/nM. This higher sensitivity was attributed to the biocatalytic product used as biorecognition element for the hybridization event. Another hypothesis is the increased probe density immobilized on the surface. In order to confirm the increased probe density on the electrode surface, two different experiments were performed: a chronocoulometric detection and EDX measurements. Both measure failed. Chronocoulometric detection gives high aspecific signals, probably due to the adsorbtion of ruthenium complex on the graphite surface. The EDX measurement was performed in order to quantify probes through the sulfur atom of the thiolated capture probe. Unfortunately, sulfur was also present on the negative control, probably due to the electrodeposition process made in presence of sulfuric acid.

In a second strategy biotin-tagged liposomes have been tested. Liposomes, owing to their large surface area, are capable of carrying a large number of streptavidin conjugated alkaline phosphatase molecules. Compared to enzyme assay, liposome assay allows a 5-fold enhancement of the electroanalytical (229 kΩ/nM) signal using impedance spectroscopy and an estimated detection limit of 0.6 pM.

6.1.3 Polymer based assay

The use of inexpensive gold-based electrodes and the label-free detection scheme made this biosensor particularly attractive. Consisting of a few basic steps, such an

analytical protocol should be easily followed even by untrained personnel. The short analysis time (less than 2 h) was the last, important, advantage. The indicator-free scheme adopted relied on the increasing of electron transfer resistance after hybrid formation. It is usually accepted that the immobilization of the DNA probe onto the sensor surface plays a crucial role in genosensor preparation, deeply determining its bio-recognition capabilities. Immobilization of densely packed DNA probe layers was required during the analysis of synthetic oligonucleotides for efficiently suppressing the non-specific adsorption of such short sequences. Biotinylated conductive polymer film was used as immobilization strategy for DNA capture probe. A biotinylated monomer was potentiodynamically polymerized on the electrode surface via CV. In order to obtain the higher sensitivity of the genosensor, a characterization of electropolymerization process was performed. Calibration plot made with synthetic miRNA sequences show a linear range with 0.14 kΩ/pM (or 140 kΩ/nM) with a calculated LOD of 1.1 pM.

6.1.4 Electrochemical genosensors conclusions

Over the past decade, enormous progresses have been made towards the development of electrochemical genosensors for miRNA detection. Such devices are of considerable interest due to their promise for obtaining sequence-specific information in a faster, simpler and cheaper manner compared to traditional nucleic acid assays. The first part of the work of this thesis has described the implementation of different electrochemical geno-assays using inexpensive screen-printed electrodes as disposable transducers. Graphite and gold-based electrodes were obtained by screen-printing polymeric inks requiring low curing temperatures onto polyester flexible substrates.

In a first approach, the genoassay was developed using disposable screen printed gold electrodes (SPGE). The surface of a SPGE was modified with a thiol-tethered DNA capture probe, a spacer thiol, and then exposed to the target miRNA sequence. Electrochemical Impedence Spectroscopy (EIS) was chosen as electroanalytical technique due to its intrinsic property that allows a label-free detection scheme. Moreover, in order to increase the sensitivity of the assay, an enzyme amplification route was investigated. In this case, the hybrid formed on the electrode surface was labeled using the enzyme Alkaline-Phosphatase. The electrochemical transduction of the hybridization process was performed by means of EIS, after a biocatalyzed

conversion of a soluble substrate into an insoluble and insulating product. Sensitivity and LOD obtained were too high for the specific application. Thus, enzyme-decorated liposomes were then tested as labels in order to amplify the miRNA-electrochemical sensing. Compared to the enzyme-based scheme, the use of biotin tagged liposome increases sensitivity of 5-fold of magnitude (see table 6.1). The possibility to further increase the sensitivity of the assay by nanostructuration of the working electrode surface was also investigated using carbon screen printed electrodes modified with gold nanoclusters through electrodeposition, obtaining an highest sensitivity and a detection limit in the picomolar range.

In another approach, an electroconductive polymer film was investigated in order to obtain a label-free assay. In particular, a biotinylated bisthiophene monomer was potentiodynamically polymerized to form films on the SPGEs surface. This structure served for capture probe immobilization as recognition element of the complementary miRNA sequence via hybridization event. EIS was chosen as electroanalytical technique. The use of conductive polymer resulted in a label-free assay with sensitivity in the picomolar range.

The label based assays showed to have some important limitations (i.e. the target labeling process and analysis time needed). In contrast, the label-free impedimetric assay developed using the gold sensors offered the best performances.

Electrode	Label	Sensitivity (kΩ/nM)	LOD (pM)
SPGE	Enzyme	1.89	180.0
SPGE	Liposome	10.3	37.0
AuSPCE	Liposome	229	0.6
SPGE	Label-free	140	1.1

Table 6.1 – Sensitivities and LODs obtained with developed genosensors.

6.2 Photoelectrochemical genosensor

Preliminary results obtained for the development of a photoelectrochemical genosensor demonstrate the possibility to recognize a hybridization event of a specific miRNA sequence. Titanium dioxide electrodes are commonly used as photocurrent generator under UV illumination. The use of gold nanorods, instead, allow the possibility to obtain a photocurrent under visible light. A commercial white LED was used for the development of the genoassay in a three electrode configuration.

An enzymatic detection scheme, based on the use of streptavidin conjugated alkaline phosphatase, was proposed and preliminary calibration plot performed. This enzyme amplification produces a sensitivity of 1.85 nA/nM, with an estimated detection limit of 2 nM and an average RSD of 5%. LOD estimated is too high for the specific application, but further optimization and the possibilities to develop new assay schemes with nanoarchitectures rich in enzyme could further increase the sensitivity of the method.

6.2.1 Conclusions and future work

Preliminary results obtained with a photoelectrochemical transduction underline the possibility to develop e genosensor for miRNA detection. Enzymatic assay for hybridization event transduction is necessary, but the possibility to introduce an hairpin capture probe, coupled with a biotinylated signaling probe, could permit the development of a label free enzymatic detection scheme. Morover, the use of nanorchitectures for enzyme reach structures could further increase sensitivity.

References

1. http://www.istat.it
2. http://www.registri-tumori.it/PDF/AIOM2013/I_numeri_del_cancro_2013.pdf
3. http://www.istat.it/it/archivio/14256
4. Berenblum, I., *Classics in oncology: The mechanism of carcinogenesis: A study of the significance of cocarcinogenic action and related phenomena.* CA: A Cancer Journal for Clinicians, 1981. **31**(4): p. 241-253.
5. Berenblum, I., *Sequential Aspects of Chemical Carcinogenesis: Skin*, in *Cancer. A Comprehensive Treatise*, F. Becker, Editor. 1975, Springer US. p. 323-344.
6. Yamasaki, H., *Multistage carcinogenesis: implications for risk estimation.* Cancer and Metastasis Reviews, 1988. **7**(1): p. 5-18.
7. Spandidos, D.A. and M.L.M. Anderson, *Oncogenes and onco-suppressor genes: Their involvement in cancer.* The Journal of Pathology, 1989. **157**(1): p. 1-10.
8. Atkinson, A.J., et al., *Biomarkers and surrogate endpoints: Preferred definitions and conceptual framework*.* Clin Pharmacol Ther, 2001. **69**(3): p. 89-95.
9. WHO International Programme on Chemical Safety Biomarkers in Risk Assessment: Validity and Validation. 2001. http://www.inchem.org/documents/ehc/ehc/ehc222.htm
10. Maggino, T. and A. Gadducci, *Serum markers as prognostic factors in epithelial ovarian cancer: an overview.* European journal of gynaecological oncology, 2000. **21**(1): p. 64-69.
11. Moore, R.G., et al., *The use of multiple novel tumor biomarkers for the detection of ovarian carcinoma in patients with a pelvic mass.* Gynecologic Oncology, 2008. **108**(2): p. 402-408.
12. Gold, P. and S.O. Freedman, *DEMONSTRATION OF TUMOR-SPECIFIC ANTIGENS IN HUMAN COLONIC CARCINOMATA BY IMMUNOLOGICAL TOLERANCE AND ABSORPTION TECHNIQUES.* The Journal of Experimental Medicine, 1965. **121**(3): p. 439-462.
13. Zhou, L., J. Liu, and F. Luo, *Serum tumor markers for detection of hepatocellular carcinoma.* World J Gastroenterol, 2006. **12**(8).

14. Liu, P.P.L., et al., *Bone-Specific Alkaline Phosphatase in Plasma as Tumour Marker for Osteosarcoma.* Oncology, 1996. **53**(4): p. 275-280.
15. Calin, G.A. and C.M. Croce, *MicroRNA signatures in human cancers.* Nat Rev Cancer, 2006. **6**(11): p. 857-66.
16. Lee, R.C., R.L. Feinbaum, and V. Ambros, *The C. elegans heterochronic gene lin-4 encodes small RNAs with antisense complementarity to lin-14.* Cell, 1993. **75**(5): p. 843-854.
17. Wightman, B., I. Ha, and G. Ruvkun, *Posttranscriptional regulation of the heterochronic gene lin-14 by lin-4 mediates temporal pattern formation in C. elegans.* Cell, 1993. **75**(5): p. 855-862.
18. *The Evolution of Self-Fertile Hermaphroditism: The Fog Is Clearing.* PLOS Biology, 2004.
19. Reinhart, B.J., et al., *The 21-nucleotide let-7 RNA regulates developmental timing in Caenorhabditis elegans.* Nature, 2000. **403**(6772): p. 901-906.
20. Pasquinelli, A.E., et al., *Conservation of the sequence and temporal expression of let-7 heterochronic regulatory RNA.* Nature, 2000. **408**(6808): p. 86-89.
21. Lee, Y., et al., *MicroRNA maturation: stepwise processing and subcellular localization*. Vol. 21. 2002. 4663-4670.
22. Lee, Y., et al., *The nuclear RNase III Drosha initiates microRNA processing.* Nature, 2003. **425**(6956): p. 415-419.
23. Lund, E., et al., *Nuclear Export of MicroRNA Precursors.* Science, 2004. **303**(5654): p. 95-98.
24. Nohata, N., et al., *microRNA-1/133a and microRNA-206/133b clusters: Dysregulation and functional roles in human cancers*. 2012. Vol. 3. 2012.
25. van Rooij, E., et al., *A signature pattern of stress-responsive microRNAs that can evoke cardiac hypertrophy and heart failure.* Proceedings of the National Academy of Sciences, 2006. **103**(48): p. 18255-18260.
26. Pauley, K.M., S. Cha, and E.K.L. Chan, *MicroRNA in autoimmunity and autoimmune diseases.* Journal of Autoimmunity, 2009. **32**(3–4): p. 189-194.
27. Hébert, S.S. and B. De Strooper, *Alterations of the microRNA network cause neurodegenerative disease.* Trends in Neurosciences, 2009. **32**(4): p. 199-206.
28. Calin, G.A., et al., *Frequent deletions and down-regulation of micro- RNA genes miR15 and miR16 at 13q14 in chronic lymphocytic leukemia.* Proceedings of the National Academy of Sciences, 2002. **99**(24): p. 15524-15529.

29. Iorio, M.V. and C.M. Croce, *MicroRNA dysregulation in cancer: diagnostics, monitoring and therapeutics. A comprehensive review*. Vol. 4. 2012. 143-159.
30. Aqeilan, R.I., G.A. Calin, and C.M. Croce, *miR-15a and miR-16-1 in cancer: discovery, function and future perspectives.* Cell Death Differ, 2009. **17**(2): p. 215-220.
31. Tsuchida, A., et al., *miR-92 is a key oncogenic component of the miR-17–92 cluster in colon cancer.* Cancer Science, 2011. **102**(12): p. 2264-2271.
32. Lu, L., et al., *miR-21 Targets 15-PGDH and Promotes Cholangiocarcinoma Growth.* Molecular Cancer Research, 2014. **12**(6): p. 890-900.
33. Ji, Q., et al., *Restoration of tumor suppressor miR-34 inhibits human p53-mutant gastric cancer tumorspheres.* BMC Cancer, 2008. **8**(1): p. 266.
34. Jiang, S., et al., *MicroRNA-155 Functions as an OncomiR in Breast Cancer by Targeting the Suppressor of Cytokine Signaling 1 Gene.* Cancer Research, 2010. **70**(8): p. 3119-3127.
35. Wiklund, E.D., et al., *Coordinated epigenetic repression of the miR-200 family and miR-205 in invasive bladder cancer.* International Journal of Cancer, 2011. **128**(6): p. 1327-1334.
36. Zhang, C.-Z., et al., *MiR-221 and miR-222 target PUMA to induce cell survival in glioblastoma.* Molecular Cancer, 2010. **9**(1): p. 229.
37. Galardi, S., et al., *miR-221 and miR-222 Expression Affects the Proliferation Potential of Human Prostate Carcinoma Cell Lines by Targeting p27Kip1.* Journal of Biological Chemistry, 2007. **282**(32): p. 23716-23724.
38. Visone, R., et al., *MicroRNAs (miR)-221 and miR-222, both overexpressed in human thyroid papillary carcinomas, regulate p27Kip1 protein levels and cell cycle.* Endocrine-Related Cancer, 2007. **14**(3): p. 791-798.
39. Michael, M.Z., et al., *Reduced Accumulation of Specific MicroRNAs in Colorectal Neoplasia11Note: Susan M. O' Connor and Nicholas G. van Holst Pellekaan contributed equally to this work.* Molecular Cancer Research, 2003. **1**(12): p. 882-891.
40. Wang, B., H. Wang, and Z. Yang, *MiR-122 Inhibits Cell Proliferation and Tumorigenesis of Breast Cancer by Targeting IGF1R.* PLoS ONE, 2012. **7**(10): p. e47053.
41. Lawrie, C.H., et al., *Detection of elevated levels of tumour-associated microRNAs in serum of patients with diffuse large B-cell lymphoma.* British Journal of Haematology, 2008. **141**(5): p. 672-675.

42. Cortez, M.A., et al., *MicroRNAs in body fluids[mdash]the mix of hormones and biomarkers.* Nat Rev Clin Oncol, 2011. **8**(8): p. 467-477.
43. Di Leva, G., M. Garofalo, and C.M. Croce, *MicroRNAs in Cancer.* Annual Review of Pathology: Mechanisms of Disease, 2014. **9**(1): p. 287-314.
44. Moldovan, L., et al., *Methodological challenges in utilizing miRNAs as circulating biomarkers.* Journal of Cellular and Molecular Medicine, 2014. **18**(3): p. 371-390.
45. Di Leva G, Garofalo M, Croce CM. MicroRNAs in cancer. Annual Review of Pathology. 2014;9:287–314.
46. Garofalo, M., et al., *MicroRNA signatures of TRAIL resistance in human non-small cell lung cancer.* Oncogene, 2008. **27**(27): p. 3845-3855.
47. Li, J., et al., *Expression of serum miR-221 in human hepatocellular carcinoma and its prognostic significance.* Biochemical and Biophysical Research Communications, 2011. **406**(1): p. 70-73.
48. Di Leva, G., et al., *MicroRNA Cluster 221-222 and Estrogen Receptor α Interactions in Breast Cancer.* Journal of the National Cancer Institute, 2010. **102**(10): p. 706-721.
49. Felicetti, F., et al., *The Promyelocytic Leukemia Zinc Finger–MicroRNA-221/-222 Pathway Controls Melanoma Progression through Multiple Oncogenic Mechanisms.* Cancer Research, 2008. **68**(8): p. 2745-2754.
50. Callegari, E., et al., *Liver tumorigenicity promoted by microRNA-221 in a mouse transgenic model.* Hepatology, 2012. **56**(3): p. 1025-1033.
51. Stinson, S., et al., *TRPS1 Targeting by miR-221/222 Promotes the Epithelial-to-Mesenchymal Transition in Breast Cancer*. Vol. 4. 2011. ra41-ra41.
52. le Sage, C., et al., *Regulation of the p27Kip1 tumor suppressor by miR-221 and miR-222 promotes cancer cell proliferation*. Vol. 26. 2007. 3699-3708.
53. Garofalo, M., et al., *EGFR and MET receptor tyrosine kinase-altered microRNA expression induces tumorigenesis and gefitinib resistance in lung cancers.* Nat Med, 2012. **18**(1): p. 74-82.
54. Válóczi, A., et al., *Sensitive and specific detection of microRNAs by northern blot analysis using LNA-modified oligonucleotide probes.* Nucleic Acids Research, 2004. **32**(22): p. e175.
55. Barad, O., et al., *MicroRNA expression detected by oligonucleotide microarrays: System establishment and expression profiling in human tissues.* Genome Research, 2004. **14**(12): p. 2486-2494.

56. Liang, R.-Q., et al., *An oligonucleotide microarray for microRNA expression analysis based on labeling RNA with quantum dot and nanogold probe.* Nucleic Acids Research, 2005. **33**(2): p. e17.
57. Cissell, K., S. Campbell, and S. Deo, *Rapid, single-step nucleic acid detection.* Analytical and Bioanalytical Chemistry, 2008. **391**(7): p. 2577-2581.
58. Teo, A.K.L., C.L. Lim, and Z. Gao, *The development of electrochemical assays for microRNAs.* Electrochimica Acta, 2014. **126**: p. 19-30.
59. Hamidi-Asl, E., et al., *A review on the electrochemical biosensors for determination of microRNAs.* Talanta, 2013. **115**: p. 74-83.
60. Campuzano, S., M. Pedrero, and J.M. Pingarron, *Electrochemical genosensors for the detection of cancer-related miRNAs.* Anal. Bioanal. Chem., 2014. **406**(1): p. 27-33.
61. Thévenot, D.R., et al., *Electrochemical biosensors: recommended definitions and classification.* Biosensors & Bioelectronics, 2001. **16**(1–2): p. 121-131.
62. Cammann, K., *Bio-sensors based on ion-selective electrodes.* Fresenius' Zeitschrift für analytische Chemie, 1977. **287**(1): p. 1-9.
63. Leech, D., *Affinity biosensors.* Chemical Society Reviews, 1994. **23**(3): p. 205-213.
64. Jayasena, S.D., *Aptamers: An Emerging Class of Molecules That Rival Antibodies in Diagnostics.* Clinical Chemistry, 1999. **45**(9): p. 1628-1650.
65. Mascini, M., I. Palchetti, and S. Tombelli, *Nucleic Acid and Peptide Aptamers: Fundamentals and Bioanalytical Aspects.* Angewandte Chemie International Edition, 2012. **51**(6): p. 1316-1332.
66. Laschi, S., et al., *Development of disposable low density screen-printed electrode arrays for simultaneous electrochemical measurements of the hybridisation reaction.* Journal of Electroanalytical Chemistry, 2006. **593**(1–2): p. 211-218.
67. Labuda, J., et al., *Electrochemical nucleic acid-based biosensors: Concepts, terms, and methodology (IUPAC Technical Report)*, in *Pure and Applied Chemistry*. 2010. p. 1161.
68. Laschi, S., et al., *Enzyme-amplified electrochemical hybridization assay based on PNA, LNA and DNA probe-modified micro-magnetic beads.* Bioelectrochemistry, 2009. **76**(1–2): p. 214-220.
69. Zanardi, C., et al., *Development of a gold-nanostructured surface for amperometric genosensors.* Journal of Nanoparticle Research, 2012. **14**(10): p. 1-12.
70. Zhang, X., et al., *Photoelectrochemically active species and photoelectrochemical biosensors.* RSC Advances, 2013. **3**(9): p. 2846-2857.

71. Bard, A.J. and M. Stratmann, *Semiconductor Electrodes and Photoelectrochemistry*, in *Encyclopedia of Electrochemistry*, S. Licht, Ed., Editor. 2002, Wiley–VCH: Weinheim.
72. Mettenbörger, A., et al., *Plasma-chemical reduction of iron oxide photoanodes for efficient solar hydrogen production.* International Journal of Hydrogen Energy, 2014. **39**(10): p. 4828-4835.
73. Chuang, H.-Y., et al., *Synthesis and properties of a new conjugated polymer containing benzodithiophene for polymer solar cells.* Polymer Bulletin, 2014. **71**(5): p. 1117-1130.
74. Derry, C., et al., *Composite Semiconductor Material of Carbon Nanotubes and Poly[5,5′-bis(3-dodecyl-2-thienyl)-2,2′-bithiophene] for High-Performance Organic Thin-Film Transistors.* Journal of Electronic Materials, 2013. **42**(12): p. 3481-3488.
75. Shon, J.W., et al., *Fabrication of full-color InGaN-based light-emitting diodes on amorphous substrates by pulsed sputtering.* Sci. Rep., 2014. **4**.
76. Zhang, Y., et al., *Flexible paper-based ZnO nanorod light-emitting diodes induced multiplexed photoelectrochemical immunoassay.* Chemical Communications, 2014. **50**(12): p. 1417-1419.
77. Wang, W., et al., *Visible light induced photoelectrochemical biosensing based on oxygen-sensitive quantum dots.* Analytica Chimica Acta, 2012. **744**(0): p. 33-38.
78. Liu, Q., et al., *A visible light photoelectrochemical biosensor coupling enzyme-inhibition for organophosphates monitoring based on a dual-functional Cd0.5Zn0.5S-reduced graphene oxide nanocomposite.* Analyst, 2014. **139**(5): p. 1121-1126.
79. Wenjuan, Y., et al., *Electrogenerated trisbipyridyl Ru(II)-/nitrilotriacetic-polypyrene copolymer for the easy fabrication of label-free photoelectrochemical immunosensor and aptasensor: Application to the determination of thrombin and anti-cholera toxinantibody.* Biosensors & Bioelectronics, 2013. **42**(0): p. 556-562.
80. Liu, L., et al., *Direct detection of microRNA-126 at a femtomolar level using a glassy carbon electrode modified with chitosan, graphene sheets, and a poly(amidoamine) dendrimer composite with gold and silver nanoclusters.* Microchimica Acta, 2014: p. 1-8.
81. Bettazzi, F., et al., *Electrochemical detection of miRNA-222 by use of a magnetic bead-based bioassay.* Analytical and Bioanalytical Chemistry, 2013. **405**(2-3): p. 1025-1034.

82. Voccia, D., et al., *Alkaline-Phosphatase-Based Nanostructure Assemblies for Electrochemical Detection of microRNAs.* Journal of Nanoscience and Nanotechnology, 2015. **15**(5): p. 3378-3384.
83. Farabullini, F., et al., *Disposable electrochemical genosensor for the simultaneous analysis of different bacterial food contaminants.* Biosensors & Bioelectronics, 2007. **22**(7): p. 1544-1549.
84. Bettazzi, F., et al., *Disposable electrochemical DNA-array for PCR amplified detection of hazelnut allergens in foodstuffs.* Analytica Chimica Acta, 2008. **614**(1): p. 93-102.
85. Yu, Y., et al., *Ultrasensitive Electrochemical Detection of MicroRNA Based on an Arched Probe Mediated Isothermal Exponential Amplification.* Analytical Chemistry, 2014. **86**(16): p. 8200-8205.
86. Patel, M.K., et al., *Magnesium oxide grafted carbon nanotubes based impedimetric genosensor for biomedical application.* Biosensors & Bioelectronics, 2013. **50**(0): p. 406-413.
87. Wang, J., et al., *Trace Measurements of RNA by Potentiometric Stripping Analysis at Carbon Paste Electrodes.* Analytical Chemistry, 1995. **67**(22): p. 4065-4070.
88. Millan, K.M. and S.R. Mikkelsen, *Sequence-selective biosensor for DNA based on electroactive hybridization indicators.* Analytical Chemistry, 1993. **65**(17): p. 2317-2323.
89. Nuzzo, R.G. and D.L. Allara, *Adsorption of bifunctional organic disulfides on gold surfaces.* Journal of the American Chemical Society, 1983. **105**(13): p. 4481-4483.
90. Herne, T.M. and M.J. Tarlov, *Characterization of DNA Probes Immobilized on Gold Surfaces.* Journal of the American Chemical Society, 1997. **119**(38): p. 8916-8920.
91. Levicky, R., et al., *Using Self-Assembly To Control the Structure of DNA Monolayers on Gold: A Neutron Reflectivity Study.* Journal of the American Chemical Society, 1998. **120**(38): p. 9787-9792.
92. Steel, A.B., T.M. Herne, and M.J. Tarlov, *Electrochemical Quantitation of DNA Immobilized on Gold.* Analytical Chemistry, 1998. **70**(22): p. 4670-4677.
93. Lucarelli, F., et al., *Electrochemical and piezoelectric DNA biosensors for hybridisation detection.* Anal Chim Acta, 2008. **609**(2): p. 139-59.
94. Jin, J. and J. Grote, *Materials Science of DNA*. 2012, Boca Raton, FL (USA): CRC Press, Taylor & Francis Group.

95. Obika, S., et al., *Stability and structural features of the duplexes containing nucleoside analogues with a fixed N-type conformation, 2'-O,4'- C-methyleneribonucleosides* Tetrahedron Lett 1998. **39**: p. 5401-5404.
96. Kvaerno, L. and J. Wengel, *Investigation of restricted backbone conformations as an explanation for the exceptional thermal stabilities of duplexes involving LNA (Locked Nucleic Acid):[dagger] synthesis and evaluation of abasic LNA.* Chemical Communications, 1999(7): p. 657-658.
97. Patolsky, F., G. Zheng, and C.M. Lieber, *Nanowire-Based Biosensors.* Analytical Chemistry, 2006. **78**(13): p. 4260-4269.
98. Nair, P.R. and M.A. Alam, *Dimensionally Frustrated Diffusion towards Fractal Adsorbers.* Physical Review Letters, 2007. **99**(25): p. 256101.
99. Merkoçi, A., *Electrochemical biosensing with nanoparticles.* FEBS Journal, 2007. **274**(2): p. 310-316.
100. Zhang, P., et al., *An electrochemiluminescent microRNA biosensor based on hybridization chain reaction coupled with hemin as the signal enhancer.* Analyst, 2014. **139**(11): p. 2748-2753.
101. Xu, Q. and J.J. Davis, *The Diagnostic Utility of Electrochemical Impedance.* Electroanalysis, 2014. **26**(6): p. 1249-1258.
102. Guan, J.-G., Y.-Q. Miao, and Q.-J. Zhang, *Impedimetric biosensors.* Journal of Bioscience and Bioengineering, 2004. **97**(4): p. 219-226.
103. Gao, Z. and Z. Yang, *Detection of MicroRNAs Using Electrocatalytic Nanoparticle Tags.* Analytical Chemistry, 2006. **78**(5): p. 1470-1477.
104. Gao, Z. and Y.H. Yu, *A microRNA biosensor based on direct chemical ligation and electrochemically amplified detection.* Sensors and Actuators B-Chemical, 2007. **121**(2): p. 552-559.
105. Gao, Z. and Y.H. Yu, *Direct labeling microRNA with an electrocatalytic moiety and its application in ultrasensitive microRNA assays.* Biosensors & Bioelectronics, 2007. **22**(6): p. 933-940.
106. Peng, Y. and Z. Gao, *Amplified Detection of MicroRNA Based on Ruthenium Oxide Nanoparticle-Initiated Deposition of an Insulating Film.* Analytical Chemistry, 2011. **83**(3): p. 820-827.
107. Peng, Y., G. Yi, and Z. Gao, *A highly sensitive microRNA biosensor based on ruthenium oxide nanoparticle-initiated polymerization of aniline.* Chemical Communications, 2010. **46**(48): p. 9131-9133.

108. Yang, H., et al., *Direct, Electronic MicroRNA Detection for the Rapid Determination of Differential Expression Profiles.* Angewandte Chemie International Edition, 2009. **48**(45): p. 8461-8464.
109. Pöhlmann, C. and M. Sprinzl, *Electrochemical Detection of MicroRNAs via Gap Hybridization Assay.* Analytical Chemistry, 2010. **82**(11): p. 4434-4440.
110. Gao, Z., *A highly sensitive electrochemical assay for microRNA expression profiling.* Analyst, 2012. **137**(7): p. 1674-1679.
111. Gao, Z. and Y. Peng, *A highly sensitive and specific biosensor for ligation- and PCR-free detection of MicroRNAs.* Biosensors & Bioelectronics, 2011. **26**(9): p. 3768-3773.
112. Yin, H., et al., *An electrochemical signal 'off-on' sensing platform for microRNA detection.* Analyst, 2012. **137**(6): p. 1389-95.
113. Zhou, Y., et al., *MicroRNA-21 detection based on molecular switching by amperometry.* New Journal of Chemistry, 2012. **36**(10): p. 1985-1991.
114. Liu, L., et al., *Highly sensitive and label-free electrochemical detection of microRNAs based on triple signal amplification of multifunctional gold nanoparticles, enzymes and redox-cycling reaction.* Biosensors and Bioelectronics, 2014. **53**(0): p. 399-405.
115. Wang, J., et al., *Microfabricated thick-film electrochemical sensor for nucleic acid determination.* Analyst, 1996. **121**(7): p. 965-969.
116. Wang, J., et al., *Indicator-free electrochemical DNA hybridization biosensor.* Analytica Chimica Acta, 1998. **375**(3): p. 197-203.
117. Lucarelli, F., et al., *Coupling of an indicator-free electrochemical DNA biosensor with polymerase chain reaction for the detection of DNA sequences related to the apolipoprotein E.* Analytica Chimica Acta, 2002. **469**(1): p. 93-99.
118. Case-Green, S.C. and E.M. Southern, *Studies on the base pairing properties of deoxyinosine by solid phase hybridisation to oligonucleotides.* Nucleic Acids Research, 1994. **22**(2): p. 131-136.
119. Erdem, A. and G. Congur, *Label-free voltammetric detection of MicroRNAs at multi-channel screen printed array of electrodes comparison to graphite sensors.* Talanta, 2014. **118**(0): p. 7-13.
120. Gao, Z., et al., *A Label-Free Biosensor for Electrochemical Detection of Femtomolar MicroRNAs.* Analytical Chemistry, 2013. **85**(3): p. 1624-1630.
121. Fan, Y., et al., *Detection of microRNAs using target-guided formation of conducting polymer nanowires in nanogaps.* Journal of the American Chemical Society, 2007. **129**(17): p. 5437-5443.

122. Zhang, G.-J., et al., *Label-free direct detection of MiRNAs with silicon nanowire biosensors.* Biosensors and Bioelectronics, 2009. **24**(8): p. 2504-2508.
123. Labib, M., et al., *Three-mode electrochemical sensing of ultralow microRNA levels.* J Am Chem Soc, 2013. **135**(8): p. 3027-38.
124. Campuzano, S., et al., *Magnetobiosensors Based on Viral Protein p19 for MicroRNA Determination in Cancer Cells and Tissues.* Angewandte Chemie International Edition, 2014. **53**(24): p. 6168-6171.
125. Torrente-Rodríguez, R.M., et al., *Direct Determination of miR-21 in Total RNA Extracted from Breast Cancer Samples Using Magnetosensing Platforms and the p19 Viral Protein as Detector Bioreceptor*. Electroanalysis, 2014. **26**(10): p. 2080-2087.
126. Brigitte, S., et al., *Nanopatterning of gold colloids for label-free biosensing.* Nanotechnology, 2007. **18**(15): p. 155306.
127. Wanekaya, A.K., et al., *Nanowire-Based Electrochemical Biosensors.* Electroanalysis, 2006. **18**(6): p. 533-550.
128. Bangham, A.D. and R.W. Horne, *Negative staining of phospholipids and their structural modification by surface-active agents as observed in the electron microscope.* Journal of Molecular Biology, 1964. **8**(5): p. 660-IN10.
129. Gregoriadis, G. and B.E. Ryman, Biochem. J., 1971. **124**.
130. Akbarzadeh, A., et al., *Liposome: classification, preparation, and applications.* Nanoscale Research Letters, 2013. **8**(1): p. 102.
131. Alfonta, L., A.K. Singh, and I. Willner, *Liposomes Labeled with Biotin and Horseradish Peroxidase: A Probe for the Enhanced Amplification of Antigen−Antibody or Oligonucleotide−DNA Sensing Processes by the Precipitation of an Insoluble Product on Electrodes.* Analytical Chemistry, 2000. **73**(1): p. 91-102.
132. Katz, E., I. Willner, and J. Wang, *Electroanalytical and Bioelectroanalytical Systems Based on Metal and Semiconductor Nanoparticles.* Electroanalysis, 2004. **16**(1-2): p. 19-44.
133. Guo, S. and E. Wang, *Synthesis and electrochemical applications of gold nanoparticles.* Analytica Chimica Acta, 2007. **598**(2): p. 181-192.
134. Faraday, M., *The Bakerian Lecture: Experimental Relations of Gold (and Other Metals) to Light.* Philosophical Transactions of the Royal Society of London, 1857. **147**.
135. Kimling, J., et al., *Turkevich Method for Gold Nanoparticle Synthesis Revisited.* The Journal of Physical Chemistry B, 2006. **110**(32): p. 15700-15707.

136. Brust, M., et al., *Synthesis of thiol-derivatised gold nanoparticles in a two-phase Liquid-Liquid system.* Journal of the Chemical Society, Chemical Communications, 1994(7): p. 801-802.
137. Sharma, V., K. Park, and M. Srinivasarao, *Colloidal dispersion of gold nanorods: Historical background, optical properties, seed-mediated synthesis, shape separation and self-assembly.* Materials Science and Engineering: R: Reports, 2009. **65**(1–3): p. 1-38.
138. http://www.scielo.br/scielo.php?pid=S0103-50532010000700003&script=sci_arttext
139. Stone, J., S. Jackson, and D. Wright, *Biological applications of gold nanorods.* Wiley Interdisciplinary Reviews: Nanomedicine and Nanobiotechnology, 2011. **3**(1): p. 100-109.
140. Martin, C.R., *Nanomaterials: A Membrane-Based Synthetic Approach.* Science, 1994. **266**(5193): p. 1961-1966.
141. Yu, et al., *Gold Nanorods: Electrochemical Synthesis and Optical Properties.* The Journal of Physical Chemistry B, 1997. **101**(34): p. 6661-6664.
142. Jana, N.R., L. Gearheart, and C.J. Murphy, *Seed-Mediated Growth Approach for Shape-Controlled Synthesis of Spheroidal and Rod-like Gold Nanoparticles Using a Surfactant Template.* Advanced Materials, 2001. **13**(18): p. 1389-1393.
143. Pal, T., et al., *Organized Media as Redox Catalysts.* Langmuir, 1998. **14**(17): p. 4724-4730.
144. Nikoobakht, B. and M.A. El-Sayed, *Preparation and Growth Mechanism of Gold Nanorods (NRs) Using Seed-Mediated Growth Method.* Chemistry of Materials, 2003. **15**(10): p. 1957-1962.
145. Kim, F., J.H. Song, and P. Yang, *Photochemical Synthesis of Gold Nanorods.* Journal of the American Chemical Society, 2002. **124**(48): p. 14316-14317.
146. Niidome Y, Yamada S, Nishioka K, et al, Methods for manufacturing metal nanorods and use thereof, US20100143184A1 (2010).
147. Han, X., et al., *An electrochemical DNA biosensor based on gold nanorods decorated graphene oxide sheets for sensing platform.* Analytical Biochemistry, 2013. **443**(2): p. 117-123.
148. Congur, G., et al., *Voltammetric and impedimetric DNA detection at single-use graphite electrodes modified with gold nanorods.* Colloids and Surfaces B: Biointerfaces, 2013. **112**(0): p. 61-66.

149. Sheridan, E., J. Hjelm, and R.J. Forster, *Electrodeposition of gold nanoparticles on fluorine-doped tin oxide: Control of particle density and size distribution.* Journal of Electroanalytical Chemistry, 2007. **608**(1): p. 1-7.
150. E. Budevski, G. Staikov, W.J. Lorenz, Electrochemical Phase Formation and Growth-An Introduction to the Initial Stages of Metal Deposition, VCH, Weinheim, 1996.
151. Finot, M.O., G.D. Braybrook, and M.T. McDermott, *Characterization of electrochemically deposited gold nanocrystals on glassy carbon electrodes.* Journal of Electroanalytical Chemistry, 1999. **466**(2): p. 234-241.
152. El-Deab, M.S. and T. Ohsaka, *Hydrodynamic voltammetric studies of the oxygen reduction at gold nanoparticles-electrodeposited gold electrodes.* Electrochimica Acta, 2002. **47**(26): p. 4255-4261.
153. Dai, X., et al., *Anodic Stripping Voltammetry of Arsenic(III) Using Gold Nanoparticle-Modified Electrodes.* Analytical Chemistry, 2004. **76**(19): p. 5924-5929.
154. Oyama, T., T. Okajima, and T. Ohsaka, *Electrodeposition of Gold at Glassy Carbon Electrodes in Room-Temperature Ionic Liquids.* Journal of The Electrochemical Society, 2007. **154**(6): p. D322-D327.
155. Komsiyska, L. and G. Staikov, *Electrocrystallization of Au nanoparticles on glassy carbon from HClO4 solution containing [AuCl4]−.* Electrochimica Acta, 2008. **54**(2): p. 168-172.
156. O'Mullane, A.P., et al., *Premonolayer Oxidation of Nanostructured Gold: An Important Factor Influencing Electrocatalytic Activity.* Langmuir, 2009. **25**(6): p. 3845-3852.
157. Suárez, M.F., et al., *Evidence for Nucleation-Growth, Redistribution, and Dissolution Mechanisms during the Course of Redox Cycling Experiments on the C60/NBu4C60 Solid-State Redox System: Voltammetric, SEM, and in Situ AFM Studies.* The Journal of Physical Chemistry B, 1999. **103**(27): p. 5637-5644.
158. Fletcher, S., et al., J. Electroanal. Chem. , 1983. **159**.
159. Jaymand, M., *Conductive polymers/zeolite (nano-)composites: under-exploited materials.* RSC Advances, 2014. **4**(64): p. 33935-33954.
160. Travas-Sejdic, J., et al., *Intrinsically conducting polymer nanowires for biosensing.* Journal of Materials Chemistry B, 2014. **2**(29): p. 4593-4609.
161. Lange, U., N.V. Roznyatovskaya, and V.M. Mirsky, *Conducting polymers in chemical sensors and arrays.* Analytica Chimica Acta, 2008. **614**(1): p. 1-26.

162. Palaniappan, S. and A. John, *Polyaniline materials by emulsion polymerization pathway.* Progress in Polymer Science, 2008. **33**(7): p. 732-758.
163. Arora, K., et al., *Escherichia coli Genosensor Based on Polyaniline.* Analytical Chemistry, 2007. **79**(16): p. 6152-6158.
164. Tosar, J.P., et al., *Template and catalytic effects of DNA in the construction of polypyrrole/DNA composite macro and microelectrodes.* Biosensors and Bioelectronics, 2013. **41**(0): p. 294-301.
165. Peng, H., et al., *Synthesis of a functionalized polythiophene as an active substrate for a label-free electrochemical genosensor.* Polymer, 2007. **48**(12): p. 3413-3419.
166. Porfireva, A.V., et al., *Impedimetric Aptasensors Based on Carbon Nanotubes – Poly(methylene blue) Composite.* Electroanalysis, 2010. **22**(19): p. 2187-2195.
167. Debiemme-Chouvy, C. and M. Gallois, *Characterization of a very thin overoxidized polypyrrole membrane: application to H2O2 determination.* Surface and Interface Analysis, 2010. **42**(6-7): p. 1144-1147.
168. Ivanov, S., et al., *Electrocatalytically active nanocomposite from palladium nanoparticles and polyaniline: Oxidation of hydrazine.* Sensors and Actuators B: Chemical, 2010. **150**(1): p. 271-278.
169. Sakmeche, N., et al., *Application of sodium dodecylsulfate (SDS) micellar solution as an organized medium for electropolymerization of thiophene derivatives in water.* Synthetic Metals, 1997. **84**(1–3): p. 191-192.
170. Aeiyach, S., E.A. Bazzaoui, and P.-C. Lacaze, *Electropolymerization of thiophene on oxidizable metals in organic media.* Journal of Electroanalytical Chemistry, 1997. **434**(1–2): p. 153-162.
171. Roncali, J., *Conjugated poly(thiophenes): synthesis, functionalization, and applications.* Chemical Reviews, 1992. **92**(4): p. 711-738.
172. Gningue-Sall, D., et al., *Electrosynthesis and characterization of poly(3-methoxythiophene)-polybithiophene composite films prepared in micellar media on Pt and Fe substrates.* Physical Chemistry Chemical Physics, 1999. **1**(8): p. 1731-1734.
173. Sosnowska, M., et al., *Piezomicrogravimetric and Impedimetric Oligonucleotide Biosensors Using Conducting Polymers of Biotinylated Bis(2,2'-bithien-5-yl)methane as Recognition Units.* Analytical Chemistry, 2013. **85**(15): p. 7454-7461.
174. Yamanda, N. M.; Karner, R. B.; Chang, E-W. In Electrical and Optical Polymer Systems: Foundamentals methods and application; Wise, D. L., Ed.; Mercel Dekker: New York, 1998

175. Wilchek, M. and E.A. Bayer, *The avidin-biotin complex in bioanalytical applications.* Analytical Biochemistry, 1988. **171**(1): p. 1-32.
176. Bard A.J., F.L.R., *Electrochemical Methods: Fundamentals and Applications.* 2nd ed. 2001, New York: Wiley.
177. Finklea, H.O., *Photoelectrochemistry: Introductory concepts.* Journal of Chemical Education, 1983. **60**(4): p. 325.
178. Strehlow, W.H. and E.L. Cook, *Compilation of Energy Band Gaps in Elemental and Binary Compound Semiconductors and Insulators.* Journal of Physical and Chemical Reference Data, 1973. **2**(1): p. 163-200.
179. Safa Kasap, P.C., *Springer handbook of electronic and photonic materials*. 2006, New York: Springer. 1046.
180. Krishnan, R., *Fundamentals of Semiconductor Electrochemistry and Photoelectrochemistry*, in *Encyclopedia of Electrochemistry*. 2007, Wiley-VCH Verlag GmbH & Co. KGaA.
181. O'Regan, B. and M. Gratzel, *A low-cost, high-efficiency solar cell based on dye-sensitized colloidal TiO2 films.* Nature, 1991. **353**(6346): p. 737-740.
182. Agarwal, M., et al., *SnO2 Nanoparticle-Based Passive Capacitive Sensor for Ethylene Detection.* Journal of Nanomaterials, 2012. **2012**: p. 5.
183. Shang, G., et al., *Facile Synthesis of Mesoporous Tin Oxide Spheres and Their Applications in Dye-Sensitized Solar Cells.* The Journal of Physical Chemistry C, 2012. **116**(38): p. 20140-20145.
184. Andreas, K., et al., *Polyimide membrane with ZnO piezoelectric thin film pressure transducers as a differential pressure liquid flow sensor.* Journal of Micromechanics and Microengineering, 2003. **13**(4): p. S103.
185. Wang, J.X., et al., *Hydrothermally grown oriented ZnO nanorod arrays for gas sensing applications.* Nanotechnology, 2006. **17**(19): p. 4995.
186. Özgür, Ü., et al., *A comprehensive review of ZnO materials and devices.* Journal of Applied Physics, 2005. **98**(4): p. -.
187. Djurišić, A.B. and Y.H. Leung, *Optical Properties of ZnO Nanostructures.* Small, 2006. **2**(8-9): p. 944-961.
188. Wang, Z.L., *ZnO nanowire and nanobelt platform for nanotechnology*. Materials Science and Engineering: R: Reports, 2009. **64**(3–4): p. 33-71.

189. Djurišić, A.B., A.M.C. Ng, and X.Y. Chen, *ZnO nanostructures for optoelectronics: Material properties and device applications.* Progress in Quantum Electronics, 2010. **34**(4): p. 191-259.
190. E. de Jongh, P., D. Vanmaekelbergh, and J. J. Kelly, *Cu2O: a catalyst for the photochemical decomposition of water?* Chemical Communications, 1999(12): p. 1069-1070.
191. Tennakone, K., A.R. Kumarsinghe, and P.M. Sirimanne, *The effect of methyl viologen ion on photocurrent and stability of Cu2O photocathodes in I−/I3− redox electrolyte.* Journal of Photochemistry and Photobiology A: Chemistry, 1995. **88**(1): p. 39-41.
192. Xiong, L., et al., *p-Type and n-type Cu2O semiconductor thin films: Controllable preparation by simple solvothermal method and photoelectrochemical properties.* Electrochimica Acta, 2011. **56**(6): p. 2735-2739.
193. Nair, M.T.S., et al., *Chemically deposited copper oxide thin films: structural, optical and electrical characteristics.* Applied Surface Science, 1999. **150**(1–4): p. 143-151.
194. Wang, G., J. Xu, and H. Chen, *Progress in the studies of photoelectrochemical sensors.* Science in China Series B: Chemistry, 2009. **52**(11): p. 1789-1800.
195. Willner, I., F. Patolsky, and J. Wasserman, *Photoelectrochemistry with Controlled DNA-Cross-Linked CdS Nanoparticle Arrays.* Angewandte Chemie International Edition, 2001. **40**(10): p. 1861-1864.
196. Gill, R., M. Zayats, and I. Willner, *Semiconductor Quantum Dots for Bioanalysis.* Angewandte Chemie International Edition, 2008. **47**(40): p. 7602-7625.
197. Zhang, X., et al., *Aptamer based photoelectrochemical cytosensor with layer-by-layer assembly of CdSe semiconductor nanoparticles as photoelectrochemically active species.* Biosensors and Bioelectronics, 2011. **26**(8): p. 3674-3678.
198. Freeman, R., J. Girsh, and I. Willner, *Nucleic Acid/Quantum Dots (QDs) Hybrid Systems for Optical and Photoelectrochemical Sensing.* ACS Applied Materials & Interfaces, 2013. **5**(8): p. 2815-2834.
199. Gratzel, M., *Photoelectrochemical cells.* Nature, 2001. **414**(6861): p. 338-344.
200. Shipway, A.N., E. Katz, and I. Willner, *Nanoparticle Arrays on Surfaces for Electronic, Optical, and Sensor Applications.* ChemPhysChem, 2000. **1**(1): p. 18-52.
201. Maino, G., et al., *Electrochemically assisted deposition of transparent, mechanically robust TiO2 films for advanced applications.* Journal of Nanoparticle Research, 2013. **15**(11): p. 1-10.

202. Spadavecchia, F., et al., *Role of Pr on the Semiconductor Properties of Nanotitania. An Experimental and First-Principles Investigation.* The Journal of Physical Chemistry C, 2012. **116**(43): p. 23083-23093.
203. Binetti, E., et al., *Nanocomposites based on highly luminescent nanocrystals and semiconducting conjugated polymer for inkjet printing.* Nanotechnology, 2012. **23**(7): p. 075701.
204. Lahav, M., et al., *Photoelectrochemistry with Integrated Photosensitizer−Electron Acceptor and Au-Nanoparticle Arrays.* Journal of the American Chemical Society, 2000. **122**(46): p. 11480-11487.
205. Nasr, C., P.V. Kamat, and S. Hotchandani, *Photoelectrochemical behavior of coupled SnO2|CdSe nanocrystalline semiconductor films.* Journal of Electroanalytical Chemistry, 1997. **420**(1–2): p. 201-207.
206. Hojeij, M., et al., *Nanoporous Photocathode and Photoanode Made by Multilayer Assembly of Quantum Dots.* ACS Nano, 2008. **2**(5): p. 984-992.
207. Baş, D. and İ.H. Boyacı, *Quantitative Photoelectrochemical Detection of Biotin Conjugated CdSe/ZnS Quantum Dots on the Avidin Immobilized ITO Electrodes.* Electroanalysis, 2009. **21**(16): p. 1829-1834.
208. Vogel, R., P. Hoyer, and H. Weller, *Quantum-Sized PbS, CdS, Ag2S, Sb2S3, and Bi2S3 Particles as Sensitizers for Various Nanoporous Wide-Bandgap Semiconductors.* The Journal of Physical Chemistry, 1994. **98**(12): p. 3183-3188.
209. Wang, G.-L., et al., *Label-free photoelectrochemical immunoassay for α-fetoprotein detection based on TiO2/CdS hybrid.* Biosensors and Bioelectronics, 2009. **25**(4): p. 791-796.
210. Sheeney-Haj-Ichia, L., et al., *Enhanced Photoelectrochemistry in CdS/Au Nanoparticle Bilayers.* Advanced Functional Materials, 2004. **14**(5): p. 416-424.
211. Chandrasekharan, N. and P.V. Kamat, *Improving the Photoelectrochemical Performance of Nanostructured TiO2 Films by Adsorption of Gold Nanoparticles†.* The Journal of Physical Chemistry B, 2000. **104**(46): p. 10851-10857.
212. Zhu, W., et al., *Study on acetylcholinesteraseinhibition induced by endogenous neurotoxin with an enzyme-semiconductor photoelectrochemical system.* Chemical Communications, 2009(19): p. 2682-2684.
213. Feng, J., et al., *Photoelectric measurements of self-assembled and supported planar lipid bilayers: a new technique for studying apoptosis.* Electrochemistry Communications, 1999. **1**(3–4): p. 145-147.

214. Abi, A. and E.E. Ferapontova, *Unmediated by DNA Electron Transfer in Redox-Labeled DNA Duplexes End-Tethered to Gold Electrodes.* Journal of the American Chemical Society, 2012. **134**(35): p. 14499-14507.
215. Hall, D.B., R.E. Holmlin, and J.K. Barton, *Oxidative DNA damage through long-range electron transfer.* Nature, 1996. **382**(6593): p. 731-735.
216. Fink, H.-W. and C. Schonenberger, *Electrical conduction through DNA molecules.* Nature, 1999. **398**(6726): p. 407-410.
217. Schuster, G.B., *Long-Range Charge Transfer in DNA: Transient Structural Distortions Control the Distance Dependence.* Accounts of Chemical Research, 2000. **33**(4): p. 253-260.
218. Grozema, F.C., Y.A. Berlin, and L.D.A. Siebbeles, *Mechanism of Charge Migration through DNA: Molecular Wire Behavior, Single-Step Tunneling or Hopping?* Journal of the American Chemical Society, 2000. **122**(44): p. 10903-10909.
219. Zhang, C.-y., et al., *Photoelectric behavior of supercoiled DNA and its applications in molecular biology.* Bioelectrochemistry and Bioenergetics, 1998. **46**(1): p. 145-150.
220. Dill, K., S.D.H. Chan, and T.W. Gibbs, *Detection of plasmids using DNA and RNA probes and the light-addressable potentiometric sensor.* Journal of Biochemical and Biophysical Methods, 1997. **35**(3): p. 197-202.
221. Qingwen, L., et al., *Photoelectrochemistry as a novel strategy for DNA hybridization detection.* Analyst, 2000. **125**(11): p. 1908-1910.
222. Lu, W., et al., *Label-free photoelectrochemical strategy for hairpin DNA hybridization detection on titanium dioxide electrode.* Applied Physics Letters, 2006. **89**(26): p. -.
223. Lu, W., et al., *Enhanced photoelectrochemical method for linear DNA hybridization detection using Au-nanopaticle labeled DNA as probe onto titanium dioxide electrode.* Biosensors and Bioelectronics, 2008. **23**(10): p. 1534-1539.
224. Liu, S., et al., *Selective Photoelectrochemical Detection of DNA with High-Affinity Metallointercalator and Tin Oxide Nanoparticle Electrode.* Analytical Chemistry, 2006. **78**(13): p. 4722-4726.
225. Gao, Z. and N.C. Tansil, *An ultrasensitive photoelectrochemical nucleic acid biosensor.* Nucleic Acids Research, 2005. **33**(13): p. e123.
226. Tokudome, H., et al., *Photoelectrochemical deoxyribonucleic acid sensing on a nanostructured TiO2 electrode.* Applied Physics Letters, 2005. **87**(21): p. -.
227. Guo, Y., Y. Sun, and S. Zhang, *Electrochemiluminescence induced photoelectrochemistry for sensing of the DNA based on DNA-linked CdS NPs*

superstructure with intercalator molecules. Chemical Communications, 2011. **47**(5): p. 1595-1597.

228. Tel-Vered, R., et al., *Photoelectrochemistry with Ordered CdS Nanoparticle/Relay or Photosensitizer/Relay Dyads on DNA Scaffolds.* Angewandte Chemie International Edition, 2008. **47**(43): p. 8272-8276.
229. Zhao, W.-W., et al., *Energy transfer between CdS quantum dots and Au nanoparticles in photoelectrochemical detection.* Chemical Communications, 2011. **47**(39): p. 10990-10992.
230. Zhao, W.-W., et al., *Exciton-Plasmon Interactions between CdS Quantum Dots and Ag Nanoparticles in Photoelectrochemical System and Its Biosensing Application.* Analytical Chemistry, 2012. **84**(14): p. 5892-5897.
231. Wang, M., et al., *Signal-on photoelectrochemical biosensor for microRNA detection based on Bi2S3 nanorods and enzymatic amplification.* Biosensors and Bioelectronics, 2014. **53**(0): p. 232-237.
232. Yin, H., et al., *Photoelectrochemical biosensing platform for microRNA detection based on in situ producing electron donor from apoferritin-encapsulated ascorbic acid.* Biosensors and Bioelectronics, 2014. **53**(0): p. 175-181.
233. Centi, S., et al., *Detection of C Reactive Protein (CRP) in Serum by an Electrochemical Aptamer-Based Sandwich Assay.* Electroanalysis, 2009. **21**(11): p. 1309-1315.
234. Heyrovsky J., 1966. Principles of polarography. Academic press, New York and London, p. 106.
235. Hoogvliet, J.C., et al., *Electrochemical Pretreatment of Polycrystalline Gold Electrodes To Produce a Reproducible Surface Roughness for Self-Assembly: A Study in Phosphate Buffer pH 7.4.* Analytical Chemistry, 2000. **72**(9): p. 2016-2021.
236. Patolsky, F., et al., *Photoswitchable Antigen−Antibody Interactions Studied by Impedance Spectroscopy.* The Journal of Physical Chemistry B, 1998. **102**(50): p. 10359-10367.
237. Yang, M., H.C.M. Yau, and H.L. Chan, *Adsorption Kinetics and Ligand-Binding Properties of Thiol-Modified Double-Stranded DNA on a Gold Surface.* Langmuir, 1998. **14**(21): p. 6121-6129.
238. Steel, A.B., et al., *Immobilization of Nucleic Acids at Solid Surfaces: Effect of Oligonucleotide Length on Layer Assembly.* Biophysical Journal, 2000. **79**(2): p. 975-981.

239. Macdonald J.R., 1987. Impedance Spectroscopy. Wiley, New York, p.75.
240. Beloglazova, N.V., et al., *Quantum Dot Loaded Liposomes As Fluorescent Labels for Immunoassay.* Analytical Chemistry, 2013. **85**(15): p. 7197-7204.
241. Hezard, T., et al., *Gold nanoparticles electrodeposited on glassy carbon using cyclic voltammetry: Application to Hg(II) trace analysis.* Journal of Electroanalytical Chemistry, 2012. **664**(0): p. 46-52.
242. Welch, C.M., et al., *Fabrication, Characterisation and Voltammetric Studies of Gold Amalgam Nanoparticle Modified Electrodes.* ChemPhysChem, 2004. **5**(9): p. 1405-1410.
243. Asavapiriyanont, S., et al., *The electrodeposition of poly-N-methylpyrrole films from aqueous solutions.* Journal of Electroanalytical Chemistry and Interfacial Electrochemistry, 1984. **177**(1–2): p. 245-251.
244. Gelderman, K., L. Lee, and S.W. Donne, *Flat-Band Potential of a Semiconductor: Using the Mott–Schottky Equation.* Journal of Chemical Education, 2007. **84**(4): p. 685.
245. http://www.sigmaaldrich.com/catalog/product/fluka/60134?lang=it&region=IT
246. De Gryse, R., et al., *On the Interpretation of Mott-Schottky Plots Determined at Semiconductor/Electrolyte Systems.* Journal of The Electrochemical Society, 1975. **122**(5): p. 711-712.
247. Mohr, P.J.a.T., Barry N. and Newell, David B., *CODATA recommended values of the fundamental physical constants: 2006.* Rev. Mod. Phys., 2008. **80**(2).
248. Löberg, J., et al., *Electronic Properties of TiO(2) Nanoparticles Films and the Effect on Apatite-Forming Ability.* International Journal of Dentistry, 2013. **2013**: p. 139615.